Bioimaging of Nitric Oxide

Tetsuo Nagano†

Graduate School of Pharmaceutical Sciences, The University of Tokyo, Hongo, Bunkyo-ku, Tokyo 113-0033, Japan

Tetsuhiko Yoshimura*

Institute for Life Support Technology, Yamagata Public Corporation for the Development of Industry, Yamagata 990-2473, Japan

Received August 20, 2001

Contents

* To whom correspondence should be addressed. Phone: +81-23-647-3133. Fax: +81-23-647-3138. E-mail: yoshi@ymgt-techno.or.jp.
† Fax: +81−3−5841−4855. E-mail: tlong@mol.f.u-tokyo.ac.jp.

I. Introduction

Human beings are highly receptive to an enormous amount and variety of information from the external environment, and more than 90% of it is thought to be visual. It is generally said that an appeal to the

10.1021/cr010152s CCC: $39.75
Published on Web 03/15/2002

Tetsuo Nagano was born in 1949 in Tokyo, Japan. He graduated in pharmaceutical sciences at the University of Tokyo. After completing his Ph.D. with work on development of bio-active heterocyclic compounds in 1977 under supervision of Professor Toshihiko Okamoto at the University of Tokyo, he became an assistant professor at the same University. In 1983–1985 he joined Professor Fridovich's group as a research associate in biochemistry at Duke University and studied a novel detection method for reactive oxygen species, especially for singlet oxygen. After postdoctoral studies, he joined again the University of Tokyo as an associate professor and changed his research field, moving from organic chemistry to chemical biology. His main research interests are in the molecular-design, synthesis and applications of novel bio-imaging probes for physiologically active species such as nitric oxide, Zn^{2+}, singlet oxygen, reactive oxygen, caspase, etc. He was awarded the Pharmaceutical Society of Japan Award for Young Scientists in 1990, Ichimura Scientific Prize in 1999 and Mochida Prize in 2000. Currently, he is a full professor at Graduate School of Pharmaceutical Sciences, the University of Tokyo.

Tetsuhiko Yoshimura is a deputy director general of Institute for Life Support Technology (ILST) at Yamagata, Japan, and a research director of the Laboratories of Applied Biomedicinal Chemistry and Applied Environmental Science in the institute. He was born in Gifu, Japan, in 1944, and educated at Osaka University, Osaka Japan, receiving BA in 1967. He earned Ph.D. degree in nuclear engineering in 1972 at Osaka University and the thesis title was "Studies on the Chemical and Electronic Structures of Octa-Coordinated Uran(IV) Complexes". In 1972 he accepted a position at the Environmental Science Institute of Hyogo Prefecture, Kobe Japan as a researcher, and promoted to a chief researcher in 1976. There he studied NO complexes of iron porphyrins and hemoproteins using various spectroscopic methods. The scope of such studies included biological effects of atmospheric NO and the structure–function relationship of cytochromes c′ which are found in denitrifying and photosynthetic bacteria and have a high affinity for NO. In 1992, he moved to Yamagata, where he joined ILST as a research director for the Division of Bioinorganic Chemistry. After joining ILST, he extended his studies to include the determination and elucidation of endogenously produced NO in mammals and its EPR imaging, which is the topic of the current review. Recently he authored an educative book, entitled "NO from Space to Cells" (in Japanese) which is directed to nonscientist readers. He is consistently interested in the role of NO in biological systems and his current projects include in vivo and in vitro researches on the functional consequences of NO production during inflammation lesions in gastrointestinal tract and brain.

eye is more effective than that to the ear, which may be the basis of the proverb "Seeing is believing". To be able to "see into the body" or "see into cells" is essential in the diagnosis and treatment of disease as well as for research into the basic processes of life. Moreover, it is desirable that seeing into the body and cells is accomplished by using noninvasive techniques, without cutting into the body or isolating of cellular constituents. Therefore, we believe that techniques to visualize physiological or pathophysiological changes in the body and cells become increasingly important in biomedical sciences. In this article, we will review the background and current status of imaging techniques for approach on biological nitric oxide (NO), i.e., bioimaging of NO, with emphasis on the imaging techniques that utilize electron paramagnetic resonance (EPR) spectrometry and fluorometry.

NO is a small uncharged free radical containing one unpaired electron. NO exists in space as an interstellar molecule[1−3] and in the atmosphere of Venus and Mars.[4,5] On earth, NO has been recognized as an atmospheric pollutant and a potential health hazard. However, in 1987 it was reported that NO is identical with endothelium-derived relaxing factor (EDRF), which is biosynthesized in the living body.[6−8] It is now widely known that NO is an ubiquitous messenger molecule in the cardiovascular, nervous, and immune systems.[9−13] In addition, L-arginine-derived NO has been found in a wide variety of organisms ranging from mammals to invertebrates, bacteria, and plants. Although NO is a relatively stable free radical, it readily and rapidly reacts with free radicals and metal-containing proteins in biological systems, exerting physiological or pathophysiological effects, and therefore, in situ NO detection is required to elucidate the biological roles of NO. In vivo and in situ visualization of NO using bioimaging techniques should provide us with a comprehensive understanding of the production and diffusion processes of NO.

Newly developed analytical techniques have revealed numerous roles of NO in various biological systems.[14−18] NO detection assays include the following: (1) chemiluminescence technique using the reaction of NO with ozone or luminol; (2) fluorometry using a fluorescent NO indicator; (3) spectrophotometry using the formation of NO−hemoglobin (NO−Hb); (4) EPR spectrometry using spin (NO) traps such as Hb, organic compounds, and iron−dithiocarbamate complexes; and (5) electrochemical method using microelectrodes specific to NO. Other indirect assays include spectrophotometry, fluorometry, and radiometry of stable biological metabolites of NO or L-arginine such as nitrite, nitrate, and L-citrulline. We can apply any method(s) of choice to detect and quantify NO, but we need to choose the one that is most suitable for a specific purpose, because each method described above has both merits and demerits.

The chemiluminescence method, for instance, requires a gas-phase reaction of NO with ozone.[6,19] Although very sensitive and selective for NO, the method required purging of aqueous samples with an inert gas to strip NO into an analyzer. Therefore, it is incapable of monitoring intracellular NO. The other chemiluminescence method with luminol has limitations for the functional analysis of NO, such as the use of cytotoxic H_2O_2.[20−22] Electrochemical sensing using microsensors provides in situ real-time detection of NO.[23] However, the only spatial information is directly at the electrode tip and is therefore influenced by the placement of the probe. These methods have been invaluable for studying NO-related biochemistry, but to achieve a more detailed understanding, a new method is required which is appropriate for studies in living cells in terms of selectivity and experimental feasibility.

For in vivo and in situ NO determination, minimal invasiveness is a necessity. It has been shown that the chemiluminescence technique, fluorometry, EPR spectrometry, and electrochemical method are feasible to detect NO in vivo or in situ. Among them, EPR spectrometry and assays that use luminescence or fluorescence could be employed for in vivo and in situ detection and imaging, because these methods are not only less invasive, but also highly sensitive.

So far, three real-time bioimaging techniques have been developed to evaluate the spatial distribution of endogenously produced NO and applied to animal and cellular model studies: (1) in vivo imaging in living small animals by an EPR technique using an efficient NO-trapping reagent,[24] (2) intracellular imaging in living cells and tissues by using newly synthesized fluorescent indicators,[25] and (3) intracellular imaging in activated macrophages by using a luminol−chemiluminescence technique,[20] which has the limitations mentioned above. These techniques represent an extension of the cumulative knowledge and progress in analytical techniques for other bioactive components, such as reactive oxygen species (ROS) and calcium ion. We hope that this review encourages the developments of the bioimaging based on the other techniques. Such bioimaging of bioradicals including NO and oxygen radicals in biological systems would be developed into a critical tool in etiological assessments in near future.

A. Fundamental Issues in Bioimaging of NO

An understanding of the biochemical and physicochemical properties of NO in biological situations is required for its detection, quantification, and imaging. No doubt, there will be detailed discussions of the fundamentals of NO elsewhere in this thematic issue of *Chemical Reviews*. Here, we briefly address the level, solubility, lifetime, and diffusibility of NO in biological systems.

NO is biosynthesized by three distinct mammalian NO synthase isoforms.[26,27] Neuronal NOS (nNOS or NOS I) and endothelial NOS (eNOS or NOS III) are constitutively expressed in neuronal and endothelial cells, respectively, and thus, both enzymes are also referred to as cNOS, while inducible NOS (iNOS or NOS II) is expressed in cells involved in inflammation such as macrophages and microglias through stimulation with cytokines and/or endotoxins. Although cNOS and iNOS do not show a significant difference in specific activity, cNOS activity is Ca^{2+}-dependent whereas iNOS activity is Ca^{2+}-independent, and these NOS's are expressed at different levels from each other. Since the enzyme activity of cNOS is dependent on transiently raised concentrations of intracellular Ca^{2+}, the NO levels produced in stimulated endothelial and neuronal cells are low (submicromolar at the cellular level) relative to those (1−10 μM) in macrophages;[28] in addition, the formation rate of NO in the former cells is higher than in the case of NO generated by other NOS.[29,30] Thus, cNOS is a transiently activated and low-output isoform while iNOS expression results in a sustained production and high-output of NO. Moreover, excessive production of NO has been realized to be responsible for various pathophysiolgies, while far lower levels of NO are produced under physiological conditions.[27]

The basal rate of NO formation in rats was evaluated through the measurement of the appearance rate of nitrate residues in plasma during exposure of rats to $^{18}O_2$.[31] The rates in anaesthetized and awake rats were in the ranges of 0.33−0.85 and 0.36−0.72 μmol kg^{-1} h^{-1}, respectively. It was suggested that the figures mainly reflect NO formation in the vascular endothelium and the neuronal tissue. In humans, the rate was estimated to be 0.9 μmol kg^{-1} h^{-1}.

NO solubility in oxygen-free water is 1.9 mM at 25 °C.[32] NO is more soluble in organic solvents such as methanol (14 mM), toluene (11 mM), and *n*-hexane (18 mM), suggesting that it is lipid-soluble and may readily dissolve in the cell membrane. The most popular reaction of NO in oxygen-containing biological fluids can be an oxidation reaction with oxygen molecule (O_2). The reaction of NO with O_2 takes place in aqueous solution according to following equation.

$$4NO + O_2 + 2H_2O \rightarrow 4NO_2^- + 4H^+ \qquad (1)$$

The rate law for the formation of NO_2^- in this reaction was found to be second order in NO concentration and first order in O_2 concentration: $d[NO_2^-]/dt = k[NO]^2[O_2]$. The rate constant has been reported to be $3-12 \times 10^6$ M^2 s^{-1}.[33−35] When [NO] is 1 μM and [O_2] is less than 100 μM, the half-life of NO is estimated to be more than 15 min. Thus, the autoxidation of NO may be markedly slow in oxygen-containing biological fluids. However, it has been clearly demonstrated that the reaction of NO with O_2 in hydrophobic phase proceeds 300 times more rapidly than in the aqueous phase because NO and O_2 concentrations are much higher in the former phase than in the latter phase.[36] This finding suggests that the autoxidation of NO and the subsequent reactions occur rapidly within the membrane.[37] Reported values for the half-life of NO under physiological conditions range from 0.1 to 5 s.[9,37,38] It has recently been demonstrated that the half-life in whole blood was shortened to millisecond order owing to the rapid reaction of NO with oxyhemoglobins.[39]

When using Fick's second law of diffusion and the diffusion coefficient of NO, the diffusion distances of

NO at a given half-life can be estimated, assuming both concentrations at the site of production and at the site of action. The diffusion coefficient of NO in liposomes was 1.3×10^{-5} cm^2 s^{-1} at 20 °C.[40] When NO concentrations at the production and action sites are 1 μM and 10 nM, respectively, the diffusion distances at half-life values of 1 ms, 0.1 s, and 5 s are estimated to be 11, 110, and 760 μm, which are 1−70 times the cell diameter of 10 μm.[40] This suggests that endogenously produced NO may be able to exert its biological effects on an enormous number of cells.

B. Bioimaging of NO by Electron Paramagnetic Resonance (EPR) Spectrometry

EPR spectroscopy is a specific technique to detect and characterize molecules with unpaired electron(s). In the last two decades, the EPR technique has attracted increasing attention from both biologists and medicinal scientists due to increasing interest in reactive oxygen radicals in biological systems. Since NO was added as a new member of the group of endogenously produced radicals (bioradicals) in 1987, endogenous NO has provided a challenging target for EPR spectrometric detection. Although NO itself is an EPR-active molecule and it is detectable with an EPR technique in chemical systems, the EPR signal of NO in biological systems is hardly detectable with a straightforward EPR technique, probably because of the short lifetime and low concentration of NO. The EPR spin-trapping technique can be applied to overcome these difficulties.[41−52] This technique enables one to conduct in vitro and in vivo NO measurements in biological systems. For many years, spin trapping has been used for the detection of unstable free radicals such as hydroxyl (•OH) and superoxide ($O_2^{\bullet-}$) in biological and chemical systems.[53,54] Several spin-trapping compounds (spin traps) that selectively react with and trap NO have been developed and applied to biological NO measurements, such as iron complexes with dithiocarbamate derivatives (Fe−DTC complexes). Among NO-trapping reagents, Fe−DTC complex alone has been applied to in vivo measurements of NO.

EPR imaging is considered to be the most effective technique available for noninvasive observation of the spatial distribution of free radicals.[55,56] In vivo EPR imagings were first performed using an exogenous, synthetic, and stable free radical which was locally administered to small animals. Early in vivo direct EPR spin-trapping detection of bioradicals was difficult,[57−68] and subsequent improvement of low-frequency EPR instrumentation increased the feasibility of successful in vivo EPR imaging of bioradicals.[68] The NO adducts of the Fe−DTC traps are very stable in biological media, and the first in vivo EPR detection and imaging of endogenous NO was successfully accomplished.[24]

In section II, we will review the progress and current status of in vitro and in vivo detection and imaging of NO in biological systems by EPR and related techniques. For more information on EPR spectrometry for various bioradicals, several general reviews and books are available.[41−52,55,56,63−70]

C. Bioimaging of NO by Fluorometry

Generally, biofunctional species-reactive fluorescent indicators which allow bioimaging with high spatial and temporal resolution in conjunction with fluorescence microscopy are useful for elucidation of biological functions. For instance, experimental studies on Ca^{2+}-dependent signal transduction in cells were greatly facilitated by the development of fluorescent indicators for Ca^{2+}.[71,72] Thus, fluorescence methods were expected to be well suited for the bioimaging of NO production in biological samples with both spatial and temporal resolution.

To develop useful fluorescent NO probes, the following criteria should be satisfied: (1) Fluorescent probes should react with NO or species derived from NO to yield the corresponding fluorescent products without forming byproducts at room temperature at atmospheric pressure under physiological pH conditions in an aqueous solution; (2) The reaction should be specific for NO or species derived from NO; (3) Both of the probes and the products should be stable, especially to light, because laser microscopy is used for bioimaging; (4) The fluorescence properties of the probes should be different in the presence and in the absence of NO; (5) Visible light is desirable for excitation to diminish autofluorescence and photodamage to living systems; (6) The probes should be membrane-permeable so that they can enter living cells for bioimaging.

NO is converted by reaction with O_2 and H_2O into NO_2^- and NO_3^-. In addition, ROS such as $O_2^{\bullet-}$, •OH, etc., are often generated concomitantly with formation of NO. Thus, a practical detection method is required which is satisfactory for studies in living cells in terms of distinguishability of NO from ROS.

The use of NO-reactive fluorescent probes, in conjunction with confocal laser microscopy, should provide an NO bioimaging technique which is suitable for real-time analysis of intracellular NO. They can be applied to imaging in vivo in whole animal, although some surgical operations might be required to expose the dye-loaded region to the light. Nagano et al. succeeded in NO imaging on the surface of rat brain (unpublished data). In section III, we will review the development of workable probes for bioimaging of NO.

II. EPR Imaging of NO

A. Background

1. EPR Spectroscopy

EPR spectroscopy (which is also known as electron spin resonance or ESR) explores the magnetic moment associated with the unpaired electron(s) in free radicals and paramagnetic metal ions.[73] It has been applied for the detection of free radicals and paramagnetic metal ions in various biological materials. When an unpaired electron in a paramagnetic molecule is subjected to an external magnetic field (H), the energy level of the electron splits into two quantum states with an energy difference (ΔE). When microwaves (frequency, ν) are applied to the

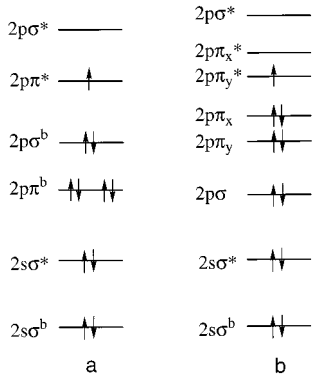

Figure 1. Presumed filling of the molecular orbitals for free NO molecule (a) and for the molecule in crystalline field (b).

system, energy absorption occurs if the following relation is strictly fulfilled: $\Delta E = h\nu = g\beta H$, where h is Planck's constant, g is a proportionality constant called the g-value, and β is the Bohr magneton. For instrumental reasons, the magnetic field is scanned with a fixed microwave frequency. Conventional EPR spectrometers employ a microwave frequency of approximately 9.5 GHz (this frequency is customarily called the X-band). However, a large volume of wet biological samples such as the tissues, organs, and the whole body of animals cannot be measured with a conventional X-band spectrometer because of the high dielectric loss of water at the frequencies[74] and small size of the EPR cavity resonator; in fact, aqueous specimens with a volume of less than about 100 μL are measurable in an X-band spectrometer. EPR spectroscopy at lower frequencies eases the restriction on sample size and water content.[40,55,56] The inner diameter of a loop−gap resonator in which the sample is inserted has been reported to be 25 mm in an instrument with a frequency of 1.1−1.3 GHz[75] and 41 mm in an instrument with a frequency of 700−800 MHz.[62] At present, EPR spectrometers operating at S-band (1.6−4 GHz) and L-band (0.4−1.6 GHz) microwave frequency and at radio frequency (0.2−0.4 GHz) are utilized for in vivo measurements of the whole body of small animals,[68] though the sensitivity is much lower than that of X-band instruments.[48]

2. EPR Detection of NO

The electronic configuration of NO, with 11 valence electrons as exemplified in Figure 1, is $(K^2K^2)(2s\sigma^b)^2(2s\sigma^*)^2(2p\pi^b)^4(2p\sigma^b)^2(2p\pi^*)^1$. Thus, NO is a free radical with one unpaired electron in the antibonding π orbital. Therefore, EPR is considered to be the most appropriate tool for its detection.

The electronic ground state of NO is expressed by the term symbol, $^2\Pi_{1/2,3/2}$. The $^2\Pi_{1/2}$ state is nonmagnetic, owing to the exact cancellation between the orbital and spin magnetic moment of the electron, and thus, EPR can be observed only from the $^2\Pi_{3/2}$ state. The paramagnetic character of NO arises from the $^2\Pi_{3/2}$ state, whose energy is 120 cm^{-1} higher than the ground $^2\Pi_{1/2}$ state.[76] Direct EPR measurements of NO are possible under two special conditions: NO in a pressure-controlled gas phase or trapped or adsorbed in inorganic matrixes.

While the rotational angular momentum is quenched in liquid and solid phases of paramagnetic molecules, in the gaseous phase it couples strongly with electronic spin and orbital angular momentum, which explains the many lines in gas-phase EPR spectra. Beringer and Castle were the first to observe an X-band spectrum of gaseous NO at a pressure of 1.0 mmHg; it extended over 26 mT with the center field at approximately 860 mT.[76] Subsequent detailed measurements have revealed that each of nine lines is doubled by removal of the Λ-degeneracy.[77] As a result, the spectrum consists of 27 lines: 9 and 18 lines arising from magnetic− and electric−dipole transitions, respectively.[78] These measurements have been carried out at NO pressures from 0.01 to 1 mmHg under careful gas pressure control.[79]

When NO is in a crystalline field such as in an adsorbed state or in inorganic matrixes, the spin−orbit coupling can be partially quenched and the π-antibonding level split (Figure 1b). Characteristic anisotropic EPR spectra of immobilized NO can be obtained at low temperature. Thus, EPR spectra of NO adsorbed on MgO, ZnO, ZnS, and zeolite were reported by Lunsford;[80−83] crystal-field analysis using the EPR parameters and the chemical state of NO adsorbed on a cation in a adsorbent matrix was identified and allowed evaluation of the interaction of NO with the structure of the adsorbents.[81−86] Recent studies with Q- (∼34 GHz) and W-band (∼95 GHz) EPR and electron nuclear double resonance (ENDOR) spectroscopies have identified new adsorbed states of NO in zeolites.[87−89] Furthermore, in EPR studies on the interaction of NO with metalloproteins, 'unusual' EPR signals have been observed at liquid helium temperature in the presence of excess NO.[90−96] These anomalous and characteristic signal line shapes are quite similar to those of NO adsorbed in inorganic matrixes. This fact suggests that the unusual EPR signals did not originate from the interaction of NO with metalloproteins but from nonspecific interaction of excess NO with cations such as Na^+ and K^+ in buffer solutions.

In this section, we concentrated on the EPR spectroscopies of NO in the gas phase and in inorganic matrixes. The electronic structures of NO and its related compounds and the EPR spectroscopies of various nitrosylmetallocomplexes in biological situations have been detailed in recent reviews and books.[41,46,47,97−100]

3. Spin-Trapping Technique

Direct EPR detection of endogenous free radicals in biological samples requires that the free radical of interest at steady state is present at a concentration more than the practical EPR detection limit (0.1−0.01 μM) and it has a relatively long lifetime.[101] Although such direct detection may be possible at cryogenic temperature, the in vivo detection at ambient temperature seems almost impossible because bioradicals, in general, do not have a sufficiently long lifetime to survive the measuring period. These difficulties can be overcome by applying a spin-trapping technique, which has been used for the detection of various unstable free radicals, such as

$^{\bullet}OH$ and $O_2^{\bullet-}$, in biological systems.[53,54] Spin traps react with unstable free radicals to form a relatively stable radical adduct. This long-lived adduct formation results in accumulating a steady-state formation of these free radicals, and thus, the resultant radical adduct can be detected readily by EPR spectroscopy.

Two classes of spin traps that have been very efficient and useful in trapping oxygen-centered radicals are nitrone and nitroso compounds, of which the radical adducts are relatively stable, EPR-detectable nitroxide radicals.[48,53,54] Common spin traps are as follows: *nitrone traps*: 5,5-dimethyl-1-pyrroline *N*-oxide (DMPO), 5-diethoxyphosphoryl-5-methyl-1-pyrroline-*N*-oxide (DEPMPO), α-phenyl-*N*-*tert*-butylnitrone (PBN), and α-(4-pyridyl-1-oxide)-*N*-*tert*-butylnitrone (POBN); and *nitroso traps*: 2-methyl-2-nitrosopropane (MNP) and 3,5-dibromo-4-nitrosobenzenesulfonic acid (DBNBS).

For the application of the spin-trapping principle to NO detection, several spin-trapping reagents have been developed and used in in vitro and in vivo situations as described in section II.B.1.[43−45,51,102−105]

4. In Vivo EPR Detection and Imaging of Free Radicals

EPR signals from large biological samples cannot be detected with a conventional X-band spectrometer as described in section II.A.1. EPR spectrometers operating at lower frequency are now applied to in vivo measurements of the whole body of small animals.[48]

Usage of low-frequency EPR instruments for examination of living systems was initiated in the early 1980s. Berliner et al. reported the first EPR imaging of a biologically relevant sample as a one-dimensional (1-D) image of a celery stem soaked in a solution of a stable nitroxide radical, 4-hydroxy-2,2,6,6-tetramethylpiperidine-1-yloxyl (TEMPOL).[58] Since then, many in vivo EPR imaging experiments have been successfully carried out in various localized regions of small animals and have shed light on the spatial distribution and pharmacokinetics of exogenously supplied stable radicals such as TEMPOL, 3-carbamoyl-2,2,5,5-tetramethylpyrrolidine-1-yloxyl (carbamoyl-PROXYL), and their analogues.[57−68] Furthermore, the oxygen induces the broadening of EPR signals of stable nitroxides and the other paramagnetic agents. Therefore, the application of in vivo EPR spectroscopy to the measurement of concentration or partial pressure of oxygen in tissues has been extensively developed as a promising approach to oxymetry.[65−68] This technique has a potential for noninvasive measurement of tissue oxygen status.

In contrast, short half-lives and low concentrations of endogenously synthesized and metabolically produced free radicals in physiological and pathophysiological processes make in vivo EPR detection difficult, and this is exacerbated by poor sensitivity of the spectrometer. Despite facility in in vitro spin trapping of oxygen-centered radicals, its in vivo detection has been accomplished with difficulty because of the low rate of radical adduct formation and the low stability of the adduct in biological situations.[48] Several in vivo measurements of oxygen-centered radical adducts have been nevertheless carried out by using nitrone spin traps. The hydroxyethyl radical produced by ionizing radiation (3000 Gy) in the tumor of a living mouse was measured by using a mixture of POBN and ethanol as a spin-trapping system.[106] In vivo detection of hydroxyl radical formed via oxidation of 5-aminolevulinic acid was conducted by employing DEPMPO as a spin trap in mice, suggesting that DEPMPO is a good candidate for in vivo trapping of radicals.[107,108] On the other hand, endogenously produced NO is more suitable for the in vivo detection than oxygen-centered radicals in the lifetime and the stability of radical adduct. Thus, several groups have been prompted to attempt in vivo real-time detection of NO by the use of low-frequency EPR instruments combined with newly developed spin traps for NO, and they have accomplished the detection and/or imaging of NO both in vivo and in situ. In these studies, iron complexes with dithiocarbamate derivatives (Fe−DTCs) were used as spin traps for NO. The NO adduct [NO−Fe(DTC)$_2$] exhibits an intense three-line signal at room temperature, enabling in vivo detection of endogenous NO in mouse tail, mouse abdomen, and rat head (section II.D).

B. NO-Specific Trapping

1. NO-Trapping Reagents

Conventional nitrone (DMPO) and nitroso (MNP, DBNBS) spin traps were reported to be able to trap NO and were applied to the measurement of NO in cell cultures.[109−111] However, the feasibility of these traps for use in biological NO measurement has not been established.[112,113]

Suitable compounds so far proposed for NO spin trapping are either free radicals which are highly reactive to NO or compounds containing iron ions with high affinity for NO. NO cheletropic trap (NOCT), a double carbon-centered biradical equivalent, was designed based on the former concept. As in eq 2, *o*-quinodimethane **2** generated by photolysis of 2-indanone **1** reacts with NO to yield the stable nitroxide **3**, which exhibits an EPR signal with a three-line hyperfine structure.[112]

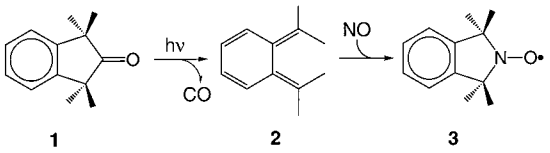

1 **2** **3** (2)

NO formation from cultured liver macrophages, Kupffer cells, was detected by using NOCTs.[112] NOCTs with improved thermal stability and water solubility have been useful in cellular NO trapping.[114,115] It is an advantage of NOCTs that they can also trap NO_2, and the EPR spectrum of NO_2 adducts is distinguishable from that of NO adducts. Unfortunately, these compounds are not commercially available. Recently, fluorescent NOCT (FNOCT) containing a fluorophoric moiety has been shown to react with NO to form a new fluorophore.[116−118] FNOCT potentially adds a new concept to a design of NO traps as shown in section III.A.6.

Nitronyl nitroxides are stable radicals originally developed as spin-labeling reagents. Nitronyl nitrox-

ides react with NO to yield imino nitroxides which are also radicals.[119−121] 2-Phenyl-4,4,5,5-tetramethylimidazoline-1-yloxyl-3-oxide (PTIO) (**4**) is one of the most stable nitronyl nitroxides known, and its reaction product **5** is 2-phenyl-4,4,5,5-tetramethylimidazoline-1-yloxyl.[120,122]

The second-order rate constants for this reaction (eq 3) are 5.15×10^3 M^{-1} s^{-1} for PTIO and 1.01×10^4 M^{-1} s^{-1} for carboxy-PTIO.[123] Following this reaction, the number of lines in the EPR spectra changes from five to seven. Nitronyl nitroxides showing such an EPR spectral change were utilized in a 'nitric oxide dosimeter' to measure concentrations of atmospheric NO.[122] Furthermore, PTIO and its water-soluble analogue (carboxy-PTIO) have been extensively applied as an NO trap for the detection of NO in biological systems.[123,124] Nitronyl and imino nitroxides are nonspecifically reduced by various biological reductants such as ascorbate, thiol-containing compounds, and superoxide, so that special care may be required to obtain an accurate NO level.[125−128] In addition, attention should be also given to the fact that NO_2, a product of eq 3, and subsequently generated nitrite have specific biological activities and cytotoxicities. In other studies, to avoid interference from the redox system in endothelial cells, carboxy-PTIO was mixed with the effluent from an endothelial cell column, and then the mixture was subjected to EPR measurements, and this modification helped in quantitative evaluation of NO from cultured endothelial cells.[125] Encapsulation of PTIO into liposome vesicles to avoid reduction is another approach to improve NO quantitation and to reduce the effect of NO_2.[127,128] NO production from rat cerebellum was measured by incorporating a nitronyl nitroxide trap into large unilamellar phosphatidylcholine liposomes.[127] Further improvement of the stability and specificity of nitronyl nitroxides was achieved by using liposomes prepared with a reverse-phase evaporation method.[128] 2-Trimethylamino PTIO was encapsulated into these liposomes, and quantitative analyses of NO produced from cultured RAW 264 cells were carried out. Nitronyl nitroxides can be utilized as a selective NO scavenger, and many pharmacological studies have been reported.[129−134]

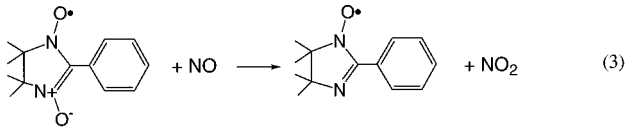

Ferrous iron complexes such as Hbs and Fe−DTC complexes have been widely applied as NO traps to various biological specimens.

NO has been employed as a useful probe for elucidating the electronic structure of a heme group and the stereochemistry of a heme environment in various hemoproteins, because it coordinates as a nitrosyl ligand to the sixth-coordination site of the heme iron with a high affinity. Nitrosyl derivatives of ferrous hemoproteins are EPR active and exhibit a characteristic EPR spectrum because an unpaired electron on NO is delocalized toward an iron d orbital.

Scheme 1. Proposed Scheme of Reductive Nitrosylation in Fe(III) Hemoproteins and Porphyrin Complexes

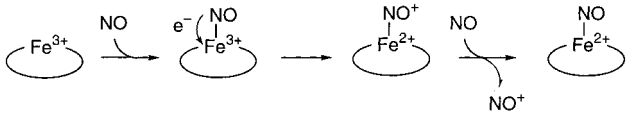

Thus, the nitrosylhemoproteins and their model complexes, nitrosyl iron(II) porphyrins, have been extensively studied by EPR spectroscopy, of which excellent achievements were introduced in recent reviews[41,42,100,135] and a book.[46] Here, we will focus on the hemoproteins as an NO spin trap. Because NO has a high affinity for ferrous Hb, NO readily binds to deoxy Hb to produce NO−Hb, which exhibits a characteristic EPR spectrum at low temperature, such as 77 K.[41] The conformational change in the α-subunit of Hb from a high-affinity R state to a low-affinity T state has been shown to lead to the appearance of the sharp three-line hyperfine structure in the EPR spectrum of NO−Hb.[46] The three-line structure is derived from the cleavage of heme iron to the proximal histidine bond on binding of NO to Hbα. Thus, three-line signal of NO−Hb is associated with the R−T equilibrium under physiological conditions, and further it can be utilized for the EPR analysis of NO−Hb.[102,136−141] In addition, the distinct three-line hyperfine structure appears in the spectrum of NO−Hb on the addition of inositol hexaphosphate, an allosteric effector of Hb, which facilitates the evaluation of NO−Hb with EPR spectrometry.[140] In the presence of O_2, however, the majority of Hb remains in its oxy form, O_2−Hb, which reacts with NO to produce met Hb and nitrate,[142] causing inaccuracies in NO−Hb methods. The carbon monoxide (CO) adduct of Hb may be a better NO trap than deoxy Hb:[143] the affinity of deoxy Hb for CO is higher than that for O_2 but lower than that for NO,[144] and therefore, NO can displace CO in CO−Hb to form NO−Hb; CO−Hb does not react with NO_2^-, while deoxy Hb reacts with NO_2^- to yield NO−Hb slowly. Moreover, Hb is an endogenous NO trap in vertebrates.[136−140] Nitrosylated Hb in blood can be utilized as a marker to assess the effect of NO on the circulation. Obviously, the use of an endogenous marker helps alleviate the external perturbation of biological systems.

On the other hand, NO also reacts with ferric hemoproteins to form nitrosyl ferric analogues. In some hemoproteins such as Hb, myoglobin, and cytochromes *c*′, the nitrosyl ferric analogues are reduced in the presence of NO to form corresponding nitrosyl ferrous analogues.[46,135] This reductive nitrosylation may be involved in in vivo trapping of NO by Hb. Reductive nitrosylation is well-known in Fe(III) hemoproteins and porphyrin complexes.[145−149] Although the detailed mechanism has not been established yet, an outline of the reaction is shown in Scheme 1 and the overall reaction formula in eq 4.

$$\text{Fe(III)(Heme)} + 2\text{NO} \rightarrow \text{NO−Fe(II)(Heme)} + \text{NO}^+ \quad (4)$$

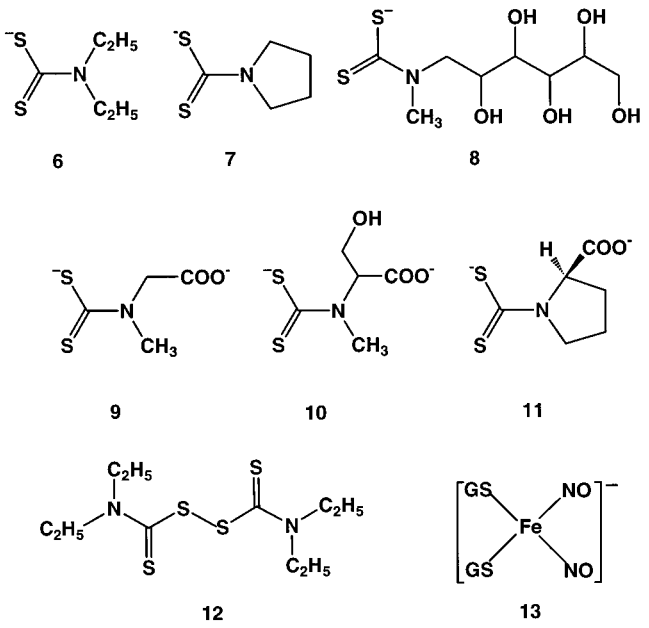

Figure 2. Chemical structures of compounds. Dithiocarbamate derivatives (**6**−**11**) used as NO-trapping reagents: dithiocarbamates to form water-insoluble iron complex (**6**−**7**) and water-soluble iron complex (**8**−**11**): **6**, *N*,*N*-diethyldithiocarbamate (DETC); **7**, pyrrolidine dithiocarbamate (PDTC); **8**, *N*-methyl-D-glucamine dithiocarbamate (MGD); **9**, *N*-(dithiocarboxy)sarcosine (DTCS); **10**, *N*-methyl-L-serine dithiocarbamate (MSD); **11**, L-proline dithiocarbamate (ProDTC); **12**, disulfiram (disulfide of DETC); **13**, diglutathionyl dinitrosyl iron complex, [DNIC−$(GS)_2$].

This reductive nitrosylation requires two NO molecules. A recent quantitative study of the reductive nitrosylation of Fe(III) hemoproteins has shown that the first nitrosyl ligand is eliminated by nucleophilic attack of OH^- to give the Fe(II) hemoproteins and nitrite ion, and then the resultant Fe(II) hemoproteins can react further with NO to give the nitrosyl complex.[149]

Cytochromes *c*′, which are hemoproteins found in a variety of denitrifying and photosynthetic bacteria, have high affinity for NO,[150,151] and the proteins can be used as bioprobes for NO, as shown in section III.A.4. Recently, NO-selective photometric or electrochemical biosensors have been developed using cytochrome *c*′ immobilized on an optical fiber or electrode or encapsulated in sol−gel glass.[152−157]

2. Dithiocarbamates

Dithiocarbamic acid is obtained as a reaction product of carbon disulfide with primary and secondary amines.[158,159] Dithiocarbamates (DTCs, Figure 2) are strong chelators of heavy metals, and *N*,*N*-diethyldithiocarbamate (DETC, **6**) has been extensively used for many years (as a colorimetric, extracting, or masking agent) in quantitative or qualitative analyses of heavy metals such as Ni, Cu, Zn, and Hg.[158−160]

DTCs and their disulfides also have antioxidant and pro-oxidant properties in biological systems. They are used worldwide as fungicides, herbicides, and insecticides with recent estimates of global consumption of 25,000−35,000 metric tons per year.[161] DTCs have been clinically used and were shown to be safe and efficient in the treatment of HIV-infected patients.[162] Biological activities of DTCs are attributed to their metal-chelating and/or thiol-delivery properties. It is suggested that some DTC biological activities may affect the physiological roles of NO.

DETC has been shown to inhibit Cu/Zn−superoxide dismutase (SOD) activity through the withdrawal of Cu from the protein both in vivo and in vitro.[163−165] This inhibition may cause an increase in the concentration of $O_2^{\bullet-}$ in vivo and a concomitant decrease in the concentration of NO, because NO and $O_2^{\bullet-}$ react at almost a diffusion-controlled rate[166] to form peroxynitrite, a more toxic species than NO. In red blood cells, DETC was demonstrated to react with O_2−Hb to produce several products, such as ROS, met Hb, sulf Hb, oxidized DETC, and lipid peroxidation products, besides inhibiting intracellular Cu/Zn−SOD.[167,168] It has been reported that disulfiram (disulfide of DETC, **12**) inhibits kidney flavoenzyme through a sulfhydryl−disulfide exchange reaction with the protein's reactive sulfhydryl group,[169] and DTCs also inhibit glutathione *S*-transferases by direct binding to the protein.[170]

Pyrrolidine dithiocarbamate (PDTC, **7**), as well as DETC, has been reported to potently inhibit oxidative activation of the nuclear transcription factor κB (NF-κB) through its action as an antioxidant.[171] NF-κB regulates gene expression in various physiological processes such as immunity, stress responses, inflammation,[172] glial and neuronal function,[173,174] and the inhibition of apoptosis.[175,176] Therefore, the inhibition of NF-κB activation by PDTC and DETC causes various biological phenomena, including inhibition of iNOS expression,[177−179] inhibition of apoptosis in thymocytes,[180] leukemic cells,[181] and L929 fibroblasts,[182] induction of heme oxygenase-1 gene expression,[183] etc.[171,174,183,184] In contrast, as a pro-oxidant, PDTC is an inducer of apoptosis in thymocytes.[185] Recently, iron complexes with *N*-(dithiocarboxy)sarcosine (DTCS, **9**) and *N*-methyl-D-glucamine dithiocarbamate (MGD, **8**) have been shown to inhibit NO production from purified nNOS in cell-free system. It was proposed that this inhibition occurred through the interference by iron−DTCs in the physiological electron flow from NADPH to nNOS heme iron, while free DTCs did not inhibit the activity.[186]

3. EPR Spectra of Nitrosyl Iron–Dithiocarbamate Complexes in Biological Specimens

Chemists have paid considerable attention to the EPR spectroscopic study of nitrosyl iron−dithiocarbamate complex, [NO−Fe(II)$(DTC)_2$], since the report by Gibson.[187] Now, not only chemists but also life scientists are greatly interested in seeing such EPR spectra in biological specimens.

At present, Fe−DTC complexes are considered useful spin-trapping reagents for NO because NO has a high affinity for them. The resultant stable NO−Fe(II)$(DTC)_2$ complex exhibit s a three-line EPR spectrum ($g_{av} \sim 2.04$; $A_N \sim 1.27$ mT) at room temperature in solution (Figure 3A) and a spectrum with axial symmetry ($g_\perp \sim 2.037$, $g_\parallel \sim 2.015$) at low temperature in the frozen state (Figure 3C), enabling one to determine in vitro and in vivo endogenous NO

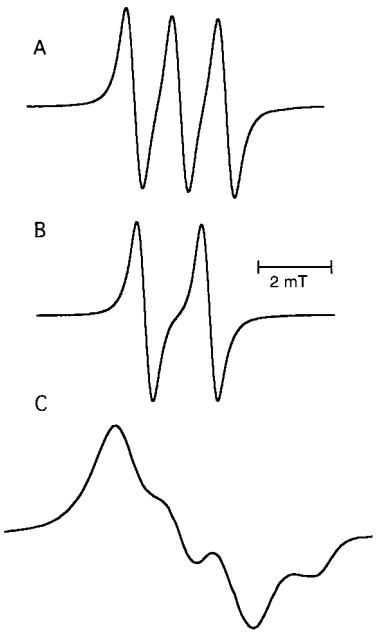

Figure 3. X-band EPR spectra of the $^{14}NO-Fe(II)(DTCS)_2$ complex at room temperature (A) and at 77 K (C) and of the $^{15}NO-Fe(II)(DTCS)_2$ complex at room temperature (B), in aqueous solution.

levels. The EPR spectrum in biological specimens at room temperature as exemplified in Figures 4, 6, 8, and 10 shows a more distorted line shape than that in Figure 3 because free rotation of the complex is restricted by the interaction of the NO complex with biological components such as membranes. Three-line (triplet) splitting originates from the hyperfine interaction of an unpaired electron with the ^{14}N nucleus ($I = 1$) in NO. If nitrogen of the NO source is labeled with ^{15}N ($I = 1/2$), a two-line (doublet) signal ($g_{av} \sim 2.04$, $A_N \sim 1.8$ mT) is observed (Figure 3B). When ^{15}N-substituted arginine as a substrate of NOS is supplied to cell culture or tissues with NOS activity in the presence of an Fe−DTC complex, the EPR spectrum exhibits a doublet line of $^{15}NO-Fe(DTC)_2$.[188−196] Furthermore, when dioxygen is replaced by ^{17}O ($I = 5/2$)-substituted dioxygen in this system, the EPR spectrum derived from $N^{17}O-Fe(DTC)_2$ can be observed, suggesting that dissolved oxygen is a sole source of oxygen in NO.[190] Thus, this isotopic substitution has been useful in the assignment of NO sources.

4. Iron–Dithiocarbamate Complexes as NO-Trapping Reagents

Vanin and colleagues were the first to use Fe−DETC complex as an NO trap in aqueous media containing 3-morpholinosydnonimine (SIN-1), NO donor.[197] Since then, Fe−DETC complex has been widely used for determination of NO generated in cell cultures, tissues, and whole animals.[50] The Fe−DETC complex is hardly soluble in aqueous solution,[198] so iron salt (in general, $FeSO_4 \cdot 7H_2O$) and DETC have to be administered separately to biological samples.

Subsequently, water-soluble iron−DTC complexes such as iron−MGD[199] and −DTCS[200] have been developed into biological NO traps. The water-solubility of these Fe−DTC complexes results from the introduction of a hydrophilic group into the DTC structure. Thus, these NO traps can be prepared as a solution of a desired concentration or used in powder form. Negatively charged Fe−DTCS complex is more water-soluble than the uncharged complex with MGD. The coordination of NO to the Fe complex alters its solubility;[201] for example, $NO-Fe(II)(DTCS)_2$, >100 mM; $NO-Fe(II)(MGD)_2$, <1 mM.[202] Other DTCs which form water-soluble iron complexes have been developed and tested for NO-trapping ability.[203−205]

The differences in water solubility among the Fe−DTC complexes allow selective usages as NO spin traps. Fe−DETC complex is essentially insoluble in water but is lipid-soluble and permeable through membranes such as the blood−brain barrier,[206,207] so it is suitable for the detection of intracellular and intramembrane NO.[105,208] Water-soluble NO traps can be transported via the circulation system and are suitable for in vivo detection of NO under physiological and pathophysiological conditions.[45] This high mobility of NO adducts in water-soluble iron complexes is useful for spin probes (section II.E.3).[200,209,210] However, water-soluble NO traps cannot permeate into lipophilic organs and tissues.[211,212]

Although transition-metal nitrosyl complexes, including Hb and Fe complexes with other ligands, are rapidly degraded in the presence of oxygen, $NO-Fe(II)(DTC)_2$ complexes are less sensitive to oxygen and their lifetime in ambient air (∼day) is much longer than that of the spin adducts of most organic spin traps (∼min). Embedding of $NO-Fe(II)(DTC)_2$ complexes in liposomes improves their air-stability, which facilitates handling.[45]

Lifetimes and pharmacokinetics of $NO-Fe(II)(MGD)_2$ and $NO-Fe(II)(DTCS)_2$ complexes were determined in in vitro and in vivo systems.[201] EPR-signal intensities of both complexes stayed unchanged over 45 min in phosphate buffer solution and exhibited longer lifetimes in the presence of glutathione and ascorbate, while the stability was diminished in the presence of $O_2^{\bullet-}$ or NO. Thus, the in vivo stability of these NO complexes in a continued flux of NO may be ascribed to some protective action of glutathione and ascorbate. The in vivo half-life of $NO-Fe(II)(DTCS)_2$ complex given by intraperitoneal injection to mice was estimated to be 41 min, and $NO-Fe(II)(MGD)_2$ complex showed approximately 1 order of magnitude shorter lifetime than DTCS complex, which may be related to the lower solubility of the latter complex in water. Fe−DTC complexes do not trap all the NO produced in the specimens, so the actual amount of NO in a sample may be underestimated. NO-trapping efficiencies of the Fe−DTC complexes depend on the DTC ligand and the medium, which may explain the difference in the efficiencies between in vitro and in vivo situations.[202] In the case of Fe−DTCS complex, the estimated trapping efficiency ranged from 40% in phosphate-buffered saline solution to 95% in Tris/HCl buffer at pH 7.4.[203] The absolute amount of NO can be estimated by considering both the observed EPR signal intensity and the trapping efficiency of the complex.

5. Reactions of NO, NO^+, NO^-, and NO_2^- with Fe–DTC Complexes

NO reacts with $Fe(II)(DTC)_2$ complex to form $NO-Fe(II)(DTC)_2$.

$$NO + Fe(II)(DTC)_2 \rightarrow NO-Fe(II)(DTC)_2 \quad (5)$$

The high-performance liquid chromatography (HPLC) profile of the reaction mixture of NO with $Fe(II)(DTCS)_2$ showed that $NO-Fe(II)(DTCS)_2$ is the only product.[213] The second-order rate constant of the reaction of NO with $Fe(II)(ProDTC)_2$ (ProDTC, **11**) was reported to be $(1.1 \pm 0.3) \times 10^8\ M^{-1}\ s^{-1}$.[204] Strict deoxygenation of the reaction media is required to accomplish the completion of the reaction as in eq 5, because $Fe(II)(DTC)_2$ is rapidly oxidized by trace amounts of oxygen to yield Fe(III) complex.[213,214] It is believed that the trapping agent, $Fe(II)(DTC)_2$ prepared by mixing iron sulfate heptahydrate ($FeSO_4 \cdot 7H_2O$) and excess DTC, reacts with NO to form a stable $NO-Fe(II)(DTC)_2$ (eq 5). However, $Fe(III)(DTC)_3$ complexes were shown to react readily with NO to form the $NO-Fe(II)(DTC)_2$ complexes in aqueous solution,[44] suggesting that the reaction occurs via reductive nitrosylation.[203,213−215]

Previously, three mechanisms for the reductive nitrosylation of $Fe(III)(DTC)_3$ complexes were proposed. Using an EPR spectroscopic approach, Yordanov et al. demonstrated that $NO-Fe(II)(DETC)_2$ complex was formed by passing NO gas through $Fe(III)(DETC)_3$ toluene solution and proposed the hypothetical reaction mechanism shown in eq 6, but the DETC radical in this scheme could not be detected[216]

$$Fe(III)(DETC)_3 + NO \rightarrow NO-Fe(II)(DETC)_2 + DETC^{\bullet} \quad (6)$$

$$2DETC^{\bullet} \rightarrow bis(DETC) \quad (7)$$

where bis(DETC) is a disulfiram, **12**.

Vanin et al. reported the reductive nitrosylation of $Fe(III)(MGD)_3$ in aqueous solution and proposed two types of mechanisms.[214] The proposed overall reactions are as follows.

$$\text{(I)}\ 2NO + Fe(III)(MGD)_2 \xrightarrow{H_2O\ (\bullet OH)} NO-Fe(II)(MGD)_2 + NO_2^- \quad (8)$$

$$\text{(II)}\ NO + Fe(III)(MGD)_2 \xrightarrow{\text{Reducing Equivalent}} NO-Fe(II)(MGD)_2 \quad (9)$$

where reducing equivalent refers to endogenous reducing agents such as ascorbate, hydroquinone, and thiol. With the use of EPR, optical, and chemiluminescence spectroscopies and electrochemical methods, Vanin et al. showed that $NO-Fe(III)(MGD)_2$ was formed as an intermediate in both mechanisms and the rate-limiting step was the reduction process of Fe(III) in $NO-Fe(III)(MGD)_2$. The mechanism of eq 8 requiring two molecules of NO is identical to that of reductive nitrosylation of Fe(III) hemoproteins (eq 4), because NO_2^- is equivalent to NO^+ in the oxidation state of the nitrogen. In biological samples with endogenous reducing agents, the mechanism of eq 9 could predominate over that of eq 8.

An HPLC and LC-electrospray ionization mass spectroscopy study by our group showed that the products of the reaction of NO with $Fe(III)(DTCS)_3$ in aqueous solution were $NO-Fe(II)(DTCS)_2$ and the dimer of DTCS in which two DTCS bind through a disulfide bond [bis(DTCS)].[213] On pulse radiolysis of a deaerated aqueous solution of $Fe(III)(DTCS)_3$ in the presence of $NaNO_2$ (NO source), the absorption change exhibited three phases, as judged from kinetic difference spectra. The reactions of the three phases are shown in eqs 10−12, in which the chemical species is expressed by considering the ionic character.

$$[Fe(III)(DTCS)_3]^{3-} + NO \rightarrow [NO-Fe(III)(DTCS)_3]^{3-} \quad (10)$$

$$[NO-Fe(III)(DTCS)_3]^{3-} + [Fe(III)(DTCS)_3]^{3-} \rightarrow [NO-Fe(II)(DTCS)_2]^{2-} + [Fe(IV)(DTCS)_3]^{2-} + DTCS^{2-} \quad (11)$$

$$[Fe(IV)(DTCS)_3]^{2-} + DTCS^{2-} \rightarrow [Fe(III)(DTCS)_3]^{3-} + 1/2\ [bis(DTCS)]^{2-} \quad (12)$$

The overall reaction is as follows

$$[Fe(III)(DTCS)_3]^{3-} + NO \rightarrow [NO-Fe(II)(DTCS)_2]^{2-} + 1/2\ [bis(DTCS)]^{2-} \quad (13)$$

The second-order rate constants of reactions 10, 11, and 12 were calculated to be $(4.8 \pm 0.9) \times 10^8$, $(2.5 \pm 0.3) \times 10^7$, and $(2.6 \pm 0.5) \times 10^6\ M^{-1} \cdot s^{-1}$, respectively. In this mechanism, unreacted $Fe(III)(DTCS)_3$ donates an electron to NO−Fe(III) complex to form $NO-Fe(II)(DTCS)_2$ and $Fe(IV)(DTCS)_3$. However, electron donors to NO−Fe(III) complex may include endogenous reducing agents such as ascorbate and glutathione in biological systems. Although the overall reaction of eq 13 is similar to eqs 6 and 7, homolytic scission of the DTCS ligand to give its radical could not be detected in this study.

As described above, the second-order rate constants of NO with both $Fe(II)(DTC)_2$ (eq 5) and $Fe(III)(DTC)_3$ (eq 10) are of the order of $10^8\ M^{-1}\ s^{-1}$. This rate constant of NO trapping is much larger than that of PTIO and its derivatives ($\sim 10^4\ M^{-1}\ s^{-1}$),[123] and further, it is by no means inferior to that of NO with O_2-Hb ($3.7 \times 10^7\ M^{-1}\ s^{-1}$)[142] or Fe(II)Hb ($1.5 \times 10^7\ M^{-1}\ s^{-1}$).[144] These results suggest that Fe−DTC complexes are very efficient as NO traps in vivo, and they should be suitable for in vivo real-time measurements of NO.

Specificity for NO is one of the most important requisites for an NO-trapping reagent. It has been demonstrated that Fe−DTC complexes react with NO^+ donors such as *S*-nitrosothiols[217] and sodium nitroprusside (SNP)[199] to exhibit EPR-active NO

adducts, although SNP is an NO^+ or NO donor depending on physiological conditions.[16] Thus, these NO traps may not be able to differentiate between NO and NO^+. Very recently, contradictory results have been reported on the reactivity of Fe−MGD complex for nitroxyl ion (NO^-). Komarov et al. reported that the reaction of an NO^- donor (Angeli's salt; $Na_2N_2O_3$) with Fe−MGD complex produced an EPR spectrum similar to that of NO under aerobic conditions, suggesting that the Fe−MGD trap does not discriminate between NO and NO^-.[218] On the contrary, Xia et al. found that $Fe(II)(MGD)_2$ complex exhibited the EPR spectrum of an NO adduct upon addition of an NO donor (*S*-nitroso-*N*-acetylpenicillamine) but not with Angeli's salt, while $Fe(III)(MGD)_3$ complex did show the EPR spectrum after reaction with both NO and NO^- donors.[193,194] These authors also showed that Fe−MGD complex can distinguish between NO and NO^-, depending on the redox state of the iron.

Nitrite (NO_2^-) and nitrate (NO_3^-) are end products of NO metabolism. The NO-trapping reaction of Fe−DTC complexes has been shown to be unaffected by NO_2^-.[217] However, recent reports indicated that Fe−MGD complex produces $NO-Fe(MGD)_2$ in the presence of NO_2^- after prolonged incubation.[219−222] The reaction of NO_2^- with Fe−MGD complex has a very small rate constant of 4.8 M^{-2} s^{-1} [221] and proceeds only in the presence of a high concentration of NO_2^- such as 100 μM[219] or <500 μM.[222] The NO_2^- level at 100 μM in the presence of Fe−MGD complex gave only a very weak EPR signal after a long period of time.[219] The NO_2^- levels in biological fluids are generally lower than the NO_3^- levels; for instance, $[NO_2^-] = 6.6 \pm 11$ μM and $[NO_3^-] = 34 \pm 18$ μM in serum of healthy humans ($n = 21$), $[NO_2^-] = 3.4 \pm 3.1$ μM and $[NO_3^-] = 7.6 \pm 4$ μM in cerebrospinal fluid of healthy humans ($n = 10$),[223] $[NO_2^-] \sim 6$ μM and $[NO_3^-] \sim 260$ μM in plasma of endotoxin-treated rats.[224] In such cases, $NO-Fe(DTC)_2$ produced from in vivo levels of NO_2^- can be much below the EPR detection limit, even though NO_2^- may interfere with NO trapping by Fe−DTC complexes. However, decreases of pH during tissue ischemia may induce the direct reduction of NO_2^-, and NO thus formed may be trapped and detected by Fe−DTC complexes.[191]

For judging whether the observed events are NOS dependent or independent, a duplicate experiment in the presence of NOS inhibitor should be carried out in the practical utilization of NO-trapping reagents. If an EPR signal from $NO-Fe(DTC)_2$ is weakened or disappeared on the addition or administration of NOS inhibitor, it is truly derived from NOS.

6. Other Features Relevant to NO Trapping by Fe–DTC Complexes

A characteristic background EPR signal with four lines is usually overlapped on the NO adduct signal at low temperature when the Fe−DETC complex is used as an NO trap,[182] and this background signal was detected after the administration of DETC alone. The large background signal sometimes interferes with the NO-derived signal. Frozen tissues or cells treated with Fe−DTCS complex or DTCs to form a water-soluble iron complex did not exhibit such a background signal.[211,225] The signal was assigned to $g_\perp$ of the $Cu(II)(DETC)_2$ complex,[211] which is formed from exogenous DETC and endogenous Cu(II) ion. It has been suggested that DETC permeates through membrane and binds with intracellular Cu(II)[197] or withdraws Cu(II) from Cu/Zn SOD and/or Cu−albumin complex in plasma.[226] Hydrophobic Fe−DETC complex may be a suitable NO trap for the detection of intracellular NO, but one must keep in mind that the EPR spectra of frozen samples treated with Fe−DETC complex always exhibit Cu−DETC and $NO-Fe(DETC)_2$ signals.

The addition or administration of exogenous NO traps can cause disturbance to biological specimens to some extent, but the feasibility of continuous and quantitative monitoring of the same biological specimen is a great advantage of this method.[103] The LD_{50} for acute toxicity of three DTCs in mice was estimated as 1870 mg/kg (orally)[227] or 1332 mg/kg (intravenously; Yoshimura, unpublished data) for $DETC\cdot Na\cdot 3H_2O$, more than 2500 mg/kg (intraperitoneally)[228] or over 7000 mg/kg (i. v., Yoshimura et al., unpublished results) for MGD·Na, 765 mg/kg for $DTCS\cdot 2NH_4\cdot 2H_2O$ (intravenously),[225] and 1942 mg/kg for $DTCS\cdot 2Na\cdot 2H_2O$ (intravenously).[225] The toxicity of Fe(DTC) complexes has not been determined. $Fe(II)(MGD)_2$ and $Fe(II)(DTCS)_2$ scarcely produced $O_2^{\bullet-}$ and yielded far less $^\bullet OH$ than the chelates such as ethylenediamine-*N*,*N*,*N*,*N*-tetraacetic acid (EDTA) frequently used to inhibit $^\bullet OH$ production.[201] This finding suggests that generation of such small amounts of free radicals by these NO traps would neither injure the organism nor affect the detection of NO, so continuous observation at ambient temperature should be feasible. Interestingly, Fe−DTC complex has been shown to be pharmacologically effective for scavenging NO under pathological conditions. Scavenging of NO after the addition or injection of Fe−MGD complex (or NOX-101; Medinox, San Diego) seemed to cause inhibition of the relaxation that was induced by acetylcholine in rat aortic ring segments,[229,230] prolongation of cardiac allograft survival, and a decrease of NF-κB DNA binding activity in rejected allografts in rats.[231] Exogenous iron supplied in NO trapping through Fe−DTC complexes may affect NO production in cells and tissues.[232,233] $NO-Fe(MGD)_2$ complex was recently demonstrated to react with $O_2^{\bullet-}$ or peroxynitrite to yield an EPR-silent species.[234] In $O_2^{\bullet-}$-generating system, this transformation into the EPR-silent state may lead to loss of the NO adduct and affect NO quantifications.

In vivo effects exerted by the addition or administration of exogenous Fe−DTC complexes may vary, depending on the conditions of use (in vivo or in vitro). Special attention should be given to such effects when using these NO traps.

C. In Vitro and Ex Vivo EPR Detection of NO Using Fe–DTC Traps

1. Detection of NO from NO Synthase and Cultured Cells

NO generated from purified nNOS has been directly measured by using Fe(II)−MGD complex,

confirming that NOS directly biosynthesizes NO from the substrate, L-arginine.[193,194] It has been shown that Fe(III) complexes with DTCS and MGD inhibited nNOS catalytic activity with IC_{50} values of 9.7 ± 0.7 μM and 25.1 ± 2.9 μM, respectively, while the free ligands did not inhibit the activity.[186] Therefore, one should pay attention to the redox state of iron in the Fe−DTC complex when Fe−DTC traps are used in cell-free systems.

After incubation of cells with the NO trap for an appropriate period, the cell suspension or supernatant is subjected to X-band EPR measurements to detect NO.[217,219,225,235] The advantage of the method is that the NO source is easily distinguishable if L-[^{15}N]arginine is used. When L-[^{15}N]arginine is added to the medium or administered to small animals instead of L-[^{14}N]arginine, a two-line EPR signal (Figure 3B) is observed if NO is derived from L-arginine.[103,188−190,236]

NO produced from macrophages, stimulated by cytokines and/or bacterial lipopolysaccharide (LPS), is detectable with the NO-trapping technique because the iNOS expressed produces a relatively high concentration of NO (>micromolar).[237] Although the NO production level in stimulated endothelium is much lower than that in macrophages, it is still detectable with NO traps.[225,238] Direct EPR detection of NO from porcine aorta endothelial cells was performed by using a water-insoluble Fe−DETC trap[238] and a water-soluble Fe−DTCS trap.[225] The lipophilic nature of the Fe−DETC complex may be an advantage for the detection of intracellular NO from membrane-bound eNOS, while water-soluble Fe−DTC traps are effective in the detection of intercellular NO diffusing out from endothelial cells.

2. Detection of NO in Resected Tissues and Organs

Fe−DTC traps have been frequently applied to NO quantification in the tissues of animal model under various pathological conditions. In most cases, after the administration of the NO trap, tissues of target organs were resected and subjected to an X-band EPR measurement at ambient and cryogenic temperature. Fe−DETC complex seems to hold an unchallenged position as an NO trap in brain tissues in animal models of ischemia,[206,207,239,240] seizure,[241,242] sepsis,[212,232,243] meningitis,[244] viral encephalitis,[245] and halothane anesthesia,[246] because Fe−DETC can pass into the brain through the blood−brain barrier.[211,212] Fe−DETC trap has been also applied to NO determinations in liver,[189,212,232,247−250] kidney,[232] intestine,[232,250] spleen,[232] heart,[232] and lung[232] of LPS-treated small animals, in regenerating rat liver,[251] in mouse stomach at adaptive relaxation,[252] and in rat jejunum and ileum under ischemia−reperfusion.[253] Hydrophobic NO−Fe(DETC)$_2$ complex formed in various organs of LPS-treated rat was extracted with organic solvent, concentrated, and subjected to the measurement.[250]

The administration of LPS, resulting in the induction of iNOS and excessive NO production, causes a septic shock syndrome in both human and animals.[254,255] Such NO production, which reaches a maximum level 6−8 h after LPS administration, was also observed in the brain tissues of rats injected intraperitoneally with LPS (plus interferon-γ, IFN-γ), exhibiting an intense EPR signal of the NO−Fe(DETC)$_2$ complex at ambient temperature (Figure 4).[243]

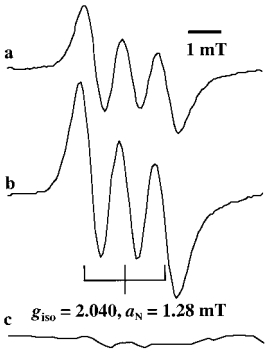

Figure 4. X-band EPR spectra of the NO−Fe(DETC)$_2$ complex at room temperature observed in the rat brain tissue. EPR spectra were recorded at 7 h after the administration of 40 mg/kg of LPS (a) and 40 mg/kg of LPS plus 100 × 10^4 U/kg of IFN-γ (b). Pretreatment with L-NMMA (100 mg/kg, intraperitoneally) completely inhibited the LPS-elicited NO formation (c). (Reprinted with permission from ref 243. Copyright 1998 Overseas Publishers Association.)

IFN-γ was used because IFN-γ is known to stimulate pathways of iNOS induction different from those of LPS.[256] In this experiment, rats received LPS with or without IFN-γ, followed by administration of Fe(SO$_4$)$_2$ and DETC solution 6.5 h later, and then EPR spectra (Figure 4) were recorded at 7 h after the LPS injection.

Although not as widely applied as the Fe−DETC trap, other water-soluble Fe−DTC complexes have also been utilized in NO measurements in live LPS-treated animals,[205,212,248,257,258] in the kidney[258] and heart[258] of LPS-treated animals, in ischemic heart of rat,[259,260] in mouse pancreas under STZ-induced diabetes,[261] in solid tumor-implanted rat,[262] and in virus-infected lung of mouse.[263] Water-soluble traps are well suited for fluid samples such as blood,[24,205,236,248] bile,[257] and urine.[24,212] It should be emphasized that NO production from nitrite in biological systems was evaluated in ischemic heart by employing an Fe−MGD trap.[191]

In blood, in addition to endogenously produced NO, the NO formation from nitrovasodilators including glyceryl trinitrate,[264,265] isosorbide dinitrate (ISDN),[196,265] and SNP[266] has been demonstrated by this NO-trapping technique.

D. In Vivo EPR Detection and Imaging of NO in Living Small Animals

The resolution of EPR images is affected by the line width and signal-to-noise (S/N) ratio of the EPR signal and the field gradient strength, and it can be improved by using a probe with a narrower line width. Nitroxide radicals most commonly used in EPR imaging or spin labeling have a line width (peak-to-peak width) of 0.14−0.16 mT.[267] In the case of the NO complex of iron shown in Figure 3A, the

width of the central line was 0.38 mT, which seems unfavorable for EPR imaging. The broad line width originates from the delocalization of an unpaired electron of NO toward the iron d orbital. Although the high resolution obtained in NMR imaging is difficult to attain in EPR imaging at present, EPR imaging is likely to be the most effective technique for noninvasive observation of the spatial distribution of free radicals.

1. Instrumentation and Imaging Techniques for In Vivo EPR Measurements

In vivo EPR detection and imaging techniques have been developed at frequency bands that cover the radio frequency of 0.2−0.4 GHz and microwave frequency region of L- (0.4−1.6 GHz) and S-bands (1.6−4 GHz). Each laboratory that is engaged in in vivo EPR imaging has made specific modifications to their EPR instrument, as reviewed in several publications.[55,56,60,61,63−69] Hereinafter, in vivo NO detection and imaging methods will be described with emphasis on the in vivo detection and imaging system developed in our institute.[45,268,269]

In vivo EPR measurements are usually carried out for rather large and water-rich samples, such as experimental animals. Since at conventional X-band (9−10 GHz) frequencies water-rich samples have a high dielectric loss which reduces the *Q*-factor of the resonant cavity,[55,56] we utilized 700 MHz microwaves to lower the dielectric loss of water. Common cavity resonators have poor filling factors even at lower microwave frequencies and have an inhomogeneous microwave field inside the resonator, while a bridged loop−gap resonator as well as a lumped circuit-resonant tank consisting of a loop conductor as the inductor and a gap as the capacitor have large filling factors. In these resonators, the electric field is attracted to the gap and a relatively homogeneous magnetic field can be obtained only in the loop. Thus, we used a two-gap-type loop−gap resonator with an interior bridge which can reduce leakage of the electric field from the gap.[59] The resonator has the dimensions of 10 mm in axial length and 41 mm in inner diameter, which can accept the head of a rat or the whole body of a mouse.

A block diagram of the EPR-computed tomography (EPR−CT) system constructed in our institute is illustrated in Figure 5. The main electromagnet has an air-cored, water-cooled, two-coil Helmholtz design. The relaxation times of an EPR-resonant system are very fast, and thus, a continuous wave (cw) method has been adopted in usual EPR measurements. Thus, the time required for EPR measurements mainly depends on the rate of the field scan. The use of the air-core magnet permitted repeated rapid field scans in a short duration because of the absence of magnetic hysteresis from an iron core.[270,271] The rapid field scan made it possible to execute a markedly increased number of signal accumulations, and it improved the S/N ratio and reduced the 1/*f* noise.[272]

The three-dimensional EPR image (i.e., EPR−CT) is constructed on the basis of Lauterbur's method,[273] known as a three-dimensional zeugmatography. For this purpose, we applied linear magnetic field gradients (1 mT/cm) along the *X*-, *Y*-, and *Z*-axes produced by magnetic field gradient coils.[62] A pair of magnetic field gradient coils for the *X*-, *Y*-, and *Z*-axes were attached to the surface of the main magnet.

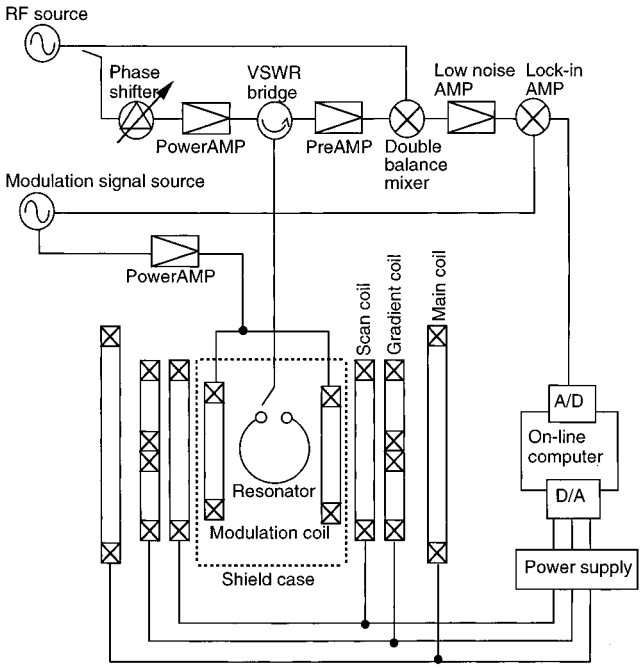

Figure 5. Block diagram of home-built EPR−CT system. The main electromagnet is air-cored, water-cooled, and two-coil Helmholtz designed. The magnetic field was scanned by regulating the current of the field scan coils. A pair of magnetic field gradient coils for the *X*-, *Y*-, and *Z*-axes are attached to the surface of the main magnet. The currents supplied for the field scan coils and the field gradient coils are controlled by an on-line computer. The microwave circuit is constructed with an RF source, a power amplifier, a VSWR bridge, a phase shifter, a preamplifier, and a double-balanced mixer for homodyne detection. The rectified signal is amplified and followed by a lock-in amplification at a frequency of magnetic field modulation. A pair of modulation coils is driven by an internal oscillator of the lock-in amplifier and a power amplifier. The spectral data are collected via an analog−digital converter using the on-line computer. (The block diagram was kindly offered by Dr. H. Yokoyama of the Institute for Life Support Technology.)

The microwave circuit was constructed with a signal source, a VSWR bridge, a phase shifter, a preamplifier, and a double-balanced mixer for homodyne detection. The rectified signal was followed by lock-in amplification at the frequency of magnetic field modulation. A pair of modulation coils was driven by an internal oscillator of the lock-in amplifier and a power amplifier operated at 100 kHz.[274] The spectral data were collected via an analog−digital converter using an on-line computer.[272]

In three-dimensional zeugmatography, projection spectra are obtained by changing the angles of the field gradient sequentially under a fixed gradient intensity in one plane. The direction of the field gradient was rotated in 20° steps, and projections were collected. The obtained data on nine spectra for each two-dimensional projection constituted a three-dimensional set. Arbitrary slice planes (i.e., CT images) can be cut from the three-dimensional data. Thus, data on 81 projection spectra were needed

under the selected field gradients to obtain one set of EPR−CT images.[62,210]

The EPR spectral data obtained under the field gradients were deconvoluted using the line shape of the zero-gradient spectrum, by a fast Fourier transform method with low-pass filtering.[275] EPR images are reconstructed from the deconvoluted data by a filtered back projection. The details of the method of construction of the image data has been described elsewhere.[45,210] Full-width at half-maximum (FWHM) required to estimate a spatial resolution[55,56] was measured from the deconvoluted spectrum that was obtained under zero gradient.[210] It was confirmed that the FWHM-to-gradient ratio could be utilized as an index for the spatial resolution.[269] This parameter is affected by the line width and S/N ratio of spectra and the gradient strength. If the pixel size is smaller than the FWHM-to-gradient ratio, then it does not represent the spatial resolution. Signals lower than 25% of the maximum signal intensity in all slices were regarded as noise when constructing the images. The images were reproduced in 256 colors.[62,210]

2. In Vivo EPR Detection of Endogenous NO

Komarov et al. first reported the in vivo real-time detection of NO in the tail of living mouse by employing the Fe−MGD trap.[199] NO production from SNP as an NO donor was monitored in the tail blood circulation as a three-line signal by using an S-band (3.5 GHz) EPR spectrometer and a loop−gap resonator with a 4 mm loop. They detected NO produced in LPS-treated mice.[236,276,277] Later, in vivo NO detection at the abdominal region of LPS-treated mice was performed by several research groups employing (1) an Fe−DETC trap with an L-band (1.14 GHz) EPR spectrometer,[247] (2) an Fe−DTCS trap with an L-band (700 MHz) EPR spectrometer,[24,278] (3) an Fe−MGD trap with an L-band (1.2 GHz) EPR spectrometer,[195,279] and an Fe−MSD trap (MSD, **10**) with an L-band (1.1 GHz) EPR spectrometer[205].

In vivo NO detection at the head region of rats was first performed in models of (i) LPS-induced sepsis and (ii) bacterial meningitis by employing the Fe−DETC trap. (i) Seven hours after the injection of LPS, the in vivo EPR (700 MHz) spectra of NO−$Fe(DETC)_2$ were obtained from the head of a living rat (Figure 6A).[243] Combined injection of LPS and IFN-γ enhanced the signal intensity (Figure 6B), and the EPR signal of NO adducts disappeared upon injection of N^G-monomethyl-L-arginine (L-NMMA), an NOS inhibitor, 30 min before NO trap injection (Figure 6C). When the brain was removed after a combined injection of LPS and IFN-γ, the EPR signal intensity from the head was greatly reduced (Figure 6D). These results clearly demonstrate that the NO−$Fe(DETC)_2$ signal observed in the head region originated from the brain tissue and from iNOS induced by both LPS and IFN-γ. (ii) In various phases during bacterial meningitis, the involvement of excessive NO synthesis has been reported.[280−286] Experimental bacterial meningitis can be induced in animals by the intraventricular inoculation of LPS/IFN-γ mixture.[281−283] Ex vivo experiments involving X-band EPR measurements showed that the NO−$Fe(DETC)_2$ signal in rat brain tissues reached a maximum in 8 h after the inoculation (Figure 7).[244]

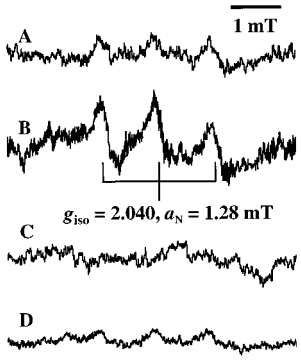

Figure 6. 700 MHz EPR spectra of the NO−$Fe(DETC)_2$ complex detected in the head regions of septic rats. In vivo EPR spectra were recorded at 7 h after the injection of 40 mg/kg of LPS (A) and 40 mg/kg of LPS plus 100×10^4 U/kg of IFN-γ (B). L-NMMA (100 mg/kg, intraperitoneally, 30 min prior to the NO trap) eliminated the NO−$Fe(DETC)_2$ signal (C). When the EPR spectrum from the head without brain, of which rat was treated in a manner similar to (B), was measured by using a 700 MHz EPR system, an NO−$Fe(DETC)_2$ signal that was rather weak in intensity was observed (D). (Reprinted with permission from ref 243. Copyright 1998 Overseas Publishers Association.)

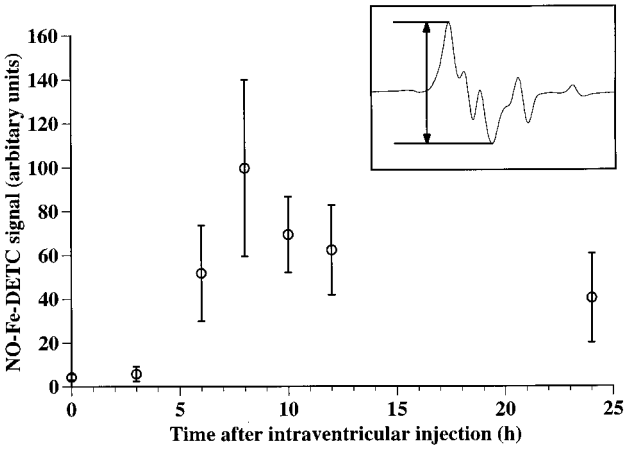

Figure 7. Sequential changes of the NO−$Fe(DETC)_2$ signal height in the rat brain tissues during experimental meningitis that was induced by the intraventricular injection of LPS plus IFN-γ X-band EPR spectra were recorded at 0, 3, 6, 8, 10, 12, and 24 h after the intraventricular injection of LPS plus IFN-γ ($n = 4$, mean ± SD). The inset shows an example of the X-band EPR spectrum of NO−$Fe(DETC)_2$ complex at liquid nitrogen temperature. (Reprinted with permission from ref 244. Copyright 1999 International Society for Cerebral Blood Flow and Metabolism.)

At that time, in vivo EPR measurements at 700 MHz were performed on the head region and a weak triplet signal was observed (Figure 8A-1). The line shape of this signal was identical to that observed in the rat's brain under sepsis (Figure 6A,B). The EPR signal of endogenous NO adducts was eliminated by pretreatment with L-NMMA (Figure 8A-2). These results showed that the in vivo EPR signal of NO adducts detected in the head of living rat originated from NOS induced by experimental meningitis. Furthermore, expression of the iNOS gene during bacterial meningitis was also verified with a

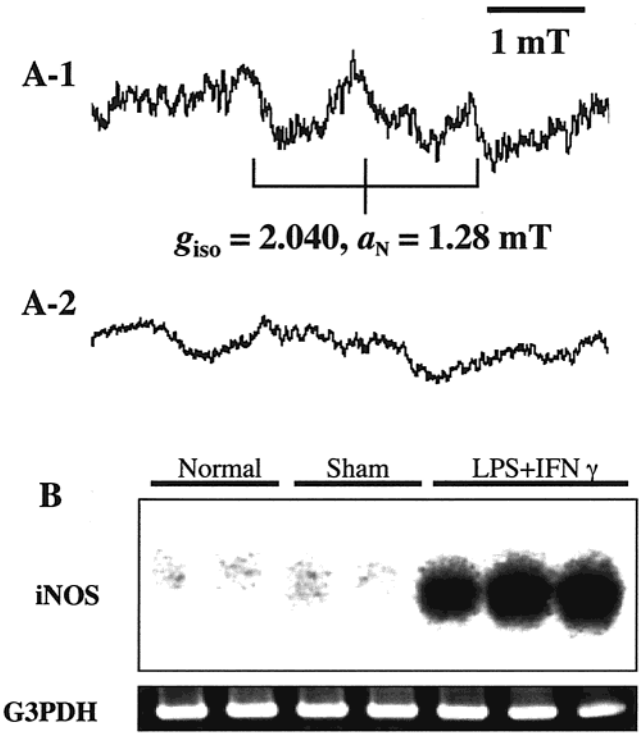

Figure 8. In vivo 700 MHz EPR spectra of the NO−Fe(DETC)$_2$ complex detected in the head region of living rat during experimental meningitis, which was induced by the intraventricular injection of LPS plus IFN-γ. (A-1) EPR spectrum recorded at 8 h after the injection of LPS plus IFN-γ. (A-2) EPR spectrum after the treatment of LPS plus IFN-γ and then of L-NMMA. (B) The RT-PCR analysis of the induction of the inducible isoform of nitric oxide synthase mRNA in the brain of the rats during experimental meningitis. (Reprinted with permission from ref 244. Copyright 1999 International Society for Cerebral Blood Flow and Metabolism.)

reverse transcriptase−polymerase chain reaction (RT-PCR) (Figure 8B). NO from the nitrovasodilator ISDN in mice has also been detected by in vivo EPR spectroscopy[196] as described in the following section.

3. In Vivo EPR Imaging of Endogenous NO

The in vivo EPR signal of NO−Fe(DTC)$_2$ in living animals showed significant intensities. Therefore, one would expect that in vivo EPR imaging of endogenously produced NO in living animals may be feasible by using the Fe−DTC traps.

First, three-dimensional EPR imaging of NO was performed in rat brain during ischemia−hypoxia. EPR images from the frozen resected brain were obtained by employing an Fe−DETC trap and an EPR imaging system with a microwave frequency of 1.2 GHz.[70,287,288] Although the observation was not in vivo, this pioneering work on EPR imaging visualized endogenously synthesized NO for the first time. To our knowledge, there have been only two studies on EPR imaging in living animals, both of which were published by our group.

To obtain in vivo EPR spectra and images from living animals, we used a home-built EPR imaging system with a 700-MHz microwave unit and a two-gap loop−gap resonator as described in section II.D.1.

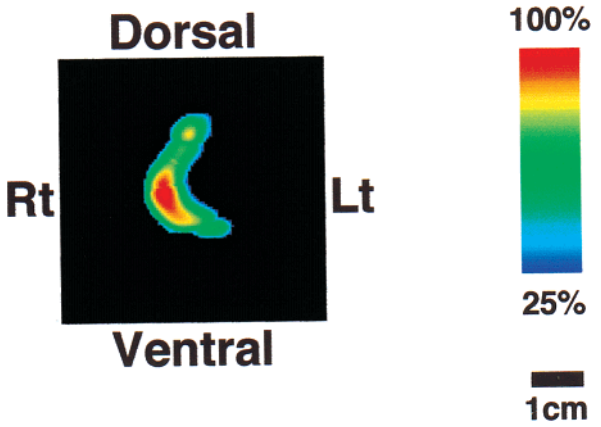

Figure 9. In vivo two-dimensional EPR projection of a cross-section of the abdominal region of an LPS-treated mouse. Signals lower than 25% of the maximum signal level in intensity were regarded as noise. The image was reproduced in 256 color levels. The spatial resolution was 6.3 mm. (Reprinted with permission from ref 24. Copyright 1999 Nature America Inc.)

The resonator was 41 mm in diameter and 10 mm in axial length, which can accommodate the head of a rat or the whole body of a mouse. We tested this system for imaging endogenous NO in living animals. We performed an imaging experiment employing NO−Fe(DTC)$_2$ complexes as a spin probe or an imaging agent to evaluate the resolution and quality of the spectral data, as described in section II.E.3.[45] We found that the NO−Fe(DTCS)$_2$ complex could be the most suitable spin probe or imaging agent among the NO−Fe(DTC)$_2$ complexes, which justifies the use of the Fe−DTCS trap as an NO imaging agent.

We conducted in vivo EPR imaging experiments of endogenously produced NO in the abdominal region in a mouse LPS-induced sepsis model mouse by using an Fe−DTCS complex as an NO trap.[24] A distinct three-line EPR signal characteristic of NO−Fe(DTCS)$_2$ was obtained from the upper abdominal region of living mice 8.5 h after LPS injection. Furthermore, the EPR signal of NO adducts disappeared in the animals preadministered with L-NMMA, an NOS inhibitor. These observations indicate that the NO adducts formed were indeed derived from NO synthesized by NOS. The two-dimensional image thus obtained showed a crescent-wise signal distribution across the right abdomen of the mouse (Figure 9), of which the outline corresponds to that of the liver.

This image was the first to show endogenously synthesized free radicals in vivo. To investigate the distribution of NO adducts in various tissues, we determined NO levels from the EPR signal intensities for different tissue homogenates from LPS-treated mice. The signal was detected in liver, kidney, whole blood, and urine but not in brain and spleen. The NO levels thus obtained are summarized in Table 1, together with the data reported by Lai and Komarov[276] and Fujii et al.[1195] All these studies show markedly high levels in liver, suggesting that the NO adducts, formed after the reaction of injected Fe−DTC complex with NO, may have been accumulated in the liver through the blood circulation.

Table 1. Distribution of NO−Fe(DTC)$_2$ Complex in Various Tissues of LPS-Treated Mice[a]

tissue	NO−Fe(MGD)$_2$ (n = 3) (Lai and Komarov, 1994)[b]	NO−Fe(DTCS)$_2$ (n = 6) (Yoshimura et al., 1996)[c]	NO−Fe(MGD)$_2$ (n = 3) (Fujii et al., 1997)[d]
liver	36.8 ± 5.4 nmol/g	96.0 ± 10.8 nmol/g	63.0 ± 10.3 nmol/g
kidney	10.9 ± 1.6	19.8 ± 1.3	11.5 ± 2.3
blood	5.4 ± 1.4	9.4 ± 1.5 nmol/ml	5.3 ± 1.4
urine		13.8 ± 2.6	9.7 ± 2.1

[a] Data are presented as a mean ± SEM. [b] From ref 276. [c] From ref 24. [d] From ref 195.

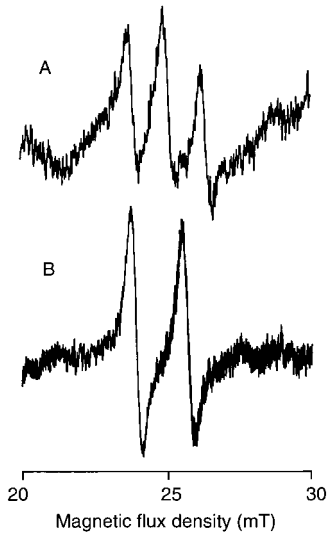

Figure 10. EPR spectra of NO−Fe(DTCS)$_2$ detected in the upper abdomen of mice treated with (a) [^{14}N]ISDN and (b) [^{15}N]ISDN, measured by a 700-MHz EPR system. (Reprinted with permission from ref 196. Copyright 1998 American Physiological Society.)

It is generally accepted that the vasodilatory effect of nitrovasodilators is mediated by the release of NO, and ISDN is well-known as a long-acting nitrovasodilator commonly used in clinical practice. NO donated from several nitrovasodilators has been detected by EPR measurements combined with the Fe−DTC-trapping method.[263−265] The second in vivo EPR imaging of NO was accomplished by the application of ISDN and the Fe−DTCS trap to a living mouse,[196] and we obtained three-dimensional images of the upper abdominal region. The in vivo EPR spectra in the upper abdomen of mice treated with [^{14}N]- or [^{15}N]ISDN were characterized by a triplet or doublet structure, respectively, which is assigned to ^{14}NO− or ^{15}NO−Fe(DTCS)$_2$ complexes (Figure 10).

The change in line shape from triplet to doublet resulted in an improvement in the S/N ratio and in the quality of the image. As is clearly shown in Figure 11, the outline of a slice image obtained with [^{14}N]-ISDN corresponds anatomically to the liver alone while that obtained with [^{15}N]ISDN corresponds to liver and kidney. In fact, the spatial resolution of the images improved from 5.7 mm ([^{14}N]ISDN) to 4.0 mm ([^{15}N]ISDN). A typical set of EPR−CT images in the $z-x$ plane of the upper abdomen of a mouse is shown in Figure 12. The ^{15}N substitution clearly provides a high-quality EPR image of NO in a living mouse. These results suggest that most NO−Fe(DTCS)$_2$ is formed in the liver and ISDN is metabolized primarily in the liver.

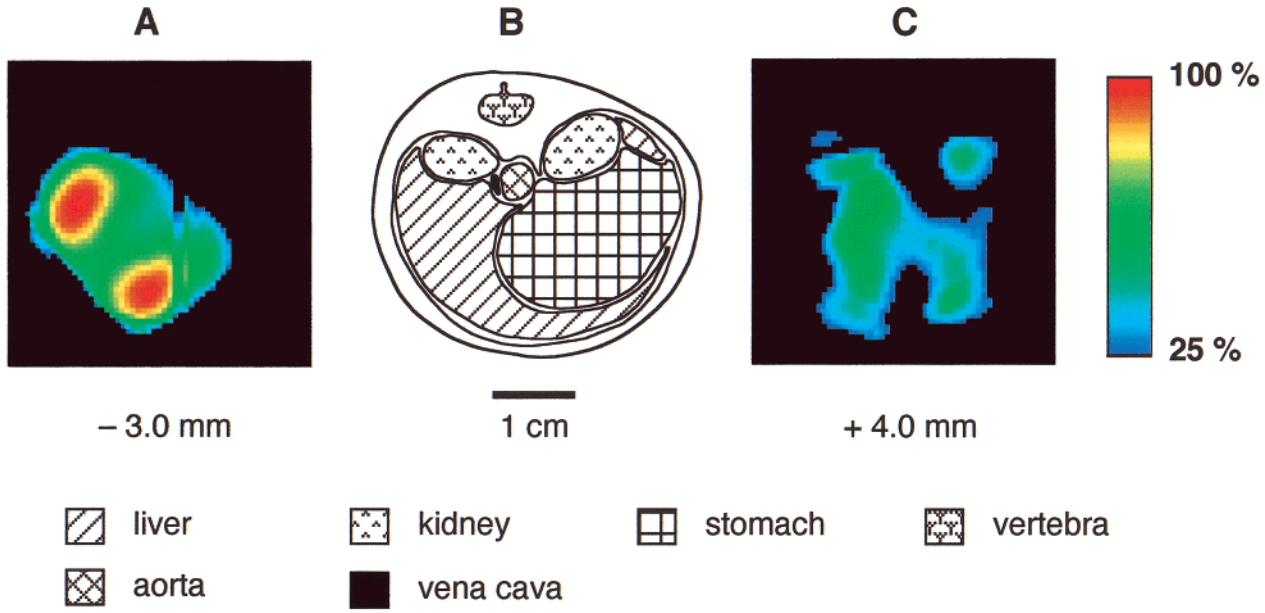

Figure 11. Typical transverse slices (thickness, 0.5 mm) of three-dimensional (3D) EPR−CT images of the ISDN-treated mice (A, C) and the illustration (B) of the upper abdominal region of mice. (A) A slice from the 3D EPR−CT images of [^{14}N]ISDN-treated mouse. (B) A schematic drawing of the cross section of the mouse upper abdomen. (C) A slice from the 3D EPR−CT images of [^{15}N]ISDN-treated mouse. The number at the bottom of A and C is the distance from the center of the loop−gap resonator in the direction of the caudal side. (Reprinted with permission from ref 196. Copyright 1998 American Physiological Society.)

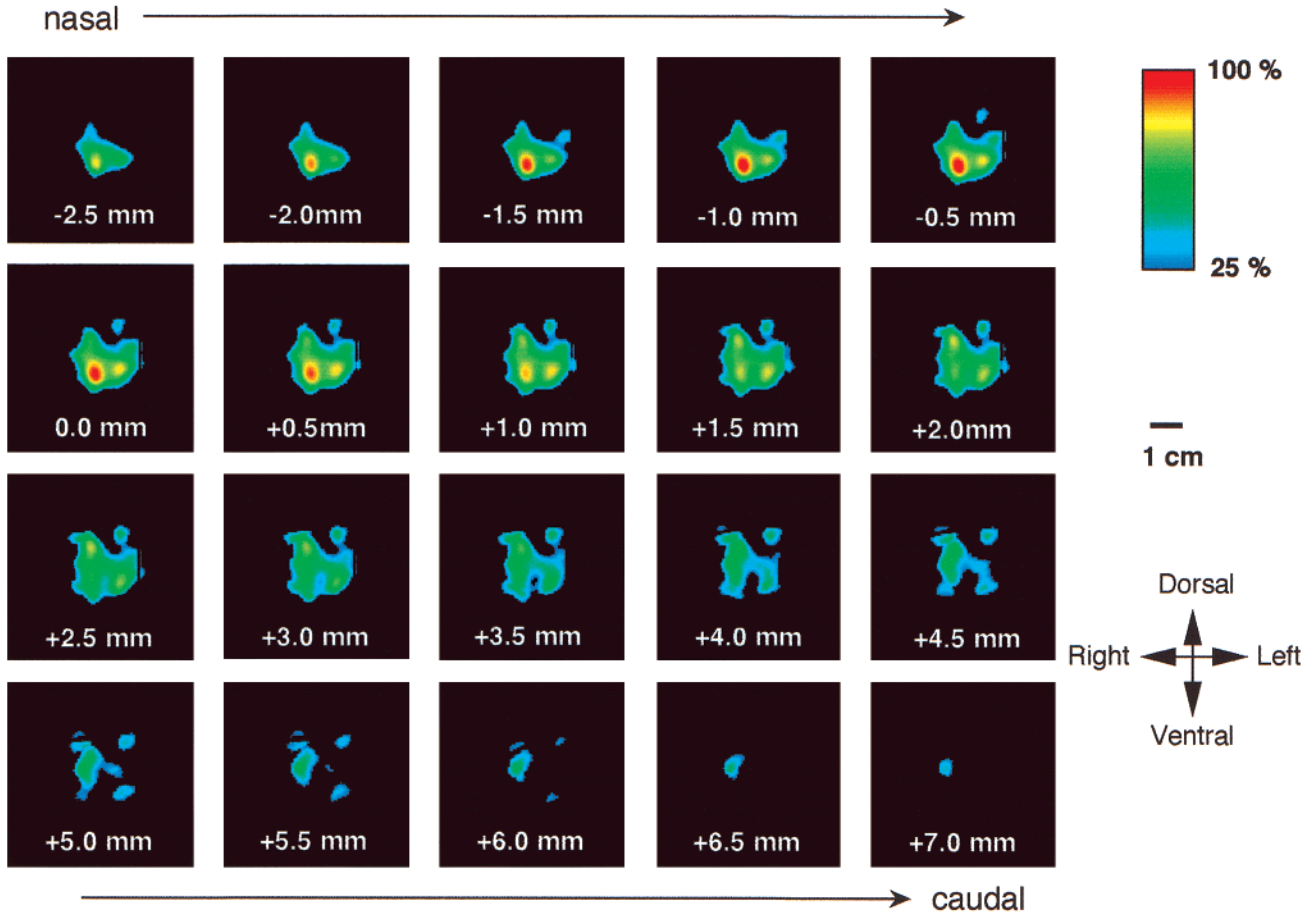

Figure 12. Typical set of EPR−CT images in the transverse plane of the upper abdomen of the mouse ca. 30 min after treatment with [^{15}N]ISDN. The thickness of each slice was 0.5 mm, and the spatial resolution was 3.95 mm. The number at the bottom of each slice image is the distance from the center of the loop−gap resonator in the direction of the caudal side. (Reprinted with permission from ref 196. Copyright 1998 American Physiological Society.)

E. EPR Detection and Imaging of Endogenous NO-Relevant Complexes

1. Nitrosylheme Complexes Produced from Infused Nitrite

It has been demonstrated by using the EPR method combined with the Fe−MGD trap that isolated hearts subjected to global ischemia generate NO by direct reduction of tissue nitrite under the acidic conditions that occur during ischemia.[191] Recently, real-time NO measurements in the whole body of mouse treated with nitrite and subjected to cardiopulmonary arrest were accomplished by using L-band (1.3 GHz) EPR spectroscopy.[289]

The in vivo EPR spectrum (Figure 13) on infusion of ^{14}N-nitrite or ^{15}N-nitrite exhibited a triplet or a doublet of which the average hyperfine coupling constants are 16.7 and 23.3 G, respectively, which agree well with those of nitrosylheme complexes.[290] These results indicate that the EPR spectrum originated from nitrosylheme complexes and that the nitrosyl group was produced from the infused nitrite. The levels were highest in lung, heart, and liver. Three-dimensional spatial mapping performed by using EPR imaging techniques also confirmed that NO formation was maximum in the lung, heart, and liver in the intact animal, revealing that mice subjected to cardiopulmonary arrest generate large amounts of NO, which is nitrite-mediated.

2. Dinitrosyl Dithiolato Iron Complex Administered as a Spin Probe

Dinitrosyl dithiolato iron complex (DNIC) is a stable, paramagnetic molecule that exhibits a characteristic EPR spectrum both in the solution state at room temperature and in the frozen state at low temperature (Figure 14).[291−294]

It is known that DNIC and nitrosothiol (RSNO) are two possible forms for stabilizing and transporting NO in biological systems.[104,295−297] The endogenous production of DNIC has been explained in terms of the binding of NO to iron−sulfur cluster-containing proteins or enzymes in mitochondria and to thiol-rich proteins in the presence of free iron.[292−294,298,299] Ex vivo and in vivo EPR spectral measurements of the abdomen of mice treated with diglutathionyl dinitrosyl iron complex, [DNIC−$(GS)_2$] **13**, showed that this complex has a relatively high affinity for the liver and kidney.[300]

In vivo real-time detection and three-dimensional imaging of DNIC−$(GS)_2$ were carried out on the abdomen of living mice by using a 700 MHz EPR system.[297] On the basis of the in vivo EPR spectra, the time course of signal intensity of the DNIC after subcutaneous injection was measured in the upper abdomen of living mice (Figure 15), The results suggested that DNIC−$(GS)_2$ is readily released into

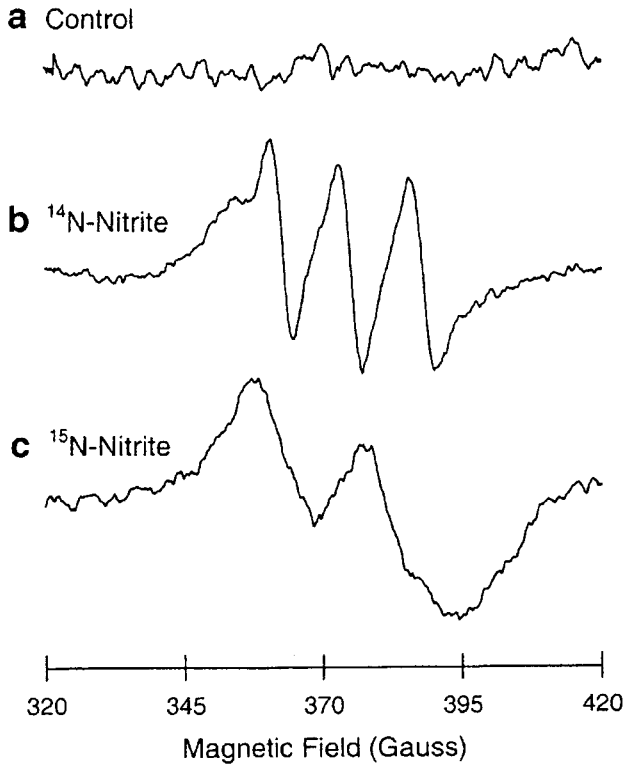

Figure 13. In vivo L-band EPR spectrum of NO measured in mice subjected to cardiopulmonary arrest. The mice were labeled (i.v.) with (a) saline, (b) 70 mg/kg (bw) of ^{14}N-nitrite, or (c) 70 mg/kg ^{15}N-nitrite and subjected to cardiopulmonary arrest with an overdose of pentobarbital 5 min later. The spectra were measured from the thoracic region of the intact animal after 120 min of cardiopulmonary arrest at ambient temperature. (Reprinted with permission from ref 289. Copyright 2001 International Society for Magnetic Resonance in Medicine.)

the circulating blood and delivered to the abdominal organs.

Figure 16 shows typical sets of EPR−CT images in the transverse plane of the upper abdomen of two living mice. The image area of the [DNIC−$(GS)_2$]-derived signal 30 min after injection (Figure 16a) was almost independent of the sites at which image slices were taken, while the high-intensity region in the images obtained 60 min after the injection (Figure 16b) gradually shifted from the nasal to the caudal direction and appeared to correspond to a specific organ, probably the liver. Accordingly, the EPR images seen in Figure 16a, b suggest that the distribution of DNIC−$(GS)_2$ shifts from the blood to organ tissues. Thus, they reflect the characteristic behavior of DNIC−$(GS)_2$ in biological systems.

3. NO–Fe(DTC)$_2$ Complexes as Spin Probes and Imaging Reagents

As described above, paramagnetic NO−Fe$(DTC)_2$ complexes are relatively stable in air and aqueous solution, suggesting that they would be applicable to in vivo EPR imaging as spin probes or imaging reagents. In vivo imaging in the rat head and in the mouse abdomen was performed after the administration of various NO−Fe$(DTC)_2$ complexes to small animals.

The rat received an intraperitoneal administration of NO−Fe$(DTCS)_2$ solution to obtain a constant

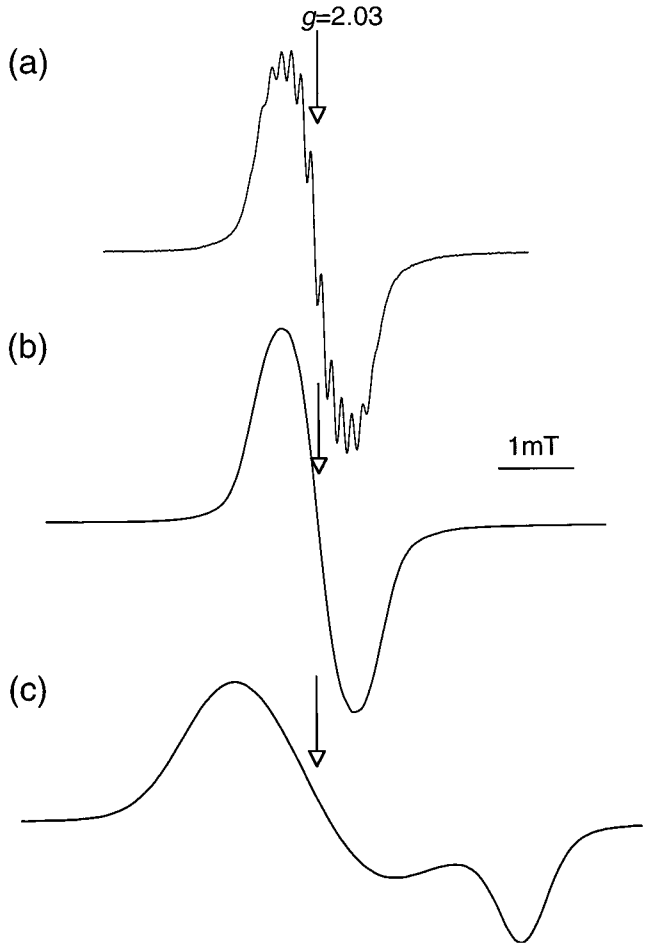

Figure 14. X-band EPR spectra of DNIC−$(GS)_2$ in HEPES buffer (15 mM, pH 7.4) at room temperature (a, b) and at 77 K (c). Instrument settings were as follows: microwave power, (a, b) 60 mW (c) 10 mW; microwave frequency, (a, b) 9.43 GHz, (c) 9.21 GHz; modulation width, (a) 0.032 mT, (b) 0.32 mT, (c) 0.63 mT at 100 kHz. (Reprinted with permission from ref 297. Copyright 1999 Pharmacological Society in Japan.)

concentration in the head.[200] The in vivo EPR spectra at the head were recorded 40 min after the injection using a 700-MHz EPR system. Figure 17 shows a two-dimensional image of the coronal section in the rat head (spatial resolution = 6.0 mm) in which the high-intensity area (ventral side) is clearly distinguished from the low-intensity area (dorsal side). The high-intensity area corresponds to the region with considerable blood circulation and/or to the extracranial tissues, while the low-intensity area corresponds to the space occupied by the rat brain. This result indicates that NO−Fe$(DTCS)_2$ scarcely passes through the blood−brain barrier.

Next, in vivo EPR detection and EPR−CT imaging in the mouse abdomen were attempted by using NO−Fe$(DTCS)_2$, NO−Fe$(MGD)_2$, and NO−Fe$(DETC)_2$ complexes as spin probes with the 700-MHz EPR system.[210] To investigate the distribution of subcutaneously (s.c.) injected spin probe complex in the mouse abdomen, the EPR signals in the resected abdominal organs were obtained. The order of signal amplitude of the complexes was NO−Fe$(DTCS)_2$ ≫ NO−Fe$(MGD)_2$, while no signals were observed in tissues of mouse given NO−Fe$(DETC)_2$. The order of intensity

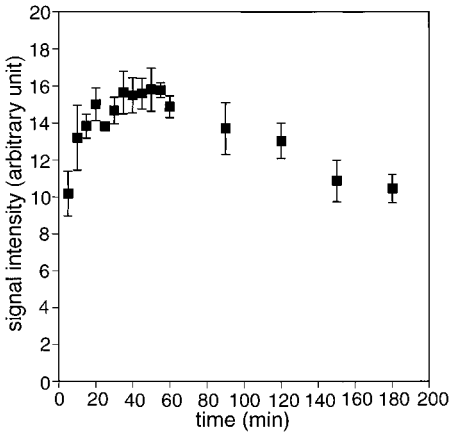

Figure 15. Time course of peak-to-peak EPR signal height detected in the upper abdomen of living mice. Each plot represents means ± SE ($n = 3$). Following the administration of DNIC−$(GS)_2$, the mice were anesthetized. Under deep anesthesia, the whole body of the mouse was held in the resonator and then spectral measurements were made every 5 min until 60 min and thereafter at 1.5, 2.0, 2.5, and 3 h by using an in vivo 700 MHz EPR spectrometer. (Reprinted with permission from ref 300. Copyright 1999 Overseas Publishers Association.)

in various organs was liver > gastrointestine ≫ blood. In vivo EPR signals were observed in the upper abdomen of living mice 40 min after s.c. administration of the spin probe complex.

NO−$Fe(DTCS)_2$ gave a high-intensity signal, while the signals of NO−$Fe(MGD)_2$ and NO−$Fe(DETC)_2$ were quite low in amplitude (the spectrum of Figure 18A was obtained with an average of 2 accumulations of 1 s scan, and those of Figure 18B,C, with an average of 64 accumulations). EPR−CT images similar to Figure 12 were reconstructed from the spectral data obtained from rats injected with NO−$Fe(DTCS)_2$, but reconstruction was not possible in the experiments with NO−$Fe(MGD)_2$ or NO−$Fe(DETC)_2$ because the spectral data had much lower S/N ratios. The high-intensity area in the EPR−CT image corresponded to the liver. These results suggest that NO−$Fe(DTCS)_2$ complex may be the most suitable spin probe or imaging agent among the NO−$Fe(DTC)_2$ complexes. Images (spatial resolution, 3.6 mm) obtained with the injection of NO−$Fe(DTCS)_2$ had low resolution compared with that obtained with nitroxide radical (about 2.3 mm).[45] However, NO−$Fe(DTCS)_2$ as a spin probe has the advantage of high chemical stability, as opposed to nitroxide, which readily loses paramagnetism in the presence of reductants.[301−303]

F. Approaches to NO Evaluation by Magnetic Resonance Imaging (MRI) Techniques

Recently, attempts have been made to overcome the limitations of EPR-based imaging in the resolution of image and the sample size by employing nuclear magnetic resonance (NMR) techniques. The proton−electron-double-resonance-imaging (PEDRI) technique is based on the enhancement of proton NMR signal intensity in the presence of radicals through the Overhauser effect.[304,305] Rat liver exposed to SNP as an NO donor exhibited intense PEDRI images,[305] suggesting that PEDRI is a potential tool for the study of NO in large biological specimens.

Several paramagnetic metal complexes have been widely used as contrast agents in magnetic resonance

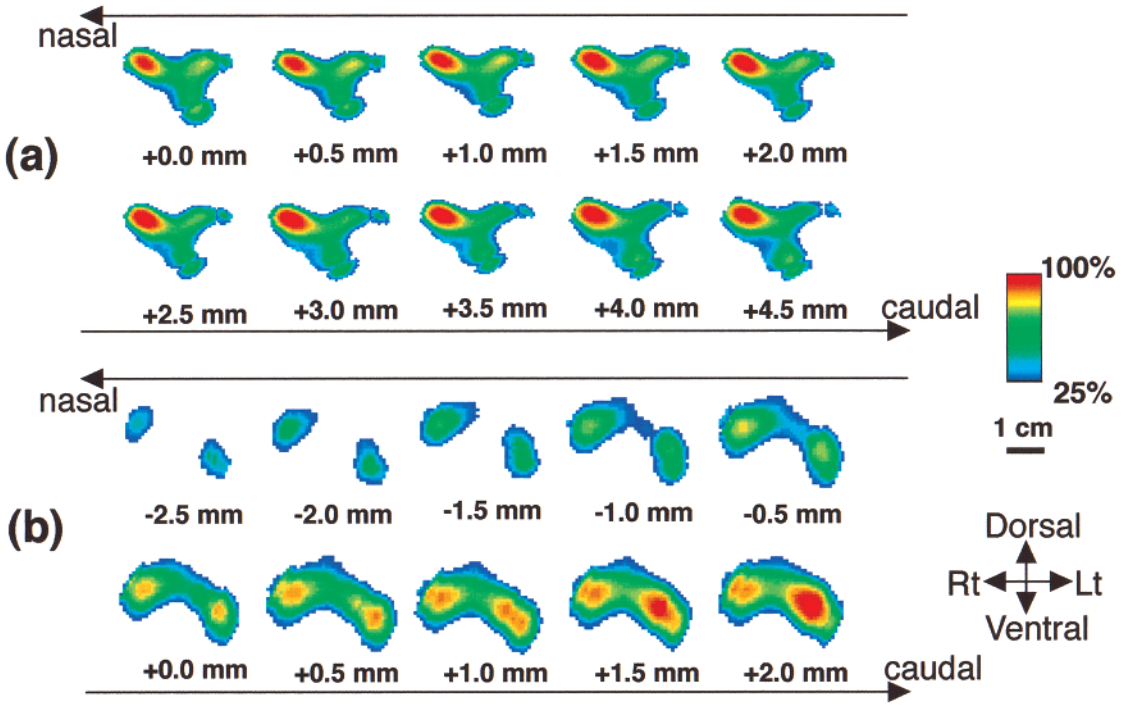

Figure 16. Typical sets of EPR−CT images of the transverse plane in the upper abdomen of living mice 30 (a) and 60 min (b) after DNIC−$(GS)_2$ injection. The mice were treated in a manner similar to that described in Figure 15. The images were reproduced in 32 colors. The thickness of each slice was 0.5 mm, and the spatial resolutions were 6.1 and 6.6 mm (a and b, respectively). The number at the bottom of each slice image is the distance from the center of the loop−gap resonator in the direction of the caudal side. (Reprinted with permission from ref 297. Copyright 1999 Pharmacological Society in Japan.)

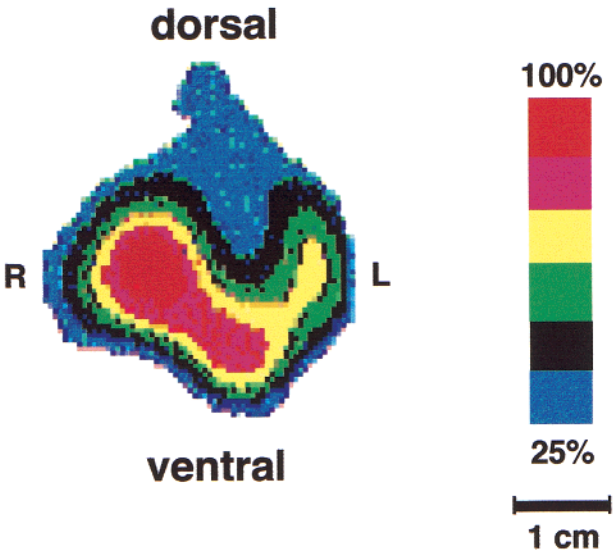

Figure 17. Two-dimensional EPR image of the coronal section in living rat head, obtained by EPR measurements at a frequency of about 700 MHz. The rat head was held in the loop−gap resonator under pentobarbital anesthesia. The rat received an intraperitoneal administration of 6 mL of the NO−Fe(DTCS)$_2$ solution to obtain a constant concentration in the head for 40 min. The spatial resolution was 6.0 mm. (Reprinted with permission from ref 200. Copyright 1995 Chemical Society of Japan.)

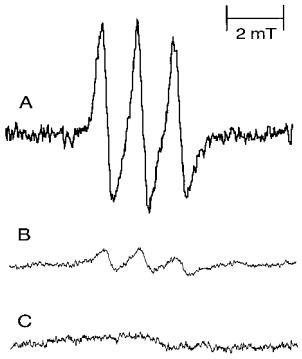

Figure 18. Representative EPR spectra in the upper abdomen of living mice 40 min after subcutaneous injection of NO−Fe(DTC)$_2$ complexes, NO−Fe(DTCS)$_2$ (A), NO−Fe(MGD)$_2$ (B), and NO−Fe(DETC)$_2$ (C), obtained by the measurements at a frequency of about 700 MHz. Accumulation number, 2 (A) or 64 (B and C). (Reprinted with permission from ref 210. Copyright 1997 Elsevier Science Inc.)

imaging (MRI) due to their ability to enhance the relaxation of neighboring protons.[306,307] Paramagnetic NO−Fe−DTC complex has been utilized to visualize NO generated in living rats with septic shock;[308] in addition, a paramagnetic nitrosyl iron complex showed contrast properties to enhance the signal intensity of SNP-perfused rat liver in MRI.[309] Thus, a paramagnetic nitrosyl iron complex may be potentially useful as a functional MRI contrast agent specific for NO in living organisms.

The effect of NO exposure to hemoglobin during MRI signal recording was explored with in vitro MRI and in vivo functional MRI (fMRI) experiments.[310] In an in vitro experiment, the MRI signal intensity of venous blood in T1-, T2-, and T2*-weighted images, in most cases, increased after the addition of aqueous NO solution, nitrite, or dithionite and nitrite to the blood while it decreased on the addition of ascorbic acid. These results seem to indicate that the transient formation of two paramagnetic species, i.e., met Hb and NO−Hb, enhances the signal intensity, while a decrease in met Hb by ascorbate reduces it. In an in vivo fMRI experiment on healthy volunteers, intravenous administration of ascorbic acid (3 g) decreased fMRI signal changes during standard tasks, suggesting a blood flow-independent effect produced by reductant.

By employing MRI techniques, the infusion of NO precursor, L-arginine, was found to increase the cerebral blood volume in nonischemic spontaneously hypertensive rats[311] and the administration of an NO donor, ISDN, increased both tumor blood flow and partial oxygen pressure in mice implanted with liver tumor in the thigh.[312]

These findings open a new perspective on the bioimaging of NO and the in vivo elucidation of NO effects by magnetic resonance techniques.

III. Fluorometric Imaging of NO

A. Development of Fluorescent Probes for NO

1. Diaminonaphthalene: DAN

NO readily decomposes to NO_2^- as a final product in the presence of O_2. Although NO_2^- is the only stable nitrogen oxide formed following decomposition in aqueous solutions in vitro, NO_3^- is found predominantly in extracellular fluids such as plasma or urine.

Griess assay is a well-known colorimetric detection method of NO_2^-. The determination of NO_2^- by use of the Griess reaction is based on a two-step diazotization reaction. Under acidic reaction conditions, NO_2^- produces a nitrosating agent which reacts with sulfanilic acid to produce the diazonium ion. This ion is then coupled to *N*-(1-naphthyl)ethylenediamine to form a chromophoric azo derivative. The Griess assay is useful for estimating total NO production, but it is not very sensitive and cannot give real-time information.

Generally, fluorometric detection is more sensitive than colorimetric detection. To enhance the sensitivity of measuring NO_2^-, Misco et al.[313] developed a rapid and sensitive fluorometric assay for quantification of NO_2^-/NO_3^-, based upon the reaction of NO_2^- with 2,3-diaminonaphthalene (DAN) to form the fluorescent product 1-(*H*)-naphthotriazole (NAT) (Scheme 2).

Scheme 2. Reaction of NO_2^- with DAN To Form NAT under Acidic Conditions

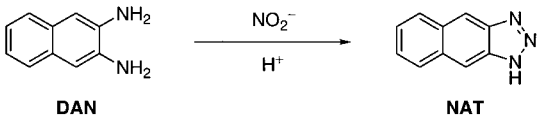

DAN NAT

The fluorescence intensity of NAT is at least 90- to 100-fold higher than that observed for an equimolar concentration of DAN when the solution is excited at 375 nm and emission is monitored at the emission maximum for NAT of 415 nm. The detection limit is

Scheme 3. Reaction of NO with DCFH To Form Dichlorofluorescein

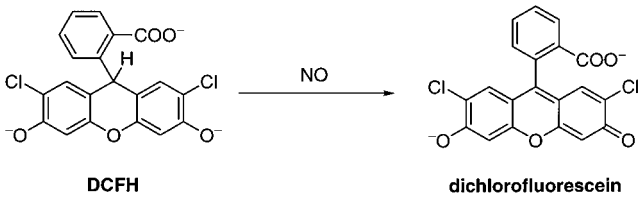

DCFH dichlorofluorescein

10 nM, which is 50−100 times more sensitive than the Griess assay. The *N*-nitrosation of DAN offers the additional advantages of specificity, sensitivity, and versatility. The assay is also adaptable to a 96-well plate format, facilitating the handling of a large number of samples including conditioned media from cell culture or NO_2^- generated by a purified enzyme.

This fluorometric determination for NO_2^- is useful in the detection and quantification of NO_2^- in biological systems. NO generated in vivo is converted into NO_2^-/NO_3^-, nitrosyl hemoproteins, nitrosylmetal complexes, and *S*-nitroso compounds in the circulation. The assay method developed by Sonoda et al.[314] involves the thermolysis of all NO-related compounds in whole blood and the detection of the resulting NO_2^- by fluorometry after enzymatic reduction. *S*-Nitroso-albumin and NO−Hb can be easily thermolyzed to NO_3^-, and relatively stable *S*-nitrosoglutathione is also degraded to NO_3^- in the presence of blood constituents with high molecular mass. After NO_3^- was reduced to NO_2^-, concentrations of NO-related compounds in blood from healthy human as well as control or LPS-stimulated rats were determined. Furthermore, they reported that the method can detect quantitatively the fraction of NO diffused and metabolized within red cells and other NO metabolites in plasma, such as NO_2^-/NO_3^- and *S*-nitroso compounds, both of which reflect NO production in vivo.[314] The method can serve as a tool for defining the role of NOS in both normal and pathophysiological processes.

However, the method cannot be adapted for NO bioimaging because of the reaction under acidic conditions, and in addition, irradiation at the excitation wavelength of 375 nm often does serious damage to living cells. Thus, reaction under neutral conditions and a longer excitation wavelength are required for NO imaging.

2. Dichlorofluorescin: DCFH

Gunasekar et al.[315] used 2,7-dichlorofluorescin (DCFH) for monitoring intracellular NO formed in neuronal cells (Scheme 3).

In a cell-free system DCFH, a nonfluorescent species, is oxidized by NO to dichlorofluorescein, a fluorescent compound. Addition of NO to a solution containing DCFH increases the fluorescent signal within 10 s, and the intensity continues to increase slowly over a 10-min period. The limit of detection is 16 μM NO. Imrich and Kobzik[316] used DCFH as a probe for quantitation of iNOS activity in activated rat lung macrophages.

The method has very low specificity for NO, because DCFH can be converted to dichlorofluorescein by various ROS as well as by autoxidation. The addition of SOD, catalase, and/or other inhibitors is required to measure formation of NO, so this approach is not readily applicable to biological systems.

Scheme 4. Reaction of NO with Fe(II) Complex of Quinoline Pendant Cyclam

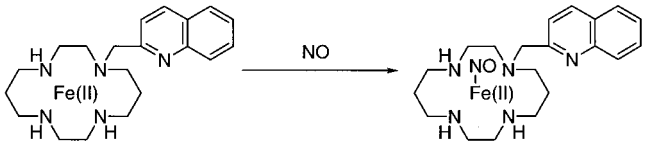

3. Iron Complexes

The iron(II) complex of quinoline pendant cyclam was designed as a mimic of the activation site of guanylate cyclase and synthesized as a fluorescent probe for NO.[317] The iron(II) complex shows fluorescence emission at 460 nm, which is quenched effectively by NO from NO-releasing agents (Scheme 4). The detection limit is poor (micromolar order), and the nature of the spectral change is not convenient for NO detection in biological systems.

Maeda et al.[318] developed a novel fluorescent probe using a new spin exchange concept. The fluorescent probe is composed of 2,2,6,6-tetramethylpiperidine-*N*-oxyl (TEMPO) labeled with acridine and Fe(II)-$(DTCS)_2$ complex. The addition of an NO-releasing reagent causes a decrease of the probe's fluorescence due to the irreversible binding of NO to the Fe(II). Using this probe, less than 100 μM NO can be detected, and the probe can be used for monitoring direct production of NO in an aqueous solution (Scheme 5). The complex has not yet been applied for bioimaging.

4. Heme Domain with Fluorescent Reporter Dye

Kopelman et al.[152,154] developed ratiometric and lifetime-based sensors which incorporate cytochrome *c′* labeled with a fluorescent reporter dye. The dye-labeled cytochrome *c′* is attached to an optical fiber via colloidal gold, along with fluorescent microspheres as intensity standards. The ratiometric sensor is completely reversible and selective over common interferents such as NO_2^-, NO_3^-, and oxygen species. Microscopic adaptation of the lifetime-based method allows direct correlation of intracellular NO levels with specific cellular activities, such as phagocytosis. The use of these two techniques allows measurement of intra- and extracellular macrophage NO.

Prior to this report, Barker and Kopelman[153] developed an NO-selective fiberoptic sensor composed of a fluorescein derivative dye attached directly to colloidal gold. The fluorescein dye rearranges as NO is adsorbed onto the gold, inducing a decrease in the fluorescence intensity of the dye. The sensor was utilized to measure NO production by BALB/c mouse macrophages.

In addition, Kopelman et al.[319] recently reported NO-selective sensors with the heme domain of soluble guanylate cyclase (sGC). The heme domain of the sGC is labeled with a fluorescent reporter dye, and changes in the dye's fluorescence intensity are ob-

Scheme 5. Reaction of NO with the Fluorescent Probe Which Is Composed of TMPO Labeled with Acridine and Fe(II)DTCS Complex

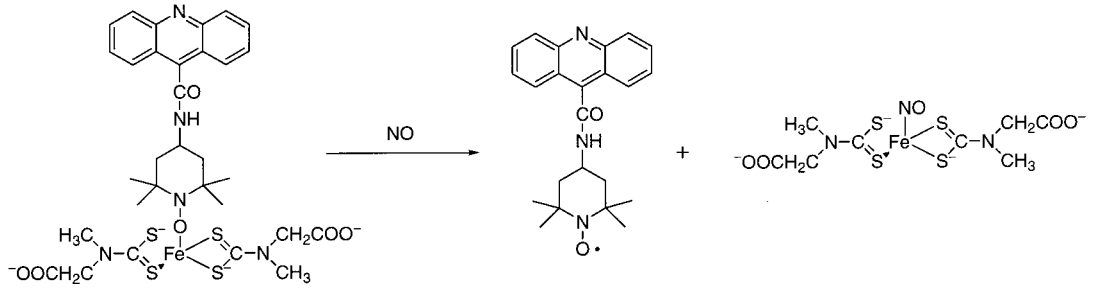

Scheme 6. Reaction of NO with Co(DATI-4) Complex To Form $Co(NO)_2$(DATI-4) Complex

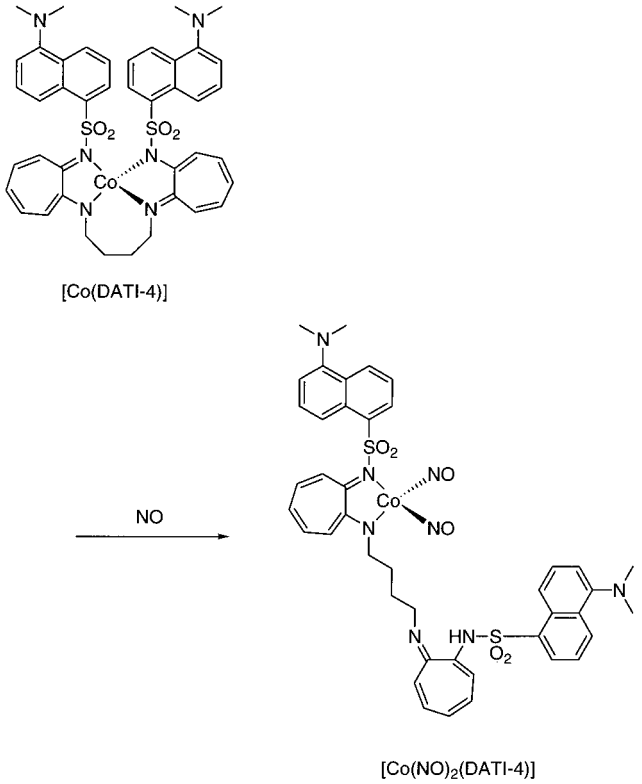

Scheme 7. Reaction of NO with FNOCT

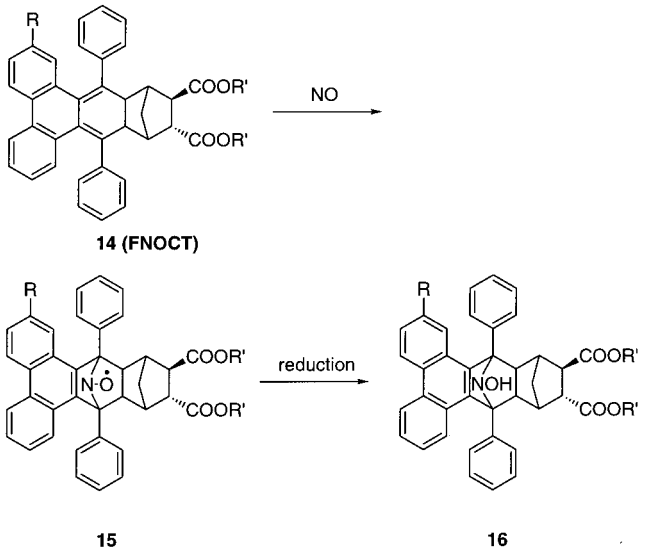

served based on the sGC heme domain's characteristic binding of NO. These sensors have fast, linear, and reversible responses to NO and are unaffected by O_2, NO_2^-, and NO_3^-.

It may be difficult to apply these methods for measurement of NO formation from NOS in endothelial cells because the limit of detection is only 8 μM NO and the lifetime-based measurements have a limit of detection of 30 μM NO.

5. Co Complex: [$Co(NO)_2$(^{R}DATI)]

A unique strategy for fluorescent NO sensing has been reported by Lippard et al.[320,321] (Scheme 6).

They prepared a family of new fluorescently labeled ligands (H^RDATI) to develop transition-metal-based NO-sensing strategies. The ligands are composed of aminotroponiminates (ATIs) with a dansyl fluorophore on one of the imine nitrogen atoms and an alkyl substituent on the other. When excited at 350 nm, the H^RDATI ligands and the diamagnetic Zn^{2+} complex fluoresce around 500 nm whereas the paramagnetic Co^{2+} complexes quench the fluorescence. The air-stable cobalt compounds react with NO to dissociate a DATI ligand and form neutral dinitrosyl complexes, [$Co(NO)_2$(^{R}DATI))]. The release of the fluorophore-containing ligand is accompanied by an increase in fluorescence intensity, thus providing a strategy for fluorescent NO sensing. This system does not exhibit reversible NO binding and has not been applied to biological systems, although the design idea provides the possibility of creating desirable sensors in the future.

6. Cheletropic Traps: FNOCTs

Sustmann et al. extended the concept of NOCT, which relies on ESR spectroscopic detection,[112,114−118] to FNOCT, incorporating a fluorophoric system (Scheme 7).

The procedure makes use of the fact that FNOCTs (**14**) react with NO in a formal cheletropic reaction to give bridged nitroxide radicals (**15**), which are required to be reduced to the corresponding hydroxylamines (**16**) as shown in Scheme 7. They reported that these nitroxides are immediately reduced under cellular conditions to the hydroxylamine derivatives (**16**), thereby generating a phenanthrene-type fluorophore.

Using the acetoxymethylesters of two FNOCTs, which can be loaded into cells, NO formed by LPS-activated alveolar macrophages can easily be detected at the single-cell level. The applicability of the trap

Scheme 8. Schematic Representation of DAN-1 EE Loading Mechanism in the Cell

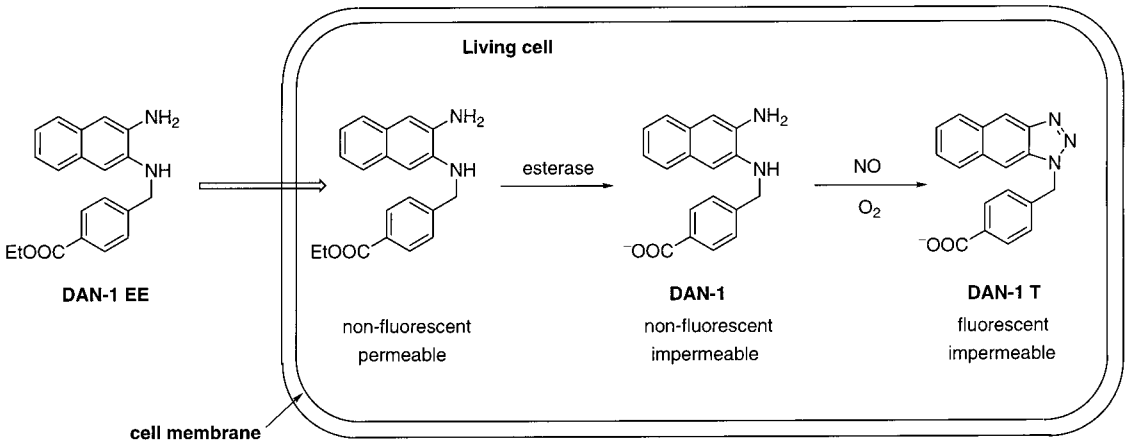

for NO detection in single, viable cells was demonstrated by the use of isolated rat alveolar macrophages. FNOCTs are nontoxic at the final concentration used. The intracellular trap can respond in the same way as in the chemical system to endogenously produced NO, while no signal was observed in unstimulated cells or in the presence of an inhibitor of cellular NO formation. Using digital fluorescence microscopy, the signal could be detected at the single-cell level, underlining the sensitivity of the method. The method is likely to be useful for studying a broad range of NO-related questions in cellular systems.

B. Development of NO Bioimaging Probes

1. Diaminofluoresceins: DAFs

In attempts to measure NO generated under physiological conditions, Nagano et al. developed a fluorometric method that exploits the ability of NO to produce *N*-nitrosating agents.[322,323] The method is based on the use of an aromatic diamino compound, DAN. The relatively nonfluorescent DAN reacts rapidly with *N*-nitrosating agent(s) to yield the highly fluorescent product (NAT), as shown in Scheme 2.

First, the key reaction of selective NO trapping was established.[324] As a result, DANs were found to react with NO to yield NATs in the presence of O_2 *under a neutral condition*. Until then, DAN had been considered as a reagent for the detection of NO_2^- under acidic conditions. However, the results obtained mean that the reaction of NO with DAN aerobically produces the fluorescent compound NAT quantitatively in an aqueous medium, *even under physiological conditions*. In fact, the fluorescence intensity increases dose-dependently on addition of NO to the DAN solution. One of the possible reaction species is nitrous anhydride (N_2O_3), which is formed as an intermediate in the autoxidation of NO to produce NO_2^-.[325,326] Under these reaction conditions, NO_2^- and NO_3^- cannot convert DAN into NAT. Therefore, the selectivity for NO of this principle is high, and it is possible to detect NO without the inhibition of its biological function because DAN does not react *directly* with NO.

However, it is impossible to use DAN itself as a probe for the imaging of NO because DAN leaks easily through cell membranes after loading. Thus, an ester group was introduced into DAN to yield DAN-1 EE, which can be transformed into DAN-1 with lower membrane permeability by esterase in the cytosol after the dye permeates through the cell membrane (Scheme 8).

The new probe DAN-1 EE was applied for NO detection in activated rat aortic smooth muscle cells, and the fluorescence intensity in activated cells increased with NO production. The increase was depressed by an inhibitor of NOS, L-NMMA. These results show that DAN-1 EE enables the bioimaging of NO.

However, the use of DAN as a detection probe for NO under neutral conditions, presents some problems such as cytotoxicity and strong autofluorescence owing to the requirement for UV excitation, the small extinction coefficient, and the poor solubility in neutral buffer.

Therefore, new fluorescent indicators were synthesized to detect NO in living cells as a means to examine the physiological functions of NO. Fluorescein is widely used in biology as a fluorophore because of its convenient excitation and emission wavelengths for biological measurement, high extinction coefficient, and high fluorescence quantum yield in water.

Diaminofluoresceins (DAFs) were therefore designed as novel probes for NO. Conversion of DAFs to the corresponding triazole forms (DAF-Ts) by reaction with NO caused little change of the absorbance maxima but greatly increased the quantum efficiency. DAFs possess favorable properties for cellular imaging applications; in particular, they have a visible excitation wavelength, which is less damaging to cells and is not subject to interference from the autofluorescence of biological samples. The increase of fluorescence intensity is dependent on the concentration of NO. Scheme 9 shows the conversion of DAF-2 to DAF-2 T by NO in the presence of O_2.[25,327,328]

The detection limit of NO by DAF-2 is 5 nM. The fluorescence of fluorescein with two phenolic OH groups is almost completely quenched by protonation. DAFs exhibit similar properties. The fluorescence of DAF-2 T strikingly decreases below pH 7. That is, DAF-2 is useful in media above pH 7. DAF-4 and

Scheme 9. Reaction of NO with DAF-2 To Form DAF-2 T

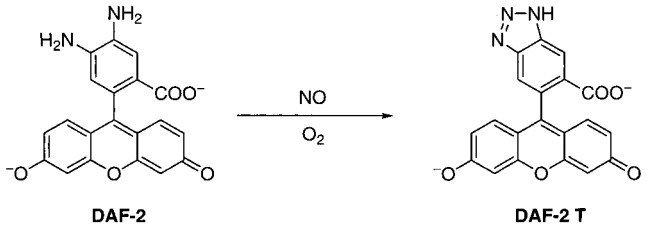

DAF-5 with the electron-withdrawing chlorine substituent were synthesized in order to lower the pK_a value, with the aim of obtaining a stable fluorescence intensity at physiological pH (Scheme 10).

The excitation and emission wavelengths of DAF-4 and DAF-5 with a chlorine atom adjacent to phenolic OH are shifted to longer wavelengths than that of DAF-2. Although the electron-withdrawing effect of the chlorine atom does lower the pK_a values of DAF-Ts, there is a reduction of their fluorescence intensity from pH 7 to 9, probably due to deprotonation of the triazole moiety.

The protonation of phenolic OH significantly reduces the fluorescence intensity because of the blue shift of the absorption wavelength owing to hindrance of electron delocalization, whereas deprotonation of the triazole ring slightly decreases the intensity because of the small electron donation to the conjugated double bonds. As a result, the chlorine substitution, lowering the pK_a value of phenolic OH, induced unstable fluorescence intensity around physiological pH.

In applications to various biological systems, the pH dependency of the fluorescence intensity of DAF-Ts can make it difficult to monitor small changes of intracellular NO level after a stimulus that shifts the intracellular pH. For example, it is reported that stimulation with bradykinin lowers the pH in vascular endothelial cells to 6.5. The instability of the fluorescence intensity was considered to arise from the triazole proton, so a methyl group was introduced (DAF-4 M1, 4 M2, 5 M1 and 5 M2; Scheme 10).

The sensitivities of these new probes to NO were examined in detail, and DAF-4 M2 was found to be the most sensitive to NO. The fluorescence intensity of the triazole form of DAF-4 M2 is stable at above pH 5.8.

On the other hand, fluorinated fluorescein derivatives are reported to be more resistant to photobleaching than fluorescein and can be efficiently excited with the 488 nm spectral line of the argon-ion laser used in confocal laser scanning microscopes.[329] Therefore, the chlorine atom was replaced with a fluorine atom. This new indicator was named DAF−FM (Scheme 10). Examination of the photobleaching in sunlight showed that the triazole form of DAF−FM (DAF−FM T) is more stable than DAF-2 T and DAF-4 T. The fluorescence intensity is stable above pH 5.8. The sensitivity of DAF−FM is 1.4 times higher than that of DAF-2. This increase of sensitivity is thought to result from the higher rate of the reaction with NO^+ equivalents due to the electron-donating effect of the methyl group.

Scheme 10. Pathway To Development of DAF−FM

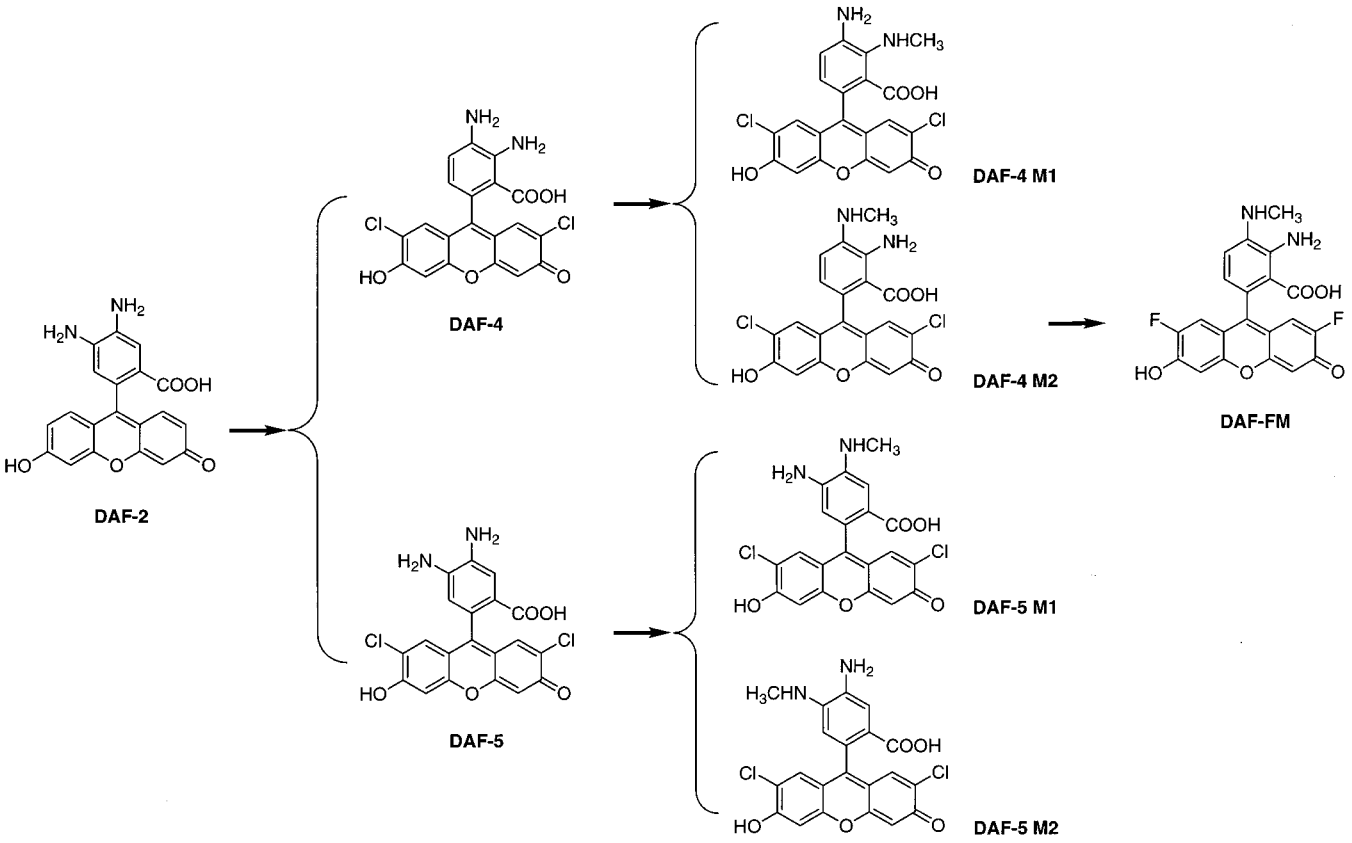

Scheme 11. Pathway To Development of DAR-4M AM

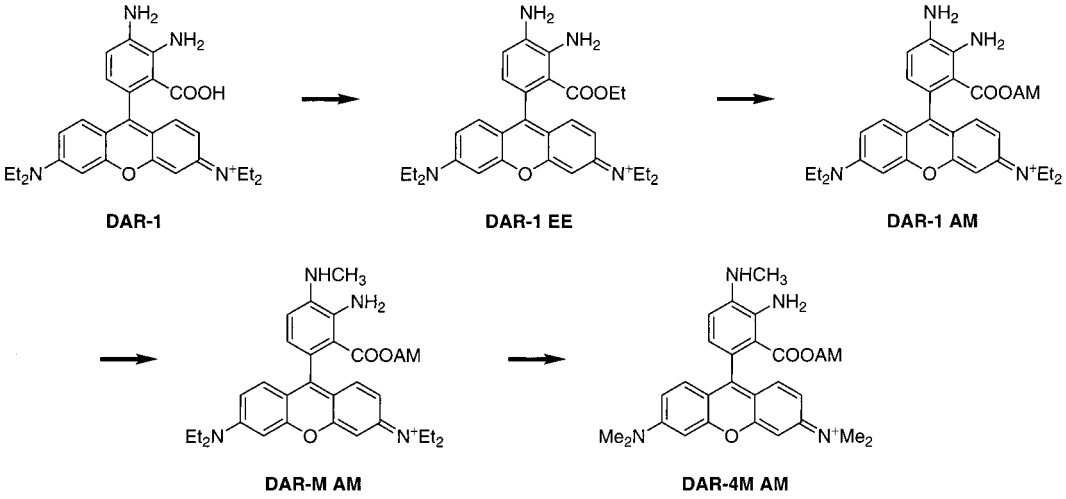

2. Diaminorhodamines: DARs

Although the practical usefulness of DAFs for functional studies of NO was confirmed, DAFs lack some desirable characteristics of NO indicators. To obtain higher photostability, longer excitation wavelength, and applicability over a wider pH range, we examined the suitability of rhodamine as the fluorophore.

DARs were designed, based on the highly fluorescent Rhodamine B fluorophore (Scheme 11), and synthesized from phthalic anhydride derivatives and *N*,*N*-diethyl-3-aminophenol.[330,331]

The reaction of DARs and NO affords the corresponding fluorescent triazole, as in the case of DAFs. To image NO in living cells, DARs should be membrane-permeable. Therefore, an ethyl group was introduced into the carboxyl group of DAR-1, anticipating that the ethyl ester, DAR-1 EE, would be hydrolyzed by cytosolic esterases after permeation through the cell membrane. As expected, when this probe was applied to imaging of NO produced by activated rat aortic smooth muscle cells, there was almost no autofluorescence of the cells, due to the longer wavelength excitation. Although the NO imaging with DAR-1 EE was successful, a difficulty in loading was encountered. It took a longer time to obtain a stable fluorescence intensity in the cells than in the case of DAF derivatives. This presumably occurred because the ethyl ester, which was attached to a bulky acid, was not readily hydrolyzed. DAR-1 EE remaining in the cytosol might be distributed to the fatty membrane in cells, and fluorescent rhodamines generally show higher fluorescence intensity in organic solvents, such as ethanol, than in water. Therefore, the hydrolysis of DAR-1 EE was examined with rat brain homogenate as an esterase preparation by means of HPLC. During a 30-min incubation, DAR-1 EE was not hydrolyzed at all. Most of the loaded DAR-1 EE was probably localized on membranes in the smooth muscle cells, in unhydrolyzed form.

Thus, the acetoxymethyl ester of DAR-1 was synthesized (DAR-1 AM; Scheme 11) because acetoxymethyl esters were reported to be easily hydrolyzed by intracellular esterases.[332] Twenty seven percent of DAR-1 AM was hydrolyzed in 30 min by rat brain homogenate. This suggests that DAR-1 AM would be useful for NO imaging in living systems. However, the triazole proton of DAR-1 T affected the fluorescence due to its pK_a value, 6.69. Therefore, a methyl group was introduced into DAR-1, as had been done in the development of DAF. The fluorescence intensity of the triazole form of DAR-M was stable above pH 4, while that of DAR-1 T was unstable at around pH 7.

For bioimaging applications, an acetoxymethyl ester was introduced into DAR-M. DAR-M AM (Scheme 11) was applied to NO imaging in bovine aortic endothelial cells. However, the difficulty in loading was hardly improved, compared to DAR-1 EE. This might be because DAR-M AM, which has four ethyl groups, is too hydrophobic to be stably distributed to the cytosol. Therefore, the fluorophore was changed to tetramethylrhodamine, and we then examined the suitability of DAR-4M AM for bioimaging (Scheme 11). The quantum efficiency of DAR-4M T is the highest of all DARs examined. Judging from NO standard curves calibrated with the indicators, the sensitivity of DAR-4M to NO is twice that of DAR-1. The detection limit of NO by DAR-4M was 7 nM. DAR-4M should offer a good signal-to-noise ratio in the examination of biological samples because of the low background fluorescence with the longer wavelength excitation, even though the quantum yield of DAR-4M T is lower than that of fluorescein probes. Moreover, DAR-4M permitted NO detection above pH 4, while DAF−FM, a fluorescein probe, can only be applied above pH 5.8.[333] When using DAFs, which have weak fluorescence, it is sometimes difficult to tell whether the cells are loaded with the dye because the autofluorescence of cells overlaps the fluorescence of DAFs. On the other hand, the cells loaded with DAR-4M could be easily distinguished because the unloaded cells had almost no fluorescence. Moreover, DARs are more photostable than DAFs.

3. Emission Mechanism

Although DAFs are fluorescein derivatives, DAFs themselves scarcely fluoresce while DAF-Ts are

Scheme 12. Frontier Orbital Energy Diagram: Illustration of the Thermodynamic Situation of the Fluorescence OFF/ON Switch Including the PET Process

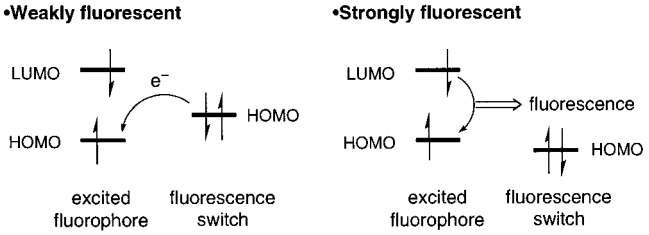

Scheme 13[a]

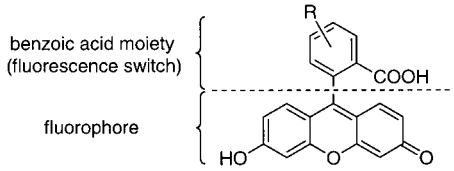

[a] The fluorescein structure was divided into two parts, the fluorescence switch and the fluorophore.

strongly fluorescent. However, the mechanisms accounting for the diminution of fluorescence in DAFs and its enhancement in DAF-Ts remain unclear. In principle, the fluorescence properties of fluorescein derivatives are controlled by the photoinduced electron transfer (PET) process from the benzoic acid moiety to the fluorophore, the xanthene ring (Scheme 12).

PET is a widely accepted mechanism for fluorescence quenching in which electron transfer from the PET donor to the excited fluorophore diminishes the fluorescence of the fluorophore. It is appropriate to divide the fluorescein structure into two parts, i.e., the benzoic acid moiety as the PET donor and the xanthene ring as the fluorophore (Scheme 13) because only small alterations in absorbance were observed among fluorescein and its derivatives and the dihedral angle between the benzoic acid moiety and the xanthene ring is almost 90°, as found by X-ray analysis,[334] which suggests there is little ground-state interaction between these two parts.

If the HOMO energy level of the benzoic acid moiety is high enough for electron transfer to the excited xanthene ring, the ϕ value will be small. In other words, fluorescein derivatives with a high ϕ value must have benzoic moieties with low HOMO energy levels. The HOMO energy levels of 3-aminobenzoic acid, 3-benzamidobenzoic acid, 3,4-diaminobenzenecarboxylic acid (DAB−COOH), and benzotriazole-5-carboxylic acid (BT-COOH), which are the benzoic moieties of aminofluorescein, benzamidofluorescein, DAF-2, and DAF-2T, respectively were estimated by semiempirical (PM3) calculations. DAB−COOH and aminobenzoic acid, which are the benzoic acid moieties of weakly fluorescent fluorescein derivatives, have higher HOMO levels than BT-COOH and amidobenzoic acid. These results are consistent with the PET mechanism (Table 2).

Scheme 14. Structures of NX and AX

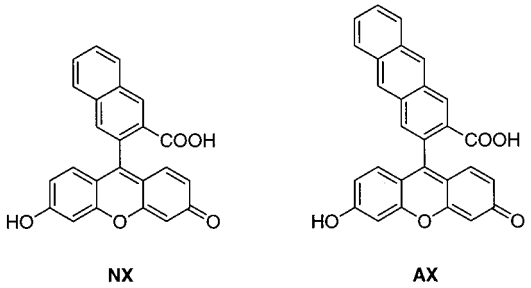

Further, to confirm this mechanism 9-[2-(3-carboxy)naphthyl]-6-hydroxy-3*H*-xanthen-3-one (NX) and 9-[2-(3-carboxy)anthryl]-6-hydroxy-3*H*-xanthen-3-one (AX) were synthesized. It is well-known that expanding the size of aromatic conjugates makes their HOMO levels higher, as does introducing electron-donating substituents. Thus, naphthoic acid and anthracene-2-carboxylic acid would have higher HOMO levels than benzoic acid, and therefore, the fluorescence properties of NX and AX would differ from those of fluorescein (Scheme 14).

The absorbance and fluorescence properties as well as the HOMO levels of the benzoic acid moieties are summarized in Table 2. The absorbance maximum (Ex_{max}) and emission maximum (Em_{max}) were not much altered among these fluorescein derivatives. However, the ϕ values were greatly altered; NX is highly fluorescent, whereas AX is almost nonfluorescent. Thus, a small change in the size of conjugated aromatics, namely, from naphthalene to anthracene, causes a great alteration of the fluorescence properties. When the HOMO levels of the benzoic acid moieties were compared, those of benzoic acid and naphthoic acid, which are present in highly fluorescent fluorescein and NX, are lower than that of the xanthene ring, while the HOMO level of anthracenecarboxylic acid, which is present in the scarcely fluorescent AX, is higher than that of the xanthene. These results are consistent with the idea

Table 2. Absorbance and Fluorescence Properties of Fluorescein, Its Derivatives, DAF-2, and DAF-2 T

	absorbance maximum (nm)	molar absorption coefficient (x 10^4 M^{-1} cm^{-1})	emission maximum (nm)	quantum efficiency	calculated HOMO level of its benzoic acid moiety (eV)
fluorescein[a,b]	492	8.0	517	0.85	−10.1
DAF-2 T	491	7.3	513	0.92	−9.71
4-benzamidofluorescein[c]	490	n.d.	n.d.	0.79	−9.29
NX	492	6.9	512	0.83	−9.14
4-aminofluorescein[c]	490	n.d.	n.d.	0.015	−8.90
DAF-2	486	7.9	513	0.005	−8.63
AX	492	6.5	510	0.003	−8.51

[a] From ref 329. [b] From Tsien, R. Y.; Waggoner, A. In *Handbook of Biological Confocal Microscopy*; Pawley, J. B., Ed.; Plenum Press: New York, 1995; p 267. [c] From Munkholm, C.; Parkinson, D. R.; Walt, D. R. *J. Am. Chem. Soc.* **1990**, *112*, 2608.

that a PET process controls the fluorescence properties of fluorescein derivatives and that these properties can be predicted from the HOMO level of the benzoic acid moiety, with a threshold at around −8.9 eV. This in turn provides a basis for developing novel fluorescence probes with fluorescein-derived structure.

C. Biological Applications of DAFs and DARs

1. Endothelial Cells

Nagano et al.[333] reported NO bioimaging in cultured bovine aortic endothelial cells using DAF−FM DA. The cultured bovine aortic endothelial cells were incubated with DAF−FM DA for 1 h for dye loading. After stimulation with bradykinin, the fluorescence intensity in the cells increased and that in the cytosol increased more than that in the nucleus. NO is produced in the cytosol, where NOS exists. This observation implies that little of the produced NO diffuses into the nucleus or if it does diffuse into the nucleus little of it is oxidized there. The augmentation of the fluorescence intensity was suppressed by an NOS inhibitor. In conclusion, DAF−FM is a useful tool for visualizing the temporal and spatial distribution of intracellular NO.

Kimura et al.[335] examined the effects of acute glucose overload on the cellular productivity of NO in bovine aortic endothelial cells (BAEC) using DAF-2. ATP induced an increase in NO production, assessed by DAF-2, mainly due to Ca^{2+} entry. In contrast, the ATP-induced increase in DAF-2 fluorescence was impaired by glucose overload. The results indicate that glucose overload impairs NO production via the O_2^--mediated attenuation of Ca^{2+} entry. In addition, Kimura et al.[336] examined in detail the mechanism by which mechanical stress induces NOS in endothelium. Hypotonic stress (HTS) induced ATP release, which evoked Ca^{2+} transients in BAEC. HTS also induced NOS, assessed by DAF-2 fluorescence. The results obtained indicate that endogenous ATP plays a central role in HTS-induced NOS in BAEC.

Broillet et al.[337] reported that Ca^{2+}, Mg^{2+}, or incident light promoted the reaction of DAF-2 and NO. However, Nagano et al. probed that the enhancement of fluorescence intensity was caused not by increasing the reaction rate between DAF-2 and NO but by promotion of NO-releasing rate of NO donors.[338]

Endothelial NOS, a Ca^{2+}/calmodulin-dependent enzyme, is critical for vascular homeostasis. To determine the signaling pathway for endogenous eNOS, Rodman et al.[339] directly measured NO production in bovine pulmonary artery endothelial cells (PAEC). Endothelial cells grown in a monolayer produce very low levels of NO which are below the detection range of traditional assays. Therefore, they employed DAF-2 DA to measure NO production in real-time. PAEC had detectable basal NO production which increased slightly after thapsigargin treatment in the presence of low extracellular Ca^{2+}. In contrast, a large increase in NO production was detected in the presence of 4 mM extracellular Ca^{2+}, suggesting that capacitative Ca^{2+} entry regulates wild-type eNOS activity.

Zharikov et al.[340] investigated possible involvement of the actin cytoskeleton in the regulation of the L-arginine/NO pathway in pulmonary artery endothelial cells (PAEC). DAF-2 DA was used for detection of NO in PAEC. They conclude that the state of actin microfilaments in PAEC regulates L-arginine transport and that this regulation can affect NO production by PAEC.

Berkels et al.[341] presented a new method to measure intracellular Ca^{2+} and NO simultaneously in endothelial cells. The method makes it possible to follow intracellular Ca^{2+} and NO distributions online and is sensitive enough to monitor changes of NO formed by the constitutive endothelial NOS.

In addition, DAR-4M AM was applied to the imaging of NO in bovine aortic endothelial cells.[321] DARs are more photostable than DAFs. The fluorescence in cells was observed after stimulation with bradykinin (Figure 19), which raises the intracellular Ca^{2+} level and thereby activates NOS, and this increase was suppressed by addition of an NOS inhibitor. DAR-4M should be useful for bioimaging of samples that have strong autofluorescence in the case of 490 nm excitation in which the intracellular pH may fall below 6.

2. Smooth Muscle Cells

DAF-2 DA was applied to the imaging of NO in cultured rat aortic smooth muscle cells by using a fluorescence microscope equipped with fluorescence filters for fluorescein chromophores.[25] Confocal laser scanning microscopy indicated that fluorescence was emitted from the whole cell body, including the nucleus. This implies that DAF-2 regenerated intracellularly by esterase is distributed throughout the whole cell. There was no indication of any cell damage caused by loading the dye. The results show that the fluorescence intensity in endotoxin- and cytokine-activated cells increased owing to DAF-2 T production from DAF-2 by reaction with NO. The fluorescence did not increase in inactivated cells, which did not produce NO. The probe is very useful for bioimaging of NO in cultured rat aortic smooth muscle cells.

Itoh et al. detected DAF−FM T using reversed-phase high-performance liquid chromatography with a fluorescence detector.[342] This sensitive method enabled them to detect the spontaneous and substance P-induced NO release from isolated porcine coronary arteries, both of which were dependent entirely on the NOS activity in vascular endothelial cells. Furthermore, they obtained fluorescence images of cultured smooth muscle cells of the rat urinary bladder after loading with DAF−FM DA. In the cells pretreated with cytokines, the fluorescence intensity increased with time after DAF−FM loading.

3. Brain Slices

The biological functions of NO in the neuronal system remain controversial. Using DAF-2 DA for direct detection of NO, Nagano et al.[343] examined both acute rat brain slices and organotypic culture

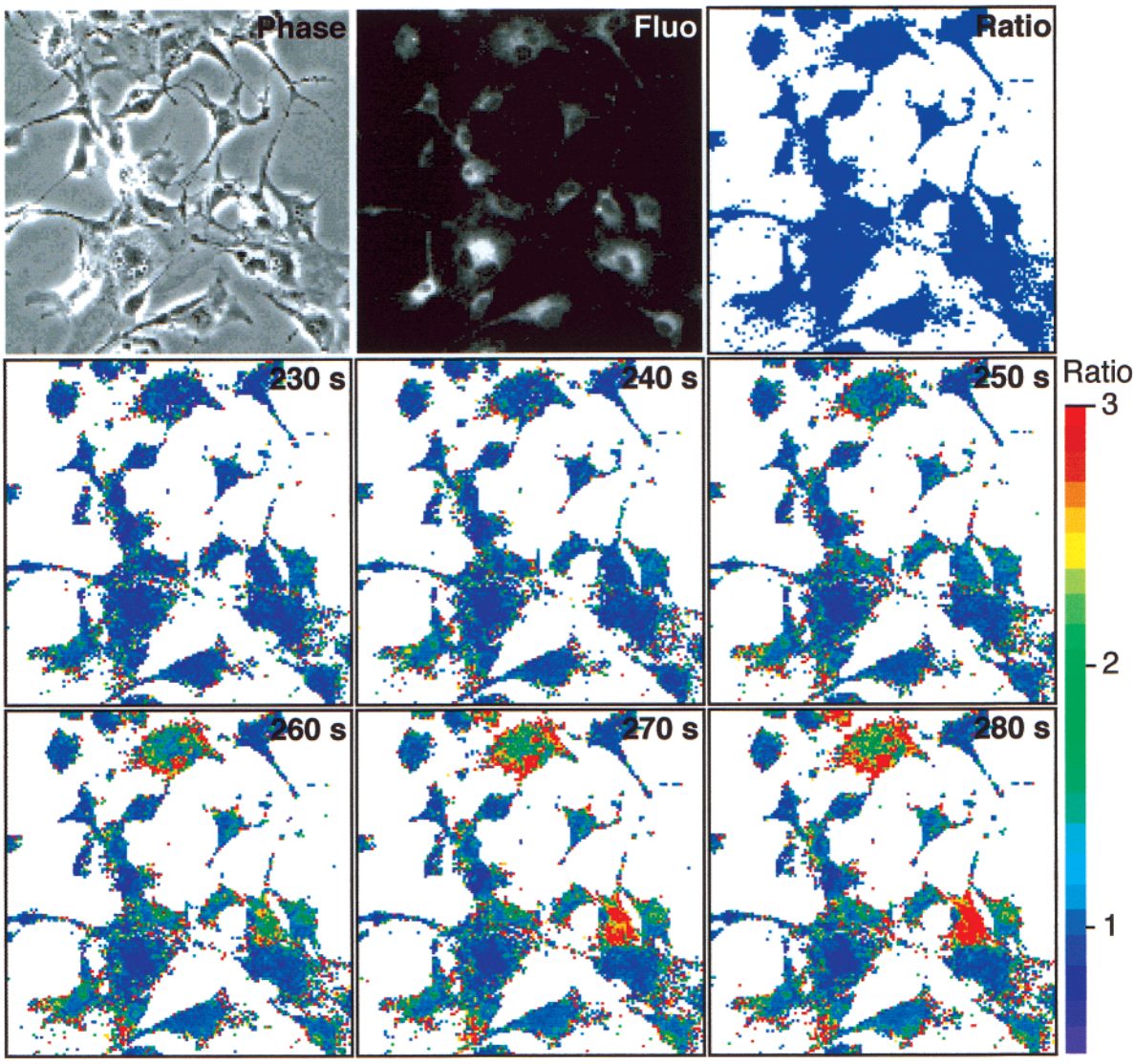

Figure 19. Bright-field and fluorescence images of cultured bovine aortic endothelial cells loaded with DAR-4M AM. The upper images are the bright-field, the fluorescence, and the fluorescence ratio images at the start of measurement, respectively. The middle and the lower images are fluorescence ratio images at the indicated times after the start of measurement. The fluorescence ratio images indicate the ratio of the intensity to the initial intensity at the start. However, areas where the fluorescence intensity was low were excluded and are shown in white. (Reprinted with permission from ref 331. Copyright 2001 American Chemical Society.)

of brain slices to ascertain NO production sites. The fluorescence intensity in the CA1 region of the hippocampus was augmented, especially after stimulation with NMDA, in acute brain slices. This NO production in the CA1 region was also confirmed in cultured hippocampus. This is the first direct evidence of NO production in the CA1 region. There were also fluorescence cells in the cerebral cortex after stimulation with NMDA. Imaging techniques using DAF-2 DA should be very useful for the clarification of neuronal NO functions (Figure 20).

DAF−FM DA was also applied to imaging of NO generated in rat hippocampal slices by exposure to an aglycemic medium.[344] NO production was observed mainly in the CA1 area and was dependent on the concentration of O_2. During exposure to an anoxic−aglycemic medium, NO was hardly produced while marked elevation of intracellular Ca^{2+} was observed. Production of NO increased sharply as soon as the perfusate was changed to the normal medium. These results suggest that NOS is activated after reperfusion rather than during ischemia.

ROS and NO are important participants in signal transduction that could provide the cellular basis for activity-dependent regulation of neuronal excitability.[345] In young rat cortical brain slices and undifferentiated PC 12 cells, paired application of depolarization/agonist stimulation and oxidation induces long-lasting potentiation of subsequent Ca^{2+} signaling that is reversed by hypoxia. This potentiation critically depends on NO production and involves cellular ROS utilization. Using the fluorescent dye DAF-2, Yermolaieva et al.[345] measured NO production in PC 12 cells during depolarization or histamine application. Application of 100 μM histamine induced a significant increase in NO production. The crucial role for NO in oxidative potentiation of Ca^{2+} signaling triggered by pairing of electrical/agonist stimulation and oxidation demonstrated here provides an insight into the cellular mechanisms involved in neuronal

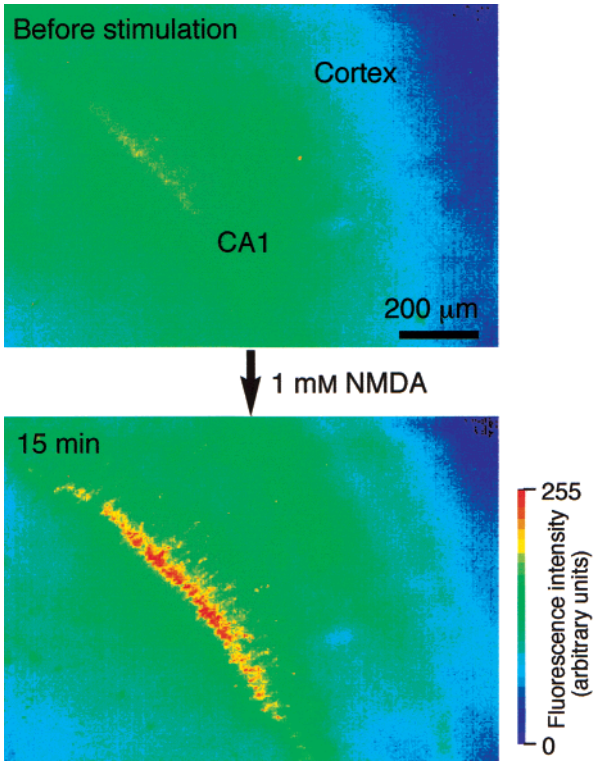

Figure 20. Fluorescence images of a rat brain slice loaded with DAF-2 DA. The fluorescence intensity is shown in pseudocolor. (Reprinted with permission from ref 343. Copyright 1998 Rapid Science Publishers.)

developmental plasticity. NO could influence its effectors by stimulating the cGMP-dependent signaling pathway and/or by acting as a weak radical.

4. Ion Channels

Most voltage-gated Na^+ channels are almost completely inactivated at depolarized membrane potentials, but in some cells a residual Na^+ current is seen that is resistant to inactivation. The biological signaling mechanisms that regulate the persistence of Na^+ channels are not well understood. Ahern et al.[346] showed that in nerve terminals and ventricular myocytes, NO reduces the inactivation of Na^+ current. This effect was independent of cGMP and blocked by *N*-ethylmaleimide. Thus, ROS act directly on the channel or a closely associated protein. Application of ionomycin to raise the intracellular Ca^{2+} concentration in myocytes activated NOS. The NO produced in response to ionomycin was detected with DAF-2 DA. They concluded that NO is a potential endogenous regulator of persistent Na^+ current under physiological and pathophysiological conditions.

Lipton et al.[347] reported that the NMDA receptor (NMDAR)-associated ion channel is modulated not only by exogenous NO, but also by endogenous NO. They examined inhibition of NMDAR responses by endogenous NO to determine the underlying molecular mechanism. For this purpose, HEK 293 cells transfected with nNOS were transiently transfected with wild-type NR1/NR2A or mutant NR1/NR2A (C399A) receptors. NMDA responses were monitored by digital Ca^{2+} imaging with fura-2. Production of endogenous NO by these HEK-nNOS cells was measured with DAF-2. It was concluded that endogenous *S*-nitrosylation may regulate ion channel activity.

5. Fertilization

Epel et al.[348] demonstrated that NO is necessary and sufficient for egg activation at fertilization. The early steps that lead to the rise in Ca^{2+} and egg activation at fertilization are unknown but are of great interest, particularly with the advent of in vitro fertilization techniques for treating male infertility and whole-animal cloning by nuclear transfer. They showed that active NOS is present at high concentration in sperm after activation by the acrosome reaction. An increase in nitrosation within eggs is evident seconds after insemination and precedes the Ca^{2+} pulse of fertilization. They used DAF-2 DA for detection of NO. It was concluded that NOS- and NO-related bioactivity satisfy the primary criteria of an egg activator, i.e.,. they are present in an appropriate place, active at an appropriate time, and necessary and sufficient for successful fertilization.

6. Inflammation

NO plays important roles in inflammatory processes. Lopez-Figueroa et al.[349] examined whether changes in NOS mRNA expression lead to similar temporal and anatomical changes in NO production in an experimental model of CNS inflammation. iNOS mRNA expression was analyzed 2, 4, 6, and 24 h after intracerebroventricular (icv) injection of interleukin-1 β or the vehicle. Increased expression of iNOS mRNA was observed surrounding the microinjection site and meninges. Using DAF-2 DA for the direct detection of NO production, they observed a significant increase in NO production after 4 and 6 h. They conclude that increase in iNOS mRNA following icv administration of IL-1 β leads to increases in NO production. They proposed that the DAF-2 DA method can be used as a potential marker in the diagnosis of CNS inflammation.

7. Drosophila

Wingrove and O'Farrell[350] reported that *Drosophila* utilizes components of the NO/cGMP signaling pathway to respond to hypoxia. Hypoxic exposure rapidly induced exploratory behavior in larvae and arrested the cell cycle. These behavioral and cellular responses were diminished by an inhibitor of NOS and by a polymorphism of cGMP-dependent protein kinase. Regions of the larvae that specialize in responding to hypoxia should express significant levels of the activities involved. They used DAF-2 DA to define possible foci of function. DAF-2 DA stained the pouch of tissue surrounding the anterior spiracles as well as neuronal-like processes within the pouch. This staining near the openings of the tracheal system is interesting because the location is consistent with a possible role in governing the opening of the spiracles to increase access to oxygen. DAF-2 DA is useful for clarification of response mechanisms to hypoxia.

8. Adrenal Zona Glomerulosa

Adrenal zona glomerulosa (ZG) cells do not contain NOS. Hanke et al.[351] conferred endothelial NOS

activity upon adrenal ZG cells through transduction with a recombinant adenovirus encoding the endothelial NOS gene (AdeNOS) to determine the effect of endogenous NO on aldosterone synthesis. AdeNOS-transduced cells exhibited DAF-2 DA fluorescence, which was blocked by pretreatment with an NOS inhibitor. In conclusion, adenovirus-mediated gene transfer of eNOS in ZG cells results in the expression of active endothelial NOS enzyme, and this endogenous NO production by ZG cells decreases aldosterone synthesis.

9. Bone Marrow Stromal Cells

Gorbunov et al. found, by the data that using the reverse transcription−polymerase chain reaction and immunofluorescence analysis of murine bone marrow stromal cells, that γ irradiation at doses of 2−50 Gy stimulates expression of iNOS.[352] The activation of iNOS was accompanied by an increase in the fluorescence of DAF-2 and accumulation of 3-nitrotyrosine within cellular proteins in a dose-dependent manner.

10. Mitochondria

NO has been implicated in the modulation of mitochondrial respiration, membrane potential, and subsequently apoptosis. Although the presence of a mitochondrial NOS has been discussed, there is no direct evidence in vivo of the presence of NO within mitochondria. Using DAF-2 DA, Lopez-Figueroa et al. observed NO production in PC 12 and COS-1 cells by conventional and confocal fluorescence microscopy.[353] The subcellular distribution of NO production is consistent with the presence of a mitochondrial NOS.

11. Retina

In the retina, NO functions in network coupling, light adaptation, neurotransmitter receptor function, and synaptic release. Neuronal NOS is present in the retina of every vertebrate species so far investigated. However, although nNOS can be found in every retinal cell type, little is known about the production of NO in specific cells or about the diffusion of NO within the retina. Blute et al.[354] used DAF-2 to image real-time NO production in turtle retina in response to stimulation with NMDA. In response to NMDA, NO was produced in somata in the ganglion cell and inner nuclear layers, in synaptic boutons and processes in the inner plexiform layer, in processes in the outer plexiform layer, and in photoreceptor inner segments. They conclude that NO may function at specific synapses, modulate gene expression, or coordinate events throughout the cell.

Matsuo reported that basal NO production is enhanced by hydraulic pressure in cultured human trabecular cells.[355] He measured the intracellular NO level in real-time using DAF-2.

12. Plants

Leaves and callus of *Kalanchoe daigremontiana* and *Taxus brevifolia* were used to investigate NO-induced apoptosis in plant cells.[356] NO production was visualized in cells and tissues with DAF-2 DA. The NO burst preceded a significant increase in nuclear DNA fragmentation and cell death. L-NMMA significantly decreased NO production and apoptosis in both species. Pedroso et al.[356,357] concluded that NO is involved in DNA damage leading to cell death and proposed a potential role of NO as a signal molecule in these plants.

Foissner et al.[358] used DAF-2 DA, in conjunction with confocal laser scanning microscopy, for in vivo real-time imaging of an elicitor-induced NO burst in tobacco. A growing body of evidence suggests that NO, an important signaling and defense molecule in mammals, plays a key role in activating disease resistance in plants, acting as a signaling molecule and possibly also as a direct antimicrobial agent. The results revealed additional similarities between plant and animal host responses to infection.

13. Conclusion

Fluorescent indicators for bioimaging of NO have been applied to various biological samples to examine production of NO. The most widely used fluorescent indicators for detecting intracellular NO are DAFs and DARs. We introduced the examples in this part.

DAFs and DARs permit the measurement of NO production in various living cells, tissues, and specimen, as shown in section III. DAF-2 DA, DAF−FM DA, and DAR-4M AM permeate through the cell membrane and are hydrolyzed to yield DAF-2, DAF−FM, and DAR-4M, respectively, which are retained in the cell owing to their relatively poor permeating ability. In conclusion, these indicators are a useful tool for visualizing the temporal and spatial distribution of intracellular NO.

IV. Concluding Remarks

In this article we have endeavored to present a comprehensive review of the status of bioimaging of NO with special emphasis on in vivo EPR spectrometry and intracellular fluorometry.

Over the past decade, EPR spectroscopic methods combined with NO-trapping techniques have emerged as important tools and have provided much important information about the roles of NO in biological systems. Marked progress in in vivo EPR imaging techniques in the low-frequency region and development of superior NO-trapping reagents have made it possible to detect and image endogenously produced or exogenously supplied NO in living small animals. At present, NO traps applicable to in vivo measurements are limited to Fe−DTC complexes. In addition, in vivo EPR imaging is not applicable to physiological levels of NO because of the limitations of currently available EPR instrumentation. However, organs or tissues with a locally high, pathological level of NO can be targets, so that this method has the potential to contribute to the diagnosis of pathophysiological conditions involving the overproduction of NO. There is no doubt that further developments of EPR instrumentation and NO traps with novel functions will open up new applications. The usage of endogenous or exogenous NO complexes

as spin probes may allow the pharmacokinetic analysis of NO-derived endogenous materials. Furthermore, we think that more attention should be given to in vivo real-time imaging of NO, which could be developed based on the combination of EPR and NMR techniques and fMRI.

On the other hand, the advantages of bioimaging with fluorescent indicators include highly sensitive detection with fine temporal and spatial resolution under microscopic observation. In section III, we introduced several fluorescence probes for investigation of the diverse physiological and pathophysiological roles of NO in tissues, in living cells, and in vivo. At the present time, DAFs and DARs are the preferred indicators for bioimaging of NO in terms of specificity, sensitivity, and handling. DAF−FM DA and DAR-4M meet the six criteria for useful bioimaging probes of NO, as described in the Introduction. DAF-2, DAF-2 DA, DAF−FM, DAF−FM DA, DAR-4M, and DAR-4M AM are commercially available. The ultimate reaction species are thought to be NO^+ equivalents such as nitric anhydride (N_2O_3), which is easily generated by the autoxidation of NO. The increase of fluorescence is based on the nitrosation reaction of DAFs or DARs in living systems. Therefore, the detection method should not interfere too much with signal transduction by NO, although it may be difficult to measure the accurate concentration of NO in the living cell in the case that the nitrosative chemistry of NO is unequally distributed throughout the cell. The specificity for NO is high because DAFs and DARs do not react in neutral solution with stable oxidized forms of NO, such as NO_2^- and NO_3^-, or ROS, such as superoxide, hydrogen peroxide, and $ONOO^-$, to yield any fluorescent product. These probes are in practical use, but generally, probes based on measurements of a single fluorescence peak intensity are known to have some problems in most applications. Even fluorescent probes with high sensitivity and specificity may be influenced by factors such as photobleaching, changes in the probe concentration, changes of environment around the probe molecule (pH, polarity, temperature, etc.), and stability under illumination. Ratiometric probes represent one answer to the problems posed by intensity measurements. Further studies on the development of novel ratiometric NO bioimaging probes are in progress.

V. Abbreviations

AM	acetoxymethyl
AX	9-[2-(3-carboxy)anthryl]−6-hydroxy-3*H*-xanthen-3-one
BAEC	bovine aortic endothelial cells
BT-COOH	benzotriazole-5-carboxylic acid
carbamoyl-PROXYL	3-carbamoyl-2,2,5,5-tetramethylpyrrolidine-1-yloxyl
cNOS	constitutive NOS
CT	computed tomography
DAB−COOH	3,4-diaminobenzenecarboxylic acid
DAF	diaminofluorescein
DAN	diaminonaphthalene
DAR	diaminorhodamine
DBNBS	3,5-dibromo-4-nitrosobenzenesulfonic acid
DCFH	dichlorofluorescin
DEPMPO	5-diethoxyphosphoryl-5-methyl-1-pyrroline-*N*-oxide
DETC	*N*,*N*-diethyldithiocarbamate
DMPO	5,5-dimethyl-1-pyrroline *N*-oxide
DNIC	dinitrosyl dithiolato iron complex
DTC	dithiocarbamate
DTCS	*N*-(dithiocarboxy)sarcosine
EDRF	endothelium-derived relaxing factor
ENDOR	electron nuclear double resonance
eNOS	endothelial NOS
EPR	electron paramagnetic resonance
ESR	electron spin resonance
Fe−DTC complexes	iron complexes with dithiocarbamate derivatives
fMRI	functional MRI
FNOCT	fluorescent NOCT
Hb	hemoglobin
HOMO	highest occupied molecular orbital
HTS	hypotonic stress
IFN-γ	interferon-γ
IL-1β	interleukin-1 β
iNOS	inducible NOS
ISDN	isosorbide dinitrate
LPS	lipopolysaccharide
MGD	*N*-methyl-D-glucamine dithiocarbamate
MNP	2-methyl-2-nitrosopropane
MRI	magnetic resonance imaging
MSD	*N*-methyl-L-serine dithiocarbamate
NF-κB	nuclear transcription factor κB
L-NMMA	N^G-monomethyl-L-arginine
NMR	nuclear magnetic resonance
nNOS	neuronal NOS
NO	nitric oxide
NOCT	NO cheletropic trap
NO−Fe(II)-$(DTC)_2$	nitrosyl iron−dithiocarbamate complex
NO−Hb	nitrosyl hemoglobin
NOS	NO synthase
NX	9-[2-(3-carboxy)naphthyl]−6-hydroxy-3*H*-xanthen-3-one
PAEC	pulmonary artery endothelial cells
PBN	α-phenyl-*N*-*tert*-butylnitrone
PDTC	pyrrolidine dithiocarbamate
PEDRI	proton−electron double-resonance imaging
POBN	α-(4-pyridyl 1-oxide)-*N*-*tert*-butylnitrone
ProDTC	L-proline dithiocarbamate
PTIO	2-phenyl-4,4,5,5-tetramethylimidazoline-1-yloxyl-3-oxide
ROS	reactive oxygen species
RSNO	*S*-nitrosothiol
RT-PCR	reverse transcriptase−polymerase chain reaction
sGC	soluble guanylate cyclase
SIN-1	3-morpholinosydnonimine
SNP	sodium nitroprusside
SOD	superoxide dismutase
TEMPOL	4-hydroxy-2,2,6,6-tetramethylpiperidine-1-yloxyl

VI. Acknowledgments

T.Y. thanks Dr. S. Fujii and Dr. H. Yokoyama for their continuous technical support and stimulating discussions. T.N. thanks Dr. H. Kojima and Dr. K. Kikuchi for experimental assistance and fruitful discussions. We acknowledge the publishers and learned societies for their generous permission to reproduce many figures. Professor Jay L. Zweier (Johns Hopkins University) was kind enough to give permission to adapt the EPR spectra in ref 289 for

Figure 13. The work was supported in part by a Grant-in-Aid to T.Y. for Scientific Research (No. 11470497) and by Grants-in-Aid to T.N. for Scientific Research (Nos. 12557217, 12470475) from the Japan Society for the Promotion of Science. The work at the University of Tokyo was also supported by a Grant-in-Aid for Scientific Research for University and Society Collaboration (No. 11794026) and grants from the Takeda Science Foundation and the Nagase Science and Technology Foundation.

VII. References

(1) Liszt, H. S.; Turner, B. E. *Astrophys. J.* **1978**, *224*, L73.
(2) McGonagle, D.; Ziurys, L. M.; Irvine, W. M.; Minh, Y. C. *Astrophys. J.* **1990**, *359*, 121.
(3) Ziurys, L. M.; McGonagle, D.; Minh, Y.; Irvine, W. M. *Astrophys. J.* **1991**, *373*, 535.
(4) Watson, A. J.; Donahue, T. M.; Stedman, D. H. *Geophys. Res. Lett.* **1979**, *6*, 743.
(5) Chameides, W. L.; Walker, J. C. G.; Nagy, A. F. *Nature* **1979**, *280*, 820.
(6) Palmer, R. M. J.; Ferrige, A. G.; Moncada, S. *Nature* **1987**, *327*, 524.
(7) Ignarro, L. J.; Buga, G. M.; Wood, K. S.; Byrns, R. E.; Chaudhuri, G. *Proc. Natl. Acad. Sci. U.S.A.* **1987**, *84*, 9265.
(8) Furchgott, R. F. *Angew. Chem., Int. Ed.* **1999**, *38*, 1870.
(9) Moncada, S.; Palmer, R. M. J.; Higgs, E. A. *Pharmacol. Rev.* **1991**, *43*, 109.
(10) Feldman, P. L.; Griffith, O. W.; Stuehr, D. J. *Chem. Eng. News.* **1993**, *71*, 26.
(11) Bredt, D. S., Snyder, S. H. *Annu. Rev. Biochem.* **1994**, *63*, 175.
(12) Kerwin, J. F., Jr.; Lancaster, J. R., Jr.; Feldman, P. L. *J. Med. Chem.* **1995**, *38*, 4343.
(13) Wink, D. A.; Mitchell, J. B. *Free Radical Biol. Med.* **1998**, *25*, 434.
(14) Archer, S. *FASEB J.* **1993**, *7*, 349.
(15) Garrel, C.; Decout, J.-L.; Fontecave, M. In *Analysis of Free Radicals in Biological Systems*; Favier, A. E., Cadet, J., Kalyanaraman, B., Fontecave, M., Pierre, J.-L., Eds.; Birhhäuser Verlag: Basel, Switzerland, 1995; p 277.
(16) *Methods in Nitric Oxide Research*; Feelisch, M., Stamler, J. S., Eds.; John Wiley & Sons: Chichester, 1996.
(17) *Methods in Enzymology*; Packer, L., Ed.; Academic Press: San Diego, CA, 1996; Vol. 268.
(18) *Nitric Oxide Protocols*; Titheradge, M. A. Ed.; Humana Press: Totawa, NJ, 1998.
(19) Hampl, V.; Walters, C.; Archer, S. L. In *Methods in Nitric Oxide Research*; Feelisch, M., Stamler, J. S., Eds.; John Wiley & Sons: New York, 1996; p 309.
(20) Leone, A. M.; Furst, V. W.; Foxwell, N. A.; Cellek, S.; Moncada, S. *Biochem. Biophys. Res. Commun.* **1996**, *221*, 37.
(21) Kikuchi, K.; Nagano, T.; Hayakawa, H.; Hirata, Y.; Hirobe, M. *J. Biol. Chem.* **1993**, *268*, 23106.
(22) Kojima, H.; Kikuchi, K.; Hirobe, M.; Nagano, T. *Neurosci. Lett.* **1997**, *233*, 157.
(23) Malinski, T.; Mesaros, S.; Tomboulian, P. *Methods Enzymol.* **1996**, *268*, 58.
(24) Yoshimura, T.; Yokoyama, H.; Fujii, S.; Takayama, F.; Oikawa, K.; Kamada, H. *Nat. Biotechnol.* **1996**, *14*, 992.
(25) Kojima, H.; Nakatsubo, N.; Kikuchi, K.; Kawahara, S.; Kirino, Y.; Nagoshi, H.; Hirata, Y.; Nagano, T. *Anal. Chem.* **1998**, *70*, 2446.
(26) Griffith, O. W.; Stuehr, D. J. *Annu. Rev. Physiol.* **1995**, *57*, 707.
(27) Kleinert, H.; Boissel, J.-P.; Schwarz, P. M.: Förstermann, U. In *Nitric Oxide Biology and Pathobiology*; Ignarro, L. J., Ed.; Academic Press: San Diego, 2000; p 105.
(28) Martletta, M. A. *Trends Biochem. Sci.* **1989**, *14*, 488.
(29) Hogg, N.; Singh, R. J.; Joseph, J.; Neese, F.; Kalyanaraman, B. *Free Radical Res.* **1995**, *22*, 47.
(30) Miranda, K. M.; Espey, M. G.; Jourd'heuil, D.; Grisham, M. B.; Fukuto, J. M.; Feelisch, M.; Wink, D. A. In *Nitric Oxide Biology and Pathobiology*; Ignarro, L. J., Ed.; Academic Press: San Diego, 2000; p 41.
(31) Sakinis, A.; Wennmalm, A. *Biochem. J.* **1998**, *330*, 527.
(32) Shaw, A. W.; Vosper, A. J. *J. Chem. Soc., Faraday Trans.* **1977**, 1239.
(33) Pogrebnaya, V. L.; Usov, A. P.; Baranov, A. V.; Nesterenko, A. I.; Bez'yazychnyi, P. I. *J. Appl. Chem. USSR* **1987**, *48*, 1004.
(34) Pires, M.; Rossi, M. J.; Ross, D. S. *Int. J. Chem. Kinet.* **1994**, *26*, 1207.
(35) Goldstein, S.; Czapski, G. *J. Am. Chem. Soc.* **1995**, *117*, 12078.
(36) Liu, X.; Miller, M. J. S.; Joshi, M. S.; Thomas, D. D.; Lancaster, J. R., Jr. *Proc. Natl. Acad. Sci. U.S.A.* **1998**, *95*, 2175.
(37) Lancaster, J. R., Jr. In *Nitric Oxide Biology and Pathobiology*; Ignarro, L. J., Ed.; Academic Press: San Diego, 2000; p 209.
(38) Furchgott, R. F.; Vanhoutte, P. M. *FASEB J.* **1989**, *3*, 2007.
(39) Liu, X.; Miller, M. J. S.; Joshi, M. S.; Sadowska-Krowicka, H.; Clark, D. A.; Lancaster, J. R., Jr. *J. Biol. Chem.* **1998**, *273*, 18709.
(40) Denicola, A.; Souza, J. M.; Radi, R.; Lissi, E. *Arch. Biochem. Biophys.* **1996**, *328*, 208.
(41) Henry, Y.; Ducrocq, C.; Drapier, J. C.; Servent, D.; Pellat, C.; Guissani, A. *Eur. Biophys. J.* **1991**, *20*, 1.
(42) Henry, Y.; Lepoivre, M.; Drapier, J. C.; Ducrocq, C.; Boucher, J.-L.; Guissani, A. *FASEB J.* **1993**, *7*, 1124.
(43) Wilcox, D. E.; Smith, R. P. *Methods: A Companion to Methods in Enzymology* **1995**, *7*, 59.
(44) Rochelle, L. G.; Kruszyna, H.; Smith, R. P. *Methods Neurosci.* **1996**, *31*, 3.
(45) Yoshimura, T.; Yokoyama, H.; Fujii, S. *J. Magn. Reson. Anal.* **1997**, *3*, 125.
(46) *Nitric Oxide Research from Chemistry to Biology: EPR Spectroscopy of Nitrosylated Compounds*; Henry, Y. A., Guissani, A., Ducastel. B., Eds.; Springer: New York, 1997.
(47) *Nitric Oxide in Transplant Rejection and Antitumor Defence*; Lukiewicz, S., Zweir, J. L., Eds.; Kluwer Academic Publishers: Boston, 1998.
(48) Pou, S.; Halpern, H. J.; Tsai, P.; Rosen, G. M. *Acc. Chem. Res.* **1999**, *32*, 155.
(49) Fujii, H.; Kazama, S.; Berliner, L. J. *Curr. Top. Biophys.* **1999**, *23*, 11.
(50) Henry, Y.; Guissani, A. *Analusis* **2000**, *28*, 445.
(51) Fujii, S.; Yoshimura, T. *Antioxid. Redox Signaling* **2000**, *2*, 879.
(52) Berliner, L. J.; Khramtsov, V.; Fujii, H.; Clanton, T. L. *Free Radical Biol. Med.* **2001**, *30*, 489.
(53) Janzen, E. G. *Acc. Chem. Res.* **1971**, *4*, 31.
(54) Buettner, G. R. *Free Radical Biol. Med.* **1987**, *3*, 259.
(55) Ohno, K. *Magn. Reson. Rev.* **1987**, *11*, 275.
(56) Eaton, G. R.; Eaton, S. S.; Ohno, K. *EPR Imaging and in vivo EPR*; CRC Press: Boca Raton, FL, 1991.
(57) Feldman, A.; Wildman, E.; Bartolinini, G.; Piette, L. H. *Phys. Med. Biol.* **1975**, *20*, 602.
(58) Berliner, L. J.; Fujii, H. *Science.* **1985**, *227*, 517.
(59) Ono, M.; Ogata, T.; Hsieh, K.-C.; Suzuki, M.; Yoshida, E.; Kamada, H. *Chem. Lett.* **1986**, *491*.
(60) Allecci, M.; Colacicchi, S.; Indovina, P. L.; Momo, F.; Pavone, P.; Sotgiu, A. *Magn. Reson. Imaging* **1990**, *8*, 59.
(61) Ohno, K.; Tsuchihashi, N. *Tr. Phys. Chem.* **1991**, *2*, 79.
(62) Ishida, S.; Matsumoto, S.; Yokoyama, H.; Mori, N.; Kumashiro, H.; Tsuchihashi, N.; Ogata. T.; Yamada, M.; Ono, M.; Kitajima, T.; Kamada, H.; Yoshida, E. *Magn. Reson. Imaging* **1992**, *10*, 109.
(63) Berliner, L. J.; Fujii, H. *Biol. Magn. Reson.* **1992**, *11*, 307.
(64) Sotgiu, A.; Placidi, G.; Gualtieri, G.; Tatone, C. *Magn. Reson. Chem.* **1995**, *33*, S160.
(65) Sotgiu, A.; Colacicchi, S.; Placidi, G.; Allacci, M. *Cell. Mol. Biol.* **1997**, *43*, 813.
(66) Swartz, H. M.; Walczak, T. *Res. Chem. Intermed.* **1996**, *22*, 511.
(67) Swartz, H. M.; Halpern, H. *Biol. Magn. Reson.* **1998**, *14*, 367.
(68) Quaresima, V.; Ferrari, M. *Phys. Med. Biol.* **1998**, *43*, 1937.
(69) Kuppusamy, P.; Zweier, J. L. In *Nitric Oxide in Transplant Rejection and Antitumor Defence*; Lukiewicz, S., Zweier, J. L. Eds.; Kuwer Academic: Boston, 1998; p 109.
(70) Kuppusamy, P.; Ohnishi, S. T.; Zweier, J. L. In *Nitric Oxide in Transplant Rejection and Antitumor Defence*; Lukiewicz, S., Zweier, J. L. Eds.; Kuwer Academic: Boston, 1998; p 119.
(71) Minta, A.; Kao, J. P. Y.; Tsien, R. Y. *J. Biol. Chem.* **1989**, *264*, 8171.
(72) Tsien, R. Y. *Biochemistry* **1980**, *19*, 2396.
(73) Weil, J. A.; Bolton, J. R.; Wertz, J. E. *Electron Paramagnetic Resonance*; John Wiley & Sons: New York, 1994.
(74) Barthel, J.; Bachhuber, K.; Buchner, R.; Hetzenauer, H. *Chem. Phys. Lett.* **1990**, *165*, 369.
(75) Lukiewicz, S. J.; Lukiewicz, S. G. *Magn. Reson. Med.* **1984**, *1*, 297.
(76) Beringer, R.; Castle, J. G. *Phys. Rev.* **1950**, *78*, 581.
(77) Brown, R. L.; Radford, H. E. *Phys. Rev.* **1966**, *147*, 6.
(78) Jinguji, M.; Ohokubo, Y.; Tanaka, I. *Chem. Phys. Lett.* **1978**, *54*, 136.
(79) Whittaker, J. W. *J. Chem. Educ.* **1991**, *68*, 421.
(80) Lunsford, J. H. *J. Chem. Phys.* **1967**, *46*, 4347.
(81) Lunsford, J. H. *J. Phys. Chem.* **1968**, *72*, 2141.
(82) Lunsford, J. H. *J. Phys. Chem.* **1968**, *72*, 4163.
(83) Lunsford, J. H. *J. Phys. Chem.* **1970**, *74*, 1518.
(84) Gardner, C. L.; Weinberger, M. A. *Can. J. Chem.* **1970**, *48*, 1317.
(85) Kasai, P. H.; Bishop, R. J. *J. Am. Chem. Soc.* **1972**, *94*, 5560.
(86) Kasai, P. H.; Gaura, R. M. *J. Phys. Chem.* **1982**, *86*, 4257.
(87) Biglino, D.; Li, H.; Erickson, R.; Lund, A.; Yahiro, H.; Shiotani, M. *Phys. Chem. Chem. Phys.* **1999**, *1*, 2887.
(88) Pöppl, A.; Rudolf, T.; Manikandan, P.; Goldfarb, D. *J. Am. Chem. Soc.* **2000**, *122*, 10194.

(89) Yahiro, H.; Lund, A.; Aasa, R.; Benetis, N. P.; Shiotanai, M. *J. Phys. Chem. A* **2000**, *104*, 7950.
(90) Galpin, J. R.; Veldink, G. A.; Vliegenthart, F. G.; Boldingh, J. *Biochim. Biophys. Acta* **1978**, *536*, 356.
(91) Salerno, J. C.; Siedow, J. N. *Biochim. Biophys. Acta* **1979**, *579*, 246.
(92) Arciero, D. M.; Lipscomb, J. D.; Huynh, B. H.; Kent, T. A.; Münch, E. *J. Biol. Chem.* **1983**, *258*, 114981.
(93) Nelson, M. J. *J. Biol. Chem.* **1987**, *262*, 12137.
(94) Burn, N. E. L.; Cheesman, M. R.; Thomson, A. J.; Moore, G. R.; Andrews, S. C.; Guest, J. R.; Harrison, P. *M. FEBS Lett.* **1993**, *323*, 261.
(95) Orville, A. M.; Lipscomb, J. D. *J. Biol. Chem.* **1993**, *268*, 8596.
(96) Whittaker, M. M.; Whittaker, J. W. *Biophys. J.* **1993**, *64*, 762.
(97) Henry, Y. A.; Ducastel. B.; Guissani, A. In *Nitric Oxide Research from Chemistry to Biology: EPR Spectroscopy of Nitrosylated Compounds*; Henry, Y. A., Guissani, A., Ducastel. B., Eds.; Springer: New York, 1997; p 15.
(98) Henry, Y. A.; Guissani, A. In *Nitric Oxide in Transplant Rejection and Antitumor Defence*; Lukiewicz, S., Zweir, J. L., Eds.; Kluwer Academic Publishers: Boston, 1998; p 1.
(99) Richter-Addo, G. B.; Legzdins, P. *Metal Nitrosyls*; Oxford University Press: New York, 1992.
(100) Cheng, L.; Richter-Addo, G. B. In *The Porphyrin Handbook*; Kadish, K. M., Smith, K. M., Guilard, R., Eds.; Academic Press: San Diego, 2000; Vol. 4, p 219.
(101) Davies, M. J.; Timmins, G. S. In *Biomedical Applications of Spectroscopy*; Clark, R. J. H., Hester, R. E., Eds.; John Wiley & Sons: New York, 1996; p 217.
(102) Singel, D. J.; Lancaster, J. R., Jr. In *Methods in Nitric Oxide Research*; Feelisch, M., Stamler, J. S., Eds.; John Wiley & Sons: Chichester, 1996, p 341.
(103) Kotake, Y. *Methods Enzymol.* **1996**, *268*, 222.
(104) Vanin, A. F.; Kleschyov, A. L. In *Nitric Oxide in Transplant Rejection and Antitumor Defence*; Lukiewicz, S., Zweir, J. L., Eds.; Kluwer Academic Publishers: Boston, 1998; p 49.
(105) Vanin, A. F. *Methods Enzymol.* **1999**, *301*, 269.
(106) Halpern, H. J.; Yu, C.; Barth, E.; Peric, M.; Rosen, G. M. *Proc. Natl. Acad. Sci. U.S.A.* **1995**, *92*, 796.
(107) Liu, K. J.; Miyake, M.; Panz, T.; Swartz, H. *Free. Radical Biol. Med.* **1999**, *26*, 714.
(108) Timmins, G. S.; Liu, K. J.; Becgara, E. J. H.; Kotake, Y.; Swartz, H. M. *Free Radical Biol. Med.* **1999**, *27*, 329.
(109) Arroyo, C. M.; Kohno, M. *Free Radical Res. Commun.* **1991**, *14*, 145.
(110) Pronai, L.; Ichimori, K.; Nozaki, H.; Nakazawa, H.; Okino, H.; Carmichael, A. J.; Arroyo, C. M. *Eur. J. Biochem.* **1991**, *202*, 923.
(111) Arroyo, C. M.; Forray, C. *Eur. I. Pharmacol.* **1991**, *208*, 157.
(112) Korth, H.-G.; Ingold, K. U.; Sustman, R.; de Groot, H.; Sies, H. *Angew. Chem., Int. Ed. Engl.* **1992**, *31*, 891.
(113) Pou, S.; Keaton, L.; Surichamorn. W.; Frigillana, P.; Rosen, G. M. *Biochim. Biophys. Acta* **1994**, *1201*, 118.
(114) Korth, H.-G.; Sustmann, R.; Lommes, P.; Paul, T.; Ernst, A., de Groot, H.; Hughes, L.; Ingold, K. U. *J. Am. Chem. Soc.* **1994**. *116*, 2767.
(115) Paul, T.; Hassan, M. A.; Korth, H.-G.; Sustmann, R.; Avila, D. V. *J. Org. Chem.* **1996**. *61*, 6835.
(116) Bätz, M.; Korth, H.-G.; Sustman, R. *Angew. Chem., Int. Ed. Engl.* **1997**, *36*, 1501.
(117) Meineke, P.; Rauen, U.; de Groot, H.; Korth, H.-G.; Sustman, R. *Chem. Eur. J.* **1999**, *5*, 1738.
(118) Meineke, P.; Rauen, U.; de Groot, H.; Korth, H.-G.; Sustman, R. *Biol. Chem.* **2000**, *381*, 575.
(119) Osiecki, J. H.; Ullman, E. *J. Am. Chem. Soc.* **1968**, *90*, 1078.
(120) Ullman, E. F.; Call, L.; Osiecki, J. H. *J. Org. Chem.* **1970**, *35*, 3623.
(121) Ullman, E. F.; Osiecki, J. H.; Boocock, D. G. B.; Darcy, R. *J. Am. Chem. Soc.* **1972**, *94*, 7049.
(122) Nadeau, J. S.; Boocock, D. G. B. *Anal. Chem.* **1977**, *49*, 1672.
(123) Akaike, T.; Yoshida, M.; Miyamoto, Y.; Sato, K.; Kohno, M.; Sasamoto, K.; Miyazaki, K.; Ueda, S.; Maeda, H. *Biochemistry* **1993**, *32*, 827.
(124) Joseph, J.; Kalyanaraman, J. J. B.; Hyde, J. S. *Biochem. Biophys. Res. Commun.* **1993**, *192*, 926.
(125) Haseloff, R. F.; Zöllner, S.; Kirilyuk, I. A.; Grigor'ev, I. A.; Reszka, R.; Bernhardt, R.; Mertsch, K.; Roloff, B.; Blasig, I. E. *Free Radical Res.* **1997**, *26*, 7.
(126) Az-ma, T.; Fujii, K.; Yuge, O. *Life Sci.* **1994**, *54*, 185.
(127) Woldman, Y. Y.; Khramtsov, V. V.; Grigor'ev, I. A.; Kiriljuk, I. A.; Utepbergenov, D. I. *Biochem. Biophys. Res. Commun.* **1994**, *202*, 195.
(128) Akaike, T.; Maeda, H. *Methods Enzymol.* **1996**, *268*, 211.
(129) Okamoto, T.; Akaike, T.; Nagano, T.; Miyajima, S.; Suga, M.; Ando, M.; Ichimori, K.; Maeda, H. *Arch. Biochem. Biophys.* **1997**, *342*, 261.
(130) Yoshida, K.; Akaike, T.; Doi, T.; Sato, K.; Ijiri, S.; Suga, M.; Ando, M.; Maeda, H. *Infect. Immun.* **1993**, *61*, 3552.
(131) Yoshida, M.; Akaike, T.; Wada, Y.; Sato, K.; Ikeda, K.; Ueda, S.; Maeda, H. *Biochem. Biophys. Res. Commun.* **1994**, *202*, 923.
(132) Maeda, H.; Noguchi, Y.; Sato, K.; Akaike, T. *Jpn. J. Cancer Res.* **1994**, *85*, 331.
(133) Konorev, E. A.; Tarpey, M. M.; Joseph, J.; Baker, J. E.; Kalyanaraman, B. *Free Radical Biol. Med.* **1995**, *18*, 169.
(134) Konorev, E. A.; Tarpey, M. M.; Joseph, J.; Baker, J. E.; Kalyanaraman B. *J. Pharmacol. Exp. Ther.* **1995**, *274*, 200.
(135) Yoshimura, T. In *Bioradicals Detected by ESR Spectroscopy*; Ohya-Nishiguchi, H., Packer, L., Eds.; Birkhäuser Verlag: Basel, 1995; p 217.
(136) Greenberg, S. S.; Wilcox, D. E.; Rubanyi, G. M. *Circ. Res.* **1990**, *67*, 1446.
(137) Wennmalm, A.; Lanne, B.; Petersson, A. *Anal. Biochem.* **1990**, *187*, 359.
(138) Westenberger, U.; Thanner, S.; Ruf, H. H.; Gersonde, K.; Sutter, G.; Trentz, O. *Free Radical Res. Commun.* **1990**, *11*, 167.
(139) Wang, Q.; Jacobs, J.; DeLeo, J.; Kruszyna, H.; Kruszyna, R.; Smith, R.; Wilcox, D. *Life Sci.* **1991**, *49*, PL55.
(140) Kosaka, H.; Shiga, T. In *Methods in Nitric Oxide Research*; Feelish, M., Stamler, J. S., Eds.; John Wiley & Sons: Chichester; 1996; p 373.
(141) Henry, Y. A.; Singel, D. J. In *Methods in Nitric Oxide Research*; Feelisch, M., Stamler, J. S., Eds.; John Wiley & Sons: Chichester; 1996; p 357.
(142) Doyle, M. P.; Hoekstra, J. W. *J. Inorg. Biochem.* **1981**, *14*, 351.
(143) Kosaka, H.; Watanabe, M.; Yoshihara, H.; Harada, N.; Shiga, T. *Biochem. Biophys. Res. Commun.* **1992**, *184*, 1119.
(144) Gibson, Q. H.; Roughton, F. J. W. *J. Physiol.* **1957**, *136*, 507.
(145) Chien, J. C. W. *J. Am. Chem. Soc.* **1969**, *91*, 2166.
(146) Wayland, B. B.; Olson, L. W. *J. Am. Chem. Soc.* **1974**, *96*, 6037.
(147) Caulton, K. G. *Coord. Chem. Rev.* **1975**, *14*, 317.
(148) Yoshimura, T.; Suzuki, S. *Inorg. Chim. Acta*, **1988**, *152*, 241.
(149) Hoshino, M.; Maeda, M.; Konishi, R.; Seki, H.; Ford, P. C. *J. Am. Chem. Soc.* **1996**, *118*, 5702.
(150) Yoshimura, T.; Suzuki, S.; Nakahara, A.; Iwasaki, H.; Masuko, M.; Matsubara, T. *Biochemistry* **1986**, *25*, 2436.
(151) Yoshimura, T.; Fujii, S.; Kamada, H.; Yamaguchi, K.; Suzuki, S.; Shidara, S.; Takakuwa, S. *Biochim. Biophys. Acta* **1996**, *1292*, 39.
(152) Barker, S. L. R.; Kopelman, R.; Meyer, T. E.; Cusanovich, M. A. *Anal. Chem.* **1998**, *70*, 971.
(153) Barker, S. L. R.; Kopelman, R. *Anal. Chem.* **1998**, *70*, 4902.
(154) Barker, S. L. R.; Clark, H. A.; Swallen, S. F.; Kopelman, R.; Tsang, A. W.; Swanson, J. A. *Anal. Chem.* **1999**, *71*, 1767.
(155) Blyth, D. J.; Aylott, J. W.; Moir, J. W. B.; Richardson, D. J.; Russel, D. A. *Analyst* **1999**, *124*, 129.
(156) Lisdat, F.; Ge, B.; Stöcklein, W.; Scheller, F. W.; Meyer, T. *Electroanalysis* **2000**, *12*, 946.
(157) Ge, B.; Meyer, T.; Schöning, M. J.; Wollenberger, U.; Lisdat, F. *Electrochem. Commun.* **2000**, *2*, 557.
(158) Coucouvanis, D. *Prog. Inorg. Chem.* **1970**, *11*, 233.
(159) Coucouvanis, D. *Prog. Inorg. Chem.* **1979**, *26*, 301.
(160) Delpine, M. *Compt. Rend. Acad. Sci.* **1908**, *146*, 981.
(161) World Health Organization. *Environ. Health Critera* **1988**, *78*, 11.
(162) Hosni, M.; Meskini, N.; Prigent, A.-F.; Anker, G.; Joulian, C.; Habib, R. E.; Lagarde, M. *Biochem. Pharmacol.* **1992**, *43*, 1319.
(163) Heikkila, R. E.; Cabbat, F. S.; Cohen, G. *J. Biol. Chem.* **1976**, *251*, 2182.
(164) Misra, H. P. *J. Biol. Chem.* **1979**, *254*, 11623.
(165) Cocco, D.; Calabrese, L.; Rigo, A.; Argese, E.; Rotillo, G. *J. Biol. Chem.* **1981**, *256*, 8983.
(166) Huie, R. E.; Padmaja, S. *Free Radical Res. Comms.* **1993**, *18*, 195.
(167) Kelner, M. J.; Alexander, N. M. *J. Biol. Chem.* **1986**, *261*, 1636.
(168) Kelner, M. J.; Bagnell, R.; Hale, B.; Alexander, N. M. *Free Radical Biol. Med.* **1989**, *6*, 355.
(169) Neims, A. H.; Coffey, D. S.; Hellerman, L. *J. Biol. Chem.* **1966**, *241*, 5941.
(170) Dierickx, P. J. *Pharmacol. Res. Commun.* **1984**, *16*, 135.
(171) Schreck, R.; Meier, B.; MÄnnel, D. N.; DrÖge, W.; Baeuerle, P. A. *J. Exp. Med.* **1992**, *175*, 1181.
(172) BaEuerle, P. A.; Baltimore, D. *Cell* **1996**, *87*, 13.
(173) O'Neill, L. A. J.; Kaltschmidt, C. *Trends Neurosci.* **1997**, *6*, 252.
(174) Kaltschmidt, B.; Sparna, T.; Kaltschmidt, C. *Antiox. Redox Signaling* **1999**, *1*, 129.
(175) Antwerp, D. J. V.; Martin, S. J.; Kafri, T.; Green, D. R.; Verma, I. M. *Science* **1996**, *274*, 787.
(176) Wang, C.-Y.; Mayo, M. W.; Baldwin, A. S., Jr. *Science* **1996**, *274*, 784.
(177) Mülsch, A.; Schray-Utz, B.; Mordvintcev, P. I.; Hauschildt, S.; Busse, R. *FEBS Lett.* **1993**, *321*, 215.
(178) Eberhardt, W.; Kunz, D.; Pfeilshifter, J. *Biochem. Biophys. Res. Commun.* **1994**, *200*, 163.
(179) Bedoya, F. J.; Flodström, M.; Eizirik, D. L. *Biochem. Biophys. Res. Commun.* **1995**, *210*, 816.
(180) Wolfe, J. T.; Ross, D.; Cohen, G. M. *FEBS Lett.* **1994**, *352*, 58.

(181) Bessho, R.; Matsubara, K.; Kubota, M.; Kuwakado, K.; Hirota, H.; Wakazono, Y.; Lin, Y. W.; Okuda, A.; Kawai, M.; Nishikomori, R.; Heike, T. *Biochem. Pharmacol.* **1994**, *48*, 1883.
(182) Albrecht, H.; Tschopp, J.; Jongeneel, C. V. *FEBS Lett.* **1994**, *351*, 45.
(183) Hattori, Y.; Akimoto, K.; Murakami, Y.; Kasai, K. *Mol. Cell. Biochem.* **1997**, *177*, 177.
(184) Altura, B. M.; Gebrewold, A. *Alcohol* **1998**, *16*, 25.
(185) Nobel, C. S. I.; Kimland, M.; Lind, B.; Orrenius, S.; Slater, A. F. G. *J. Biol. Chem.* **1995**, *270*, 26202.
(186) Yoneyama, H.; Kosaka, H.; Ohnishi, T.; Kawazoe, T.; Mizoguchi, K.; Ichikawa, Y. *Eur. J. Biochem.* **1999**, *266*, 771.
(187) Gibson, J. F. *Nature* **1962**, *196*, 64.
(188) Lancaster, J. R., Jr.; Hibbs, J. B., Jr. *Proc. Natl. Acad. Sci. U.S.A.* **1990**, *87*, 1223.
(189) Kubrina, L. N.; Caldwell, W. S.; Mordvintcev, P. I.; Malenkova, I. V.; Vanin, A. F. *Biochim. Biophys. Acta* **1992**, *1099*, 233.
(190) Kotake, Y.; Tanigawa, T.; Tanigawa, M.; Ueno, I. *Free Radical Res.* **1995**, *23*, 287.
(191) Zweier, J. L.; Wang, P.; Samouilov, A.; Kuppusamy, P. *Nat. Med.* **1995**, *1*, 804.
(192) Kuppusamy, P.; Wang, P.; Samouilov, A.; Zweier, J. L. *Magn. Reson. Med.* **1996a**, *36*, 212.
(193) Xia, Y.; Zweier, J. L. *Proc. Natl. Acad. Sci. U.S.A.* **1997**, *94*, 12705.
(194) Xia, Y.; Cardounel, A. J.; Vanin, A. F.; Zweier, J. L. *Free Radical Biol. Med.* **2000**, *29*, 793.
(195) Fujii, H.; Koscielniak, J.; Berliner, L. J. *Magn. Reson. Med.* **1997**, *38*, 565.
(196) Fujii, S.; Suzuki, Y.; Yoshimura, T.; Kamada, H. *Am. J. Physiol.* **1998**, *274*, G857.
(197) Mordvintcev, P.; Mülsch, A.; Busse, R.; Vanin, A. *Anal. Biochem.* **1991**, *199*, 142.
(198) Mülsch, A.; Mordvintcev, P.; Vanin, A. *Neuroprotocols* **1992**, *1*, 165.
(199) Komarov, A.; Mattson, D.; Jones, M. M.; Singh, P. K.; Lai, C.-S. *Biochem. Biophys. Res. Commun.* **1993**, *195*, 1191.
(200) Yoshimura, T.; Fujii, S.; Yokoyama, H.; Kamada, H. *Chem. Lett.* **1995**, 309.
(201) Pou, S.; Tsai, P.; Porasuphatana, S.; Halpern, H. J.; Chandramouli, G. V. R.; Barth, E. D.; Rosen, G. M. *Biochim. Biophys. Acta* **1999**, *1427*, 216.
(202) Fujii, S.; Yoshimura, T. *Coord. Chem. Rev* **2000**, *198*, 89.
(203) Fujii, S.; Yoshimura, T.; Kamada, H. *Chem. Lett.* **1996**, 785.
(204) Paschenko, S. V.; Khramtsov, V. V.; Skatchkov, M. P.; Plyusnin, V. F.; Bassenge, E. *Biochem. Biophys. Res. Commun.* **1996**, *225*, 577.
(205) Nakagawa, H.; Ikota, N.; Ozawa, T.; Masumizu, T.; Kohno, M. *Biochem. Mol. Biol. Int.* **1998**, *45*, 1129.
(206) Tominaga, T.; Sato, S.; Ohnishi, T.; Ohnishi, S. T. *Brain Res.* **1993**, *614*, 342.
(207) Sato, S.; Tominaga, T.; Ohnishi, T.; Ohnishi, S. T. *Biochim. Biophys. Acta* **1993**, *1181*, 195.
(208) Ohnishi, S. T. In *Nitric Oxide Protocols*. Titheradge, M. A., Ed.; Humana Press: Totawa, NJ, 1998; p 129.
(209) Yoshimura, T. *CVD Grand Round Ser.* **1996**, *3*, 1.
(210) Yokoyama, H.; Fujii, S.; Yoshimura, T.; Ohya-Nishiguchi, H.; Kamada, H. *Magn. Reson. Imaging* **1997**, *15*, 249.
(211) Suzuki, Y.; Fujii, S.; Tominaga, T.; Yoshimoto, T.; Yoshimura, T.; Kamada, H. *Biochim. Biophys. Acta* **1997**, *1335*, 242.
(212) Fujii, H.; Berliner, L. J. *Magn. Reson. Med.* **1999**, *42*, 599.
(213) Fujii, S.; Kobayashi, K.; Tagawa, S.; Yoshimura, T. *J. Chem. Soc., Dalton Trans.* **2000**, 3310.
(214) Vanin, A. F.; Liu, X.; Samouilov, A.; Stukan, R. A.; Zweier, J. L. *Biochim. Biophys. Acta* **2000**, *1474*, 365.
(215) Tsuchiya, K.; Jiang, J.-J.; Yoshizumi, M.; Tamaki, T.; Houchi, H.; Minakuchi, K.; Fukuzawa, K.; Mason, R. P. *Free Radical Biol. Med.* **1999**, *27*, 347.
(216) Yordanov, N. D.; Iliev, V.; Shopov, D. *Inorg. Chim. Acta* **1982**, *60*, 9.
(217) Mülsch, A.; Vanin, A.; Mordvintcev, P.; Hauschildt, S.; Busse, R. *Biochem. J.* **1992**, *288*, 597.
(218) Komarov, A. M.; Wink, D. A.; Feelisch, M.; Schmidt, H. H. H. W. *Free Radical Biol. Med.* **2000**, *28*, 739.
(219) Norby, S. W.; Weyhenmeyer, J. A.; Clarkson, R. B. *Free Radical Biol. Med.* **1997**, *22*, 1.
(220) Hiramoto, K.; Tomiyama, S.; Kikugawa, K. *Free Radical Res.* **1997**, *27*, 505.
(221) Tsuchiya, K.; Yoshizumi, M.; Houchi, H.; Mason, R. P. *J. Biol. Chem.* **2000**, *275*, 1551.
(222) Venkataraman, S.; Martin, S. M.; Schafer, F. Q.; Buettner, G. R. *Free Radical Biol. Med.* **2000**, *29*, 580.
(223) Friedberg, M. A.; Hinsdale, M. E.; Shihabi, Z. K. *J. Chromatogr.* **1997**, *A781*, 491.
(224) Paya, D.; Maupoil, V.; Schott, C.; Rochette, L.; Stoclet, J.-C. *Cardiovasc. Res.* **1995**, *30*, 952.
(225) Fujii, S.; Miyakoda, G.; Chihiro, M.; Yoshimura, T.; Kamada, H. *Chem. Lett.* **1996**, 1055.
(226) Sato, S.; Tominaga, T.; Ohnishi, T.; Ohnishi, S. T. In *Central Nervous System Trauma—Research Techniques*; Ohnishi, S. T., Ohnishi, T., Eds.; CRC Press: Boca Raton, FL, 1995; p 455.
(227) *The Merck Index*; Budavari, S., Ed.; Merck: Whitehouse Station, NJ, 1996; p 572.
(228) Shinobu, L. A.; Jones, S. G.; Jones, M. M. *Acta Pharmacol. Toxicol.* **1984**, *54*, 189.
(229) Pieper, G. M.; Lai, C.-S. *Biochem. Biophys. Res. Commun.* **1996**, *219*, 584.
(230) Pieper, G. M.; Lai, C.-S. *Jpn. J. Pharmacol.* **1999**, *80*, 359.
(231) Roza, A. M.; Cooper, M.; Pieper, G.; Hilton, G.; Dembney, K.; Lai, C.-S.; Lindholm, P.; Komorowski, P.; Felix, C.; Johnson, C.; Adams, M. *Transplantation* **2000**, *69*, 227.
(232) Kubrina, L. N.; Mikoyan, V. D.; Mordvintcev, P. I.; Vanin, A. F. *Biochim. Biophys. Acta* **1993**, *1176*, 240.
(233) Komarov, A. M.; Mak, I. T.; Weglicki, W. B. *Biochim Biophys. Acta* **1997**, *1361*, 229.
(234) Vanin, A. F.; Huisman, A.; Stroes, E. S. G.; de Ruijter-Heijstek, F. C.; Rabelink, T. J.; van Faassen, E. E. *Free Radical Biol. Med.* **2001**, *30*, 813—824.
(235) Vanin, A. F.; Mordvintcev, P. I.; Hauschildt, S.; Mülsch, A. *Biochim. Biophys. Acta* **1993**, *1177*, 37.
(236) Komarov, A. M.; Lai, C.-S. *Biochim. Biophys. Acta* **1995**, *1272*, 29.
(237) Kotake, Y.; Tanigawa, T.; Tanigawa, M.; Ueno, I.; Allen, D. R.; Lai, C.-S. *Biochim. Biophys. Acta* **1996**, *1289*, 362.
(238) Mülsch, A.; Mordvintcev, P. I.; Vanin, A. F.; Busse, R. *Biochem. Biophys. Res. Commun.* **1993**, *196*, 1303.
(239) Sato, S.; Tominaga, T.; Ohnishi, T.; Ohnishi, S. T. *Brain Res.* **1994**, *647*, 91.
(240) Tominaga, T.; Sato, S.; Ohnishi, T.; Ohnishi, S. T. *J. Cereb. Blood Flow Metab.* **1994**, *14*, 715.
(241) Mülsch, A.; Busse, R.; Mordvintcev, P. I.; Vanin, A. F.; Nielsen, E. O.; Scheel-KrÜger, J.; Olesen, S.-P. *Neuroreport* **1994**, *5*, 2325.
(242) Bashkatova, V.; Vitskova, G.; Narkevich, V.; Vanin, A.; Mikoyan, V.; Rayevsky, K. *J. Mol. Neurosci.* **2000**, *14*, 183.
(243) Suzuki, Y.; Fujii, S.; Numagami, Y.; Tominaga, T.; Yoshimoto, T.; Yoshimura, T. *Free Radical Res.* **1998**, *28*, 293.
(244) Suzuki, Y.; Fujii, S.; Tominaga, T.; Yoshimoto, T.; Fujii, S.; Akaike, T.; Maeda, H.; Yoshimura, T. *J. Cereb. Blood Flow Metab.* **1999**, *19*, 1175.
(245) Fujii, S.; Akaike, T.; Maeda, H. *Virology* **1999**, *256*, 203.
(246) Sjakste, N.; Baumane, L.; Meirena, D.; Lauberte, L.; Dzintare, M.; Kalvins, I. *Biochem. Pharmacol.* **1999**, *58*, 1955.
(247) Quaresima, V.; Takehara, H.; Tsushima, K.; Ferrari, M.; Utsumi, H. *Biochem. Biophys. Res. Commun.* **1996**, *221*, 729.
(248) Mikoyan, V. D.; Kubrina, L. N.; Serezhenkov, V. A.; Stukan, R. A.; Vanin, A. F. *Biochim. Biophys. Acta* **1997**, *1336*, 225.
(249) Komarov, A. M.; Mattson, D. L.; Mak, I. T.; Weglicki, W. B. *FEBS Lett.* **1998**, *424*, 253.
(250) Wallis, G.; Brackett, D.; Lerner, M.; Kotake, Y.; Bolli, R.; McCay, P. B. *Shock* **1996**, *6*, 274.
(251) Obolenskaya, M. Y.; Vanin, A. F.; Mordvintcev, P. I.; Mülsch, A.; Decker, K. *Biochem. Biophys. Res. Commun.* **1994**, *202*, 571.
(252) Mikoyan, V. D.; Kubrina, L. N.; Vanin, A. F. *Biochem. Mol. Biol. Int.* **1994**, *32*, 1157.
(253) Chan, K. L.; Zhang, X. H.; Fung, P. C. W.; Guo, W. H.; Tam, P. K. H. *Br. J. Surg.* **1999**, *86*, 1427.
(254) Parratt, J. R. *Br. J. Pharmacol.* **1973**, *47*, 12.
(255) Suffredini, A. F.; Fromm, R. E.; Parker, M. M.; Brenner, M.; Kovacs, J. A.; Wesley, R. A.; Parrillo, J. E. *N. Engl. J. Med.* **1989**, *321*, 280.
(256) Förstermann, U.; Gath, I.; Schwarz, P.; Closs, E. I.; Kleinert, H. *Biochem. Pharmacol.* **1995**, *50*, 1321.
(257) Reinke, L. A.; Moore, D. R.; Kotake, Y. *Anal. Biochem.* **1996**, *243*, 8.
(258) Lecour, S.; Maupoil, V.; Siri, O.; Tabard, A.; Rochette, L. *J. Cardiovasc. Pharmacol.* **1999**, *33*, 78.
(259) Zweier, J. L.; Wang, P.; Kuppusamy, P. *J. Biol. Chem* **1995**, *270*, 304.
(260) Komarov, A. M.; Kramer, J. H.; Mak, I. T.; Weglicki, W. B. *Mol. Cell. Biochem.* **1997**, *175*, 91.
(261) Tabatabaie, T.; Kotake, Y.; Wallis, G.; Jacob, J. M.; Floyd, R. A. *FEBS Lett.* **1997**, *407*, 148.
(262) Doi, K.; Akaike, T.; Horie, H.; Noguchi, Y.; Fujii, S.; Beppu, T.; Ogawa, M.; Maeda, H. *Cancer* **1996**, *77*, 1598.
(263) Akaike, T.; Noguchi, Y.; Ijiri, S.; Setoguchi, K.; Suga, M.; Zheng, Y. M.; Dietzschold, B.; Maeda, H. *Proc. Natl. Acad. Sci. U.S.A.* **1996**, *93*, 2448.
(264) Mülsch, A.; Bara, A.; Mordvintcev, P.; Vanin, A.; Busse, R. *Br. J. Pharmacol.* **1995**, *116*, 2743.
(265) Mülsch, A.; Mordvintcev, P.; Bassenge, E.; Jung, F.; Clement, B.; Busse, R. *Circulation* **1995**, *92*, 1876.
(266) Rao, D. N. R.; Cederbaum, A. I. *Arch. Biochem. Biophys.* **1995**, *321*, 363.
(267) Colacicchi, S.; Alecci, M.; Gualtieri, G.; Quarresima, V.; Ursini, C. L.; Ferrari, M.; Sotgiu, A. *J. Chem. Soc., Perkin. Trans. 2* **1993**, 2077.

(268) Sato, T.; Yokoyama, H.; Ohya, H.; Kamada, H. *Appl. Magn. Reson.* **1999**, *17*, 119.
(269) Yokoyama, H.; Lin. Y.; Itoh, O.; Ueda, Y.; Nakajima, A.; Ogata, T.; Sato, T.; Ohya-Nishiguchi, H.; Kamada, H. *Free Radical Biol. Med.* **1999**, *27*, 442.
(270) Oikawa, K.; Ogata, T.; Togashi, H.; Yokoyama, H.; Ohya-Nishiguchi, H.; Kamada, H. *Anal. Sci.* **1995**, *11*, 885.
(271) Oikawa, K.; Ogata, T.; Lin, Y.; Sato, T.; Kudo, R.; Kamada, H. *Appl. Radiat. Isot.* **1996**, *47*, 1605.
(272) Yokoyama, H.; Tsuchihashi, N.; Ogata, T.; Hiramatsu, M.; Mori, N. *MAGMA* **1996**, *4*, 247.
(273) Lauterbur, P. C. *Nature* **1973**, *242*, 190.
(274) Ishida, S.; Kumashiro, H.; Tsuchihashi, N.; Ogata, T.; Ono, M.; Kamada, H.; Yoshida, E. *Phys. Med. Biol.* **1989**, *34*, 1317.
(275) Jansson, P. A. *Deconvolution with Application in Spectroscopy*; Academic: New York, 1984.
(276) Lai, C.-S.; Komarov, A. M. *FEBS Lett.* **1994**, *345*, 120.
(277) Komarov, A. M. *Cell. Mol. Biol.* **2000**, *46*, 1329.
(278) Yoshimura, T. *Anal. Sci.* **1997**, *13*, 3, S451.
(279) Fujii, H.; Berliner, L. J. *Phys. Med. Biol.* **1998**, *43*, 1949.
(280) Pfister, H.-W.; Koedel, U.; Lorenzl, S.; Tomasz, A. *Stroke* **1992**, *23*, 1798.
(281) Tunkel, A. R.; Scheld, W. M. *Annu. Rev. Med.* **1993**, *44*, 103.
(282) Koedel, U.; Bernatowicz, A.; Paul, R.; Frei, K.; Fontana, A.; Pfister, H.-W. *Ann. Neurol.* **1995**, *37*, 313.
(283) Boje, K. M. K. *Brain Res.* **1996**, *720*, 75.
(284) Kim, Y. S.; Täuber, M. G. *Infect. Immun.* **1996**, *64*, 3148.
(285) Kornelisse, R. F.; Hoekman, K.; Visser, J. J.; Hop, W. C.; Huijmans, J. G.; van der Straaten, P. J.; van der Heijden, A. J.; Sukhai, R. N.; Neijens, H. J.; de Groot, R. *J. Infect. Dis.* **1996**, *174*, 120.
(286) Leib, S. L.; Kim, Y. S.; Black, S. M.; Turren, J. H.; Täuber, M. G. *J. Infect. Dis.* **1998**, *177*, 692.
(287) Kuppusamy, P.; Ohnishi, S. T.; Numagami, Y.; Ohnishi, T.; Zweier, J. L. *J. Cereb. Blood Flow Metab.* **1995**, *15*, 899.
(288) Kuppusamy, P.; Ohnishi, S. T.; Numagami, Y.; Ohnishi, T.; Zweier, J. L. *Res. Chem. Intermed.* **1996**, *22*, 605.
(289) Kuppusany, P.; Shanker, R. A.; Roubaud, V. M.; Zweier, J. L. *Magn. Reson. Med.* **2001**, *45*, 700.
(290) Yoshimura, T. *Bull. Chem. Soc. Jpn.* **1991**, *64*, 2819.
(291) McDonald, C. C.; Phillips, W. D.; Mower, H. F. *J. Am. Chem. Soc.* **1965**, *87*, 3319.
(292) Vanin, A. F. *Biochemistry (Moscow)* **1967**, *32*, 228.
(293) Woolum, J. C.; Tiezzi, E.; Commoner, B. *Biochim. Biophys. Acta* **1968**, *160*, 311.
(294) Foster, M. W.; Cowan, J. A. *J. Am. Chem. Soc.* **1999**, *121*, 4093.
(295) Stamler, J. S.; Singel, D. J.; Loscalzo, J. *Science* **1992**, *258*, 1898.
(296) Stamler, J. S.; Hausladen, A. *Nat. Struct. Biol.* **1998**, *5*, 247.
(297) Ueno, T.; Yoshimura, T. *Jpn. J. Pharmacol.* **2000**, *82*, 95.
(298) Reddy, D.; Lancaster, J. R.; Cornforth, D. P. *Science* **1983**, *221*, 769.
(299) Drapier, J. C.; Pellat, C.; Henry, Y. *J. Biol. Chem.* **1991**, *266*, 10162.
(300) Ueno, T.; Suzuki, S.; Fujii, S.; Vanin, A. F.; Yoshimura, T. *Free Radical Res.* **1999**, *31*, 525.
(301) Bacic, G.; Nilges, M. J.; Magin, R. L.; Walczak, T.; Swartz, H. M. *Magn. Reson. Med.* **1989**, *10*, 266.
(302) Couet, W. R.; Eriksson, U. G.; Tozer, T. N.; Tuck, L. D.; Wesbey, G. E.; Nitecki, D.; Brasch, R. C. *Pharm. Res.* **1984**, *1*, 203.
(303) Matsumoto, K.; Utsumi, H. *Biophys. J.* **2000**, *79*, 3341.
(304) Foster, M. A.; Seimenis, I.; Lurie, D. J. *Phys. Med. Biol.* **1998**, *43*, 1893.
(305) Mülsch, A.; Lurie, D. J.; Seimenis, I.; Fightlscherrer, B.; Foster, M. A. *Free Radical Biol. Med.* **1999**, *27*, 636.
(306) Merbach, A. E.; Toth, E., Eds. *The Chemistry of Contrast Agents in Medical Magnetic Resonance Imaging*; John Wiley & Sons: Chichester, 2001.
(307) Rast, S.; Borel, A.; Helm, L.; Belorizky, E.; Fries, P. H.; Merbach, A. E. *J. Am. Chem. Soc.* **2001**, *123*, 2637.
(308) Fujii, H.; Wan, X.; Zhong, J.; Berliner, L.; Yoshikawa, K. *Magn. Reson. Med.* **1999**, *42*, 235.
(309) Fichtlscherer, B.; Mülsch, A. *Radiology* **2000**, *216*, 225.
(310) Salle, F. D.; Barone, P.; Hacker, H.; Smaltino, F.; d'Ischia, M. *Neuroreport* **1997**, *8*, 461.
(311) Caramia, F.; Yoshida, T.; Hamberg, L. M.; Huang, Z.; Hunter, G.; Wanke, I.; Zaharchuk, G.; Moskowitz, M. A.; Rosen, B. R. *Magn. Reson. Med.* **1998**, *39*, 160.
(312) Jordan, B. F.; Misson, P.-D.; Demeure, R.; Baudelet, C.; Beghein, N.; Gallez, B. *Int. J. Radiat. Oncol. Biol. Phys.* **2000**, *48*, 565.
(313) Misco, T. P.; Schilling, J.; Salvemini, D.; Moore, M.: Currie, M. G. *Anal. Biochem.* **1993**, *214*, 11.
(314) Sonoda, M.; Kobayashi, J.; Takezawa, M.; Miyazaki, T.; Nakajima, T.; Shimomura, H.; Koike, K.; Satomi, A.; Ogino, H.; Omoto, R.; Komoda, T. *Anal. Biochem.* **1997**, *247*, 417.
(315) Gunasekar, P. G.; Kanthasamy, A. G.; Borowitz, J. L.; Isom, G. E. *J. Neurosci. Methods* **1995**, *61*, 15.
(316) Imrich, A.; Kobzik, L. *Nitric Oxide: Biol. Chem.* **1997**, *1*, 359.
(317) Katayama, Y.; Takahashi, S.; Maeda, M. *Anal. Chim. Acta* **1998**, *365*, 159.
(318) Soh, N.; Katayama, Y.; Maeda, M. *Analyst* **2001**, *126*, 564.
(319) Barker, S. L. R.; Zhao, Y.; Marletta, M. A.; Kopelman, R. *Anal. Chem.* **1999**, *71*, 2071.
(320) Franz, K. J.; Singh, N.; Lippard, S. J. *Angew. Chem., Int. Ed.* **2000**, *39*, 2120.
(321) Franz, K. J.; Singh, N.; Spingler, B.; Lippard, S. *Inorg. Chem.* **2000**, *39*, 4081.
(322) Kojima, H.; Sakurai, K.; Kikuchi, K.; Kawahara, K.; Nagoshi, H.; Hirata, Y.; Akaike, T.; Maeda, H.; Nagano, T. *Biol. Pharm. Bull.* **1997**, *20*, 1229.
(323) Nakatsubo, N.; Kojima, H.; Sakurai, K.; Kikuchi, K.; Nagoshi, H.; Hirata, Y.; Akaike, T.; Maeda, H.; Urano, Y.; Higuchi, T.; Nagano, T. *Biol. Pharm. Bull.* **1998**, *21*, 1247.
(324) Nagano, T.; Takizawa, H.; Hirobe, M. *Tetrahedron Lett.* **1995**, *36*, 8239.
(325) Ignarro, L. J.; Fukuto, J. M.; Griscavage, J. M.; Rogers, N. E.; Byrns, R. E. *Proc. Natl. Acad. Sci. U.S.A.* **1993**, *90*, 8103.
(326) Miles, A. M.; Chen, Y.; Owens, M. W.; Grisham, M. B. *Methods* **1995**, *7*, 40. Hirata, Y.; Nagano, T. *Anal. Chem.* **1998**, *70*, 2446.
(327) Nakatsubo, N.; Kojima, H.; Kikuchi, K.; Nagoshi, H.; Hirata, Y.; Maeda, D.; Imai, Y.; Irimura, T.; Nagano, T. *FEBS Lett.* **1998**, *427*, 263.
(328) Kojima, H.; Sakurai, K.; Kikuchi, K.; Kawahara, S.; Kirino, Y.; Nagoshi, H.; Hirata, Y.; Nagano, T. *Chem. Pharm. Bull.* **1998**, *46*, 373.
(329) Sun, W. C.; Gee, K. R.; Klaubert, d. H.; Haugland, R. P. *J. Org. Chem.* **1997**, *62*, 6469.
(330) Kojima, H.; Hirotani, M.; Urano, Y.; Kikuchi, K.; Higuchi, T.; Nagano, T. *Tetrahedron Lett.* **2000**, *41*, 69.
(331) Kojima, H.; Hirotani, M.; Nakatsubo, N.; Kikuchi, K.; Urano, Y.; Higuchi, T.; Hirata, Y.; Nagano, T. *Anal. Chem.* **2001**, *73*, 1967.
(332) Tsien, R. Y. *Nature* **1981**, *290*, 527.
(333) Kojima, H.; Urano, Y.; Kikuchi, K.; Higuchi, T.; Hirata, Y.; Nagano, T. *Angew. Chem., Int. Ed. Engl.* **1999**, *38*, 3209.
(334) Yamaguchi, K.; Tamura, Z.; Maeda, M. *Acta Crystallogr.* **1997**, *C53*, 284.
(335) Kimura, C.; Oike, M.; Koyama, T.; Ito, Y. *Am. J. Physiol.* **2001**, *280*, E171.
(336) Kimura, C.; Koyama, T.; Oike, M.; Ito, Y. *Biochem. Biophys. Res. Commun.* **2000**, *274*, 736.
(337) Broillet, M.-C.; Randin, O.; Chatton, J.-Y. *FEBS Lett.* **2001**, *491*, 227.
(338) Suzuki, N.; Kojima, H.; Urano, Y.; Kikuchi, K.; Hirata, Y.; Nagano, T. *J. Biol. Chem.*, in press.
(339) Lin, S.; Fagan, K. A.; Li, K. X.; Shaul, P. W.; Cooper, D. M. F.; Rodman, D. M. *J. Biol. Chem.* **2000**, *275*, 17979.
(340) Zharikov, S. I.; Sigova, A. A.; Chen, S. F.; Bubb, M. R.; Block, E. R. *Am. J. Physiol.* **2001**, *280*, L465.
(341) Berkels, R.; Dachs, C.; Roesen, R.; Klaus, W. *Cell Calcium* **2000**, *27*, 281.
(342) Itoh, Y.; Ma, F. H.; Hoshi, H.; Oka, M.; Noda K.; Ukai, Y.; Kojima, H.; Nagano, T.; Toda, N. *Anal. Biochem.* **2000**, *287*, 203.
(343) Kojima, H.; Nakatsubo, N.; Kikuchi, K.; Urano, Y.; Higuchi, T.; Tanaka, J.; Kudo, Y.; Nagano, T. *Neuroreport* **1998**, *9*, 3345.
(344) Kojima, H.; Hirata, M.; Kudo, Y.; Kikuchi, K.; Nagano, T. *J. Neurochem.* **2001**, *76*, 1404.
(345) Yermolaieva, O.; Brot, N.; Weissbach, H.; Heinemann, S. H.; Hoshi, T. *Proc. Natl. Acad. Sci. U.S.A.* **2000**, *97*, 448.
(346) Ahern, G. P.; Hsu, S. F.; Klyachko, V. A.; Jackson, M. B. *J. Biol. Chem.* **2000**, *275*, 28810.
(347) Choi, Y. B.; Tenneti, L.; Le, D. A.; Ortiz, J.; Bai, G.; Chen, H. S. V.; Lipton, S. A. *Nat. Neurosci.* **2000**, *3*, 15.
(348) Kuo, R. K.; Baxter, G. T.; Thompson, S. H.; Stricker, S. A.; Patton, C.; Bonaventura, J.; Epel, D. *Nature* **2000**, *406*, 633.
(349) Lopez-Figueroa, M. O.; Day, H. E. W.; River, C.; Akil, H.; Watson, S. J. *Brain Res.* **2000**, *852*, 239.
(350) Wingrove, J. A.; O'Farrell, P. H. *Cell* **1999** *98*, 105.
(351) Hanke, C. J.; O'Brien, T.; Pritchard, K. A.; Campbell, W. B. *Hypertension* **2000**, *35*, 324.
(352) Gorbunov, N. V.; Pogue-Geile, K. L.; Epperly, M. W.; Bigbee, W. L.; Draviam, R.; Day, B. W.; Wald, N.; Watkins, S. C.; Greenberger, J. S. *Radiat. Res.* **2000**, *154*, 73.
(353) Lopez-Figueroa, M. O.; Caamano, C.; Morano, M. I.; Ronn, L. C.; Akil, H.; Watson, S. J. *Biochem. Biophys. Res. Commun.* **2000**, *272*, 129.
(354) Blute, T. A.; Lee, M. R.; Eldred, W. D. *Visual Neurosci.* **2000**, *17*, 557.
(355) Matsuo, T. *Br. J. Ophthalmol.* **2000**, *84*, 631.
(356) Pedroso, M. C.; Magalhaes, J. R.; Durzan, D. *J. Exp. Bot.* **2000**, *51*, 1027.
(357) Pedroso, M. C.; Magalhaes, J. R.; Durzan, D. *Plant Sci.* **2000**, *157*, 173.
(358) Foissner, I.; Wendehenne, D.; Langebartels, C.; Durner, J. *Plant J.* **2000**, *23*, 817.

CR010152S